UNIVERSITÄT DUISBURG ESSEN

Offen im Denken

The use of mass-spectrometry-based chemical proteomics approaches in bioactivity annotation of natural products and biocatalyst discovery: Applications to the natural product Zelkovamycin and fungi

Inaugural Dissertation

for the doctoral degree of

Dr. rer. nat.

from the Faculty of Biology

University of Duisburg-Essen Germany

Submitted by

Geronimo Heilmann

born in Kempen

April 2020

The experiments underlying the present work were conducted at the Department of Chemical Biology at the University of Duisburg-Essen.

1. Examiner: Prof. Dr. Markus Kaiser

2. Examiner: Prof. Dr. Bettina Siebers

Chair of the Board of Examiners: Prof. Dr. Bayer

Date of the oral examination: 03th of September 2020

DOI: 10.17185/duepublico/73028
URN: urn:nbn:de:hbz:464-20201112-082059-5

Declarations

Declarations required for the Application of Admission to the Doctoral Examination

Declaration: In accordance with § 6 (para. 2, clause g) of the Regulations Governing the Doctoral Proceedings of the Faculty of Biology for awarding the doctoral degree Dr. rer. nat., I hereby declare that I represent the field to which the topic “The use of mass-spectrometry-based chemical proteomics approaches in bioactivity annotation of natural products and biocatalyst discovery: Applications to the natural product Zelkovamycin and fungi” is assigned in research and teaching and that I support the application of Geronimo Heilmann

Essen, 07th of April 2020 _____

Prof. Dr. Markus Kaiser

Declaration regarding previous attempts to attain a doctoral degree: I hereby declare that in accordance with the Regulations Governing the Doctoral Proceedings of the Faculty of Biology § 6 (para. 2, clause e) I have undertaken no previous attempts to attain a doctoral degree.

GERONIMO HEILMANN

Essen, 07th of April 2020 _____

Geronimo Heilmann

Declarations

Declaration regarding the commercial procurement of a doctoral supervisor (§ 6, para. 2, clause f). I hereby declare the following: The present doctoral proceedings were not initiated via commercial procurement. In particular, no organisation has been engaged by me that, for a fee, has procured a doctoral supervisor nor has fulfilled all or part of my obligations with regard to examinations. Any third party help used up to now or will continue to be used has been/is only to a scientifically justifiable extent and in keeping with the laws on examinations. I am aware that any falsehoods regarding the above statement could exclude me from the admission to the doctoral proceedings or later lead to the termination of the proceedings or to the withdrawal of the doctoral title.

GERONIMO HEILMANN

Essen, 07th of April 2020 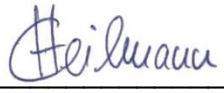

Geronimo Heilmann

Parts of this work are published in: „*Zelkovamycin is an OXPHOS inhibitory member of the argyrin natural product family*“, Chemistry – A European Journal, *accepted*

April 2020

Content

List of abbreviations

ABC	Ammonium bicarbonate
ABP	Activity-based probe
ABPP	Activity-based Protein Profiling
AMA	Antimycin A
APS	Ammonium persulfate
ATP	Adenosine triphosphate
BSA	Bovine serum albumin
CAZy	Carbohydrate-Active EnZYmes
CCCP	Carbonyl cyanide *m*-chlorophenyl hydrazone
CID	Collision-induced dissociation
Cy	Cyanine
DAPI	4′,6-diamidino-2-phenylindole
DCPIP	2,6-dichlorophenolindophenol (Tillmans reagent)
DMEM	Dulbecco's Modified Eagle's Medium
DMSO	Dimethyl sulfoxide
DNSA	3,5-Dinitrosalicylsäure
DTT	Dithiothreitol
EC	Enzyme classification
ECAR	Extracellular acidification rate
ESI	Electro spray ionization
FA	Formic acid
FBS	Fetal bovine serum
FCCP	Carbonyl cyanide-4-(trifluoromethoxy)phenylhydrazone
FP	Fluorophosphonate

GH	Glycoside hydrolase family
GO	Gene ontology
HCD	Higher-energy collisional dissociation
HRP	Horseradish peroxidase
HTP	High-throughput
IAM	Iodo acetamide
ISD	In-solution digest
JGI	Joint Genome Institute
K. lactis	*Kluyveromyces lactis*
KEGG	Kyoto Encyclopedia of Genes and Genomes
LC	Liquid chromatography
LDS	Lithium dodecyl sulfate
LFQ	Label-free quantification
LPMO	Lytic polysaccharide monooxygenases
MBR	Match between runs
MS	Mass spectrometry
MTT	Methylthiazolyldiphenyl-tetrazolium bromide
MWCO	Molecular weight cut-off
MYP	Maltose, yeast extract and peptone
nLC	nanoflow liquid chromatography
OBD	On-bead digest
OCR	Oxygen consumption rate
OXPHOS	Oxidative phosphorylation
P. chrysosporium	*Phanerochaete chrysosporium*
PBS	Phosphate-buffered saline

List of abbreviations

PDH	Pyruvate dehydrogenase
Pen/Strep	Penicillin/Streptomycin
PFK	Phosphofructokinase
pNPAc	*para*-Nitrophenol acetate
PPI	Protein-protein interaction
PTM	Post-translational modification
Rh	Rhodamine
RT	Room temperature
SDS	Sodium dodecyl sulfate
SH	Serine hydrolase
spp.	*Species pluralis*
TBS	Tris-buffered saline
TBS-T	Tris-buffered saline plus Tween-20
TBTA	Tris[(1-benzyl-1H-1,2,3-triazol-4-yl)methyl]amine
TCA	Trichloroacetic acid
TCEP	Tris(2-carboxyethyl)phosphine
TEMED	*N*, *N*, *N*', *N*'-Tetramethyl ethylenediamine
Tris	Tris(hydroxymethyl)-aminomethane

List of figures

List of figures

List of tables

Abstract

Bioactive natural compounds are a widely underexplored source of potential drugs and inhibitors. To investigate and characterize these compounds, mass spectrometry is a valuable tool. As mass spectrometry is nowadays well-configured for high throughput analysis, it is an appropriate tool for characterization of the almost indefinite number of bioactive natural compounds.

Zelkovamycin is a bioactive natural compound of the argyrin family whose bioactivity in humans is not investigated so far. This stands in contrast to its reported antibiotic effects against bacteria. On the contrary, most other reported argyrins also show promising anti-cancer effects in humans. In this work, mass spectrometric analysis in conjunction with biochemical and biological assays were used to identify an argyrin-unique OXPHOS inhibitory bioactivity of Zelkovamycin. Moreover, this PhD work revealed that Zelkovamycin is able to significantly decrease cell viability of OXPHOS-dependent skin cancer cells. Two unusual, non-canonical amino acids, a 4-methoxy tryptophan and a 2-methyl dehydrothreonine residue, are thereby essential for Zelkovamycin's bioactivity. The results highlight the potential scope of Zelkovamycin and suggests further approaches for optimizing its bioactivity.

Dead plant material is an almost indefinite feedstock of organic matter for energy production. However, its recalcitrant nature towards controlled and directed degradation severely hampers its large scale industrial use. Several fungi are however known as efficient dead plant material degraders. To this end, they secrete a huge arsenal of lignocellulolytic and accessory enzymes. Among them, *Phanerochaete chrysosporium* overtakes a prominent role as a model organism with the capacity for a complete break-down of dead plant material *via* secretion of ligninases, (hemi)cellulases and several accessory enzymes – the complete repertoire of lignocellulolytic enzymes. This PhD work shows that activity-based protein-profiling (ABPP) can be used to identify and characterize such degradation enzymes. To this end, two types of activity based probes (ABPs) were used: For the identification of plant-material degrading esterases, a fluorophosphonate-based ABP, while glycosidases were identified by a cyclophellitol-inspired ABP. Accordingly, this work points out the use of ABPP for enzymatic profiling of fungi.

Zusammenfassung

Bioaktive Naturstoffe stellen eine bisher noch unzureichend-untersuchte Quelle für Medikamente und Inhibitoren dar. Massenspektrometrie ist ein passendes Werkzeug, um diese Stoffe zu erforschen und zu charakterisieren. In der Tat kann die massenspektrometrische Analyse heutzutage im Hochdurchsatzverfahren durchgeführt werden und ist damit geeignet, die nahezu unendliche Zahl von bioaktiven Naturstoffen effizient zu charakterisieren.

Zelkovamycin ist ein bioaktiver Naturstoff aus der Argyrinfamilie, mit bisher unbekannter Bioaktivität in Menschen. Dies steht im Gegensatz zu den bekannten antibiotischen Effekten dieser Substanz. Hingegen zeigen viele Argyrine vielversprechende Effekte gegen Krebs beim Menschen. In dieser Arbeit wurde daher Massenspektrometrie in Verbindung mit biochemischen und biologischen Tests genutzt, um aufzuzeigen, dass Zelkovamycin eine für Argyrine einzigartige Bioaktivität als OXPHOS-Inhibitor besitzt. Ferner zeigt diese Doktorarbeit, dass Zelkovamycin die Zellviabilität von OXPHOS-abhängigen Hautkrebszellen signifikant reduzierte. Zwei ungewöhnliche, nicht kanonische Aminosäuren, 4-Methoxy-Tryptophan und 2-Methyldehyro-Threonin, sind dabei für die Bioaktivität von Zelkovamycin essenziell. Die Ergebnisse verdeutlichen somit das biomedizinische Potential von Zelkovamycin als Wirkstoff und deuten mögliche Optimierungsansätze zur Verbesserung der Bioaktivität an.

Totes Pflanzenmaterial ist eine nahezu unendliche organische Energiequelle. Diese kann bisher jedoch nur unzureichend genutzt werden, da dieses dazu zuerst in kontrollierter Weise in industriell-nutzbare Produkte abgebaut werden muss. Interessanterweise sind jedoch verschiedene Pilzstämme dafür bekannt, dass sie totes Pflanzenmaterial effizient abbauen können. Hierzu sekretieren sie ein großes Arsenal an lignocellulolytischen und akzessorischen Enzymen. *Phanerochaete chrysosporium* ist dabei ein gut untersuchter Modellorganismus, welcher die Fähigkeit zum vollständigen Abbau von totem Pflanzenmaterial besitzt. Zu diesem Zweck sekretiert er Ligninasen, (Hemi)cellulasen und weitere akzessorische Enzyme. In dieser Doktorarbeit wird nun gezeigt, dass Aktivitäts-basiertes Protein Profiling (ABPP) zur Identifizierung und Charakterisierung solcher Pflanzenmaterial-abbauender Enzyme verwendet werden kann. Zu diesem Zweck wurden zwei verschiedenen Typen von Aktivitäts-basierten Sonden (ABPs) eingesetzt: Zur Identifizierung von Pflanzenmaterial-abbauenden Esterasen wurde eine Fluorophosphonat-basierte ABP

verwendet, während Glycosidasen mit einer ABP auf Basis von Cyclophellitol identifiziert wurden. Dementsprechend hebt diese Arbeit den Nutzen von ABPP für ein enzymatisches Profiling in Pilzen hervor.

1 Introduction

Nature offers an uncountable number and a highly diverse repertoire of chemical compounds that may serve as starting points for various applications. In this thesis, two classes of nature-derived chemical compounds will be investigated: In the first part of the thesis, a bioactive natural product, i.e. Zelkovamycin, is in the focus while the second part of the thesis deals with the identification of natural enzymes as biocatalysts for biotechnological applications. In both parts, mass spectrometry (MS)-based approaches play an important role to mine and make these natural resources available.

Bioactive natural products are well-established starting points for drug and chemical probe design. These compounds are biosynthesized by many organisms with the aim to defend against, kill or evade competing species. Indeed, this approach occurs throughout all kingdoms of life and of all ages since appearance of life on earth.[1] Making this 'drugstore' accessible for pharmaceutical and biotechnological benefits is thus one of the biggest challenges of timely chemical biology research. Therefore, the thorough characterization of the bioactivity of natural products is an important topic.[2] In the present work, the use of MS in conjunction with further biochemical and biological approaches is used to thoroughly characterize the bioactivity of Zelkovamycin, a cyclic heptapeptide from *Streptomyces spp.*[3], in human cancer cell lines.

In the second part, the MS-driven chemical proteomics technology known as Activity-based protein profiling (ABPP) is used to identify promising enzymes for biocatalysis applications form the fungus *Phanerochaete chrysosporium* (*P. chrysosporium*).[4-7]

1.1 Natural Products

Bioactive natural products are chemical compounds biosynthesized from living organisms such as plants, fungi or microorganisms, often with the aim to display a biological effect on another organism, e.g. to defend against a pathogen invasion.[2,8] A classical example for such a compound is the fungus-derived penicillin natural product class that nowadays is probably the most widely used drug derived from a natural compound.[9,10] Due to their inherent bioactivity, natural products thus display promising starting points for the discovery of new drugs and therapeutics as well as chemical probes for biological basic research.

1.1.1 Zelkovamycin

The natural product Zelkovamycin was first reported by the Ōmura group in 1996 which isolated it from the culture broth *Streptomyces sp*. K96-0670.[3] Zelkovamycin was found to display antibiotic activity against *Xanthomonas oryzae*, *Acholeplasma laidlawii*, *Pyricularia oryzae* and *Staphylococcus aureus*. Structural elucidation by Tabata *et al*. revealed that Zelkovamycin is a cyclic heptapeptide (Fig. 1).

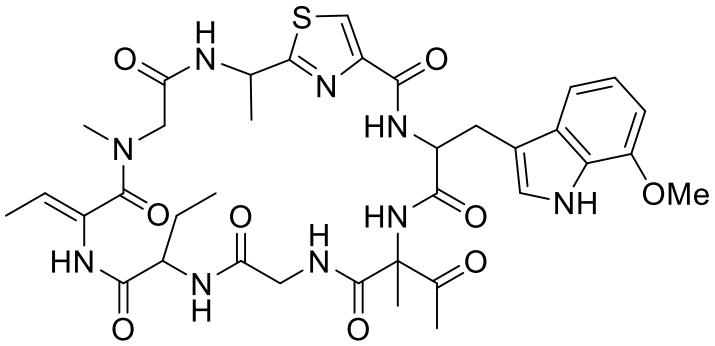

Figure 1: Proposed structure of Zelkovamycin. First published structure of Zelkovamycin by Tabata *et al*.[3] The elucidated structure lacked stereochemical assignments for the amino acid residues.

Besides the standard proteinogenic amino acid glycine, Zelkovamycin features six additional non-standard amino acids.[3,11] Among them are one unique and one very rare amino acid, namely 2-methyl dehydro threonine and 7-methoxy tryptophan, respectively.

However, total synthesis and structural assignment in the Kaiser group led to a revision of the reported structure and defined the missing stereochemistry.[12] Extensive studies by Krahn not only revealed the full stereochemical assignments for all amino acids of Zelkovamycin, but also showed that Zelkovamycin harbours a 4-methoxy instead of a 7-methoxy tryptophan residue (Fig. 2). This re-assignment of the methoxy tryptophan moiety as well as the full stereochemical assignment then revealed that Zelkovamycin is a so far unrecognized member of the natural product family of the argyrins.

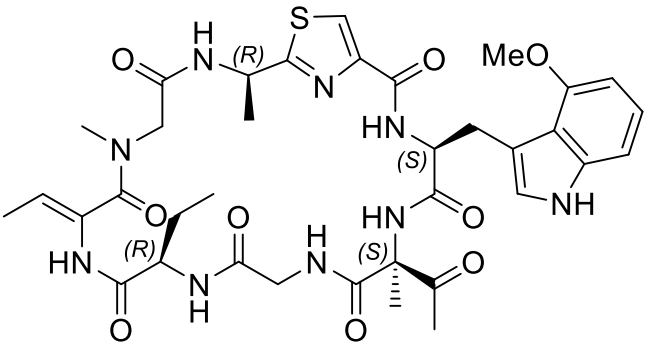

Figure 2: Revised structure of Zelkovamycin. Krahn elucidated stereochemistry of Zelkovamycin and revealed the presence of a 4-methoxy instead of a 7-methoxy tryptophan moiety in its macrocycle.[12]

So far, the argyrin family consisted of eight cycloheptapeptides (argyrin A-H), of which seven feature a 4-methoxy tryptophan.[13] The argyrins were first isolated from the myxobacterium *Archangium gephyra* in 2002 (Fig. 3).

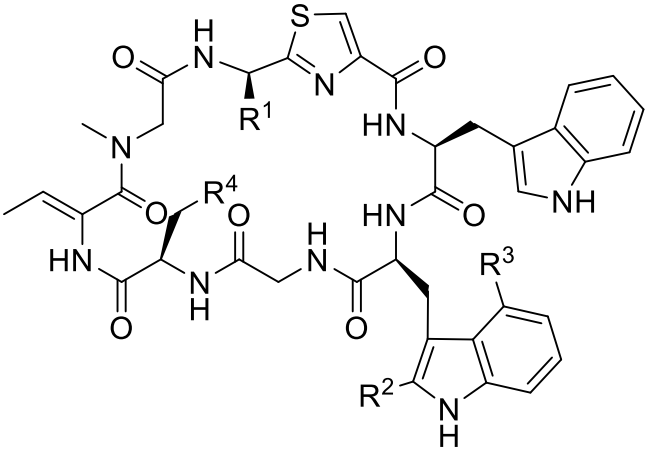

Figure 3: General structure of the argyrin natural products. A structural comparison of Argyrins and Zelkovamycin reveals strong structural similarities and pinpoints that Zelkovamycin is a member of the argyrin family.

Interestingly, besides their antibiotic properties, argyrins A and B are also highly cytotoxic for eukaryotic cells.[14,15] In 2008, Nickeleit *et al.* reported that argyrin A displays promising anticancer effects via inhibition of the proteasome and subsequent stabilization of the cyclin kinase inhibitor $p27^{kip1}$. In contrast, argyrin B was reported to target the elongation factor G in bacteria and its close homolog mitochondrial elongation factor G1 in eukaryotes. A thorough investigation of argyrin F's bioactivity again proposed the proteasome as its molecular target, thereby preventing pancreatic ductal adenocarcinoma progression in combination with Gemcitabine.[16,17] Of note, also argyrin B, C and D were reported to inhibit the proteasome in this study. Moreover, it was shown that the 4-methoxy tryptophan moiety was crucial for high bioactivity. However, as shown by Krahn, Zelkovamycin did not inhibit the proteasome nor influence $p27^{kip1}$ levels.[12] In contrast, first studies of Zelkovamycin's bioactivity demonstrated effects on cell viability of different human cancer cell lines and an

increased extracellular acidification in presence of Zelkovamycin. Since the reported bioactivity of argyrins is distinct from the observations of Krahn, a thorough investigations of the bioactivity of this new member of the argyrins is therefore warranted and was performed in this thesis.

1.1.2 Hydrolase-probes derived from natural products

Hydrolases are defined as enzymes that break a chemical bond by addition of a water molecule. Accordingly, hydrolases catalyze hydrolysis reactions. Several classification systems for enzymes have already been established. In the Expasy database, which is maintained by SwissProt, hydrolases are classified with the Enzyme Classification (EC) number 3. Further subclassifications involve the type of cleaved bond. For example, EC 3.1 consists of all enzymes that cleave ester bonds, while EC 3.2 describes enzymes that cleave glycosidic bonds.

In general, hydrolases have an essential role in many biological processes, including cellular metabolism, in which they catalyze reactions for metabolic turnover.[18] A well-known example are proteases. These enzymes break down proteins into shorter protein or peptide sequences or even single amino acids and thus participate in regulating cellular proteostasis. The resulting amino acids can then be used as an energy source or for new protein biosynthesis. Accordingly, a proper regulation of hydrolase activity is fundamental and plays an important role in many pathophysiological conditions. Nowadays, several drugs acting as protease inhibitors have been developed.[19] These include drugs vs. widespread diseases such as Alzheimer's disease, blood-clotting disorders or Type 2 diabetes.[20]

1.1.2.1 Serine hydrolases and associated probes

An important class of hydrolases is the serine hydrolase (SH) superfamily. These enzymes share a nucleophilic serine in their catalytic site.[21] Generally, classical SHs have a catalytic triad (Ser, His, Asp/Glu) that is essential for the coordinated cleavage of a substrate. While the nucleophilic Ser forms an acyl intermediate with the substrate, the His and Asp/Glu residues are important for activating the serine residue. Upon serine addition, a tetrahedral intermediate is formed and the substrate is cleaved. In a second step, the resulting acyl intermediate is cleaved. To this end, a water molecule coordinates to the electrophilic nitrogen in the His-ring. Water addition then results in the formation of another tetrahedral intermediate which immediately breaks down, resulting in the hydrolyzed product and the recovered catalytic triad. The carboxyl group of Asp or Glu serves to increase the reactivity of the His-nitrogen (Fig. 4).

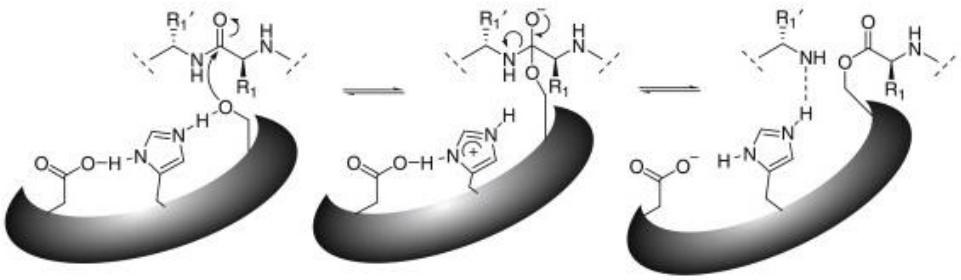

Figure 4: Catalytic mechanism of serine hydrolases. The substrate binds to the nucleophilic serine and forms a covalent product known as the acyl-enzyme intermediate. In a second step (not depicted here), this intermediate is hydrolysed by addition of water, resulting in the regeneration of the catalytic amino acids (adapted from Sieber et al).[8]

Many SH inhibitors utilize this hydrolysis mechanism and form non-hydrolyzable derivatives of the acyl-enzyme-intermediate.[7,21,22]

Accordingly, this covalent inhibition mechanism can also be used to screen for unknown SHs and subsequent annotation of these enzymes via ABPP. In 1961, Ostrowski and Banard reported for the first time the use of fluorophosphonate (FP) for inhibiting esterase activity in rat tissues.[6] For detection, FP was isotopically labelled and visualized by radiography. FP acts as a substrate mimic and binds in a similar fashion as endogenous substrates to the active site of SHs. With the emergence of ABPP in the 1990's, FPs were used as starting points for the development of activity-based probes (ABPs) vs. SHs (cf. section 1.2). [7] Liu *et al.* used a FP-biotin probe to identify serine hydrolases in rat tissue. This was the first example for 'modern ABPP' and FP rapidly became the 'workhorse' of ABPP. Successive studies with FP resulted in the identification of numerous unknown SHs throughout all kingdoms of life.[23-25] The ability of FP to target SHs (in particular esterases) is also utilized in this work to identify new SHs in thermophilic fungi (cf. section1.1.2.2 and 1.3). In this study, a derivative of the original FP-biotin, FP-alkyne, was most frequently used (Fig. 5). It was developed from classical FP-probes for improved *in vivo* labelling by substitution of the biotin-moiety with an alkyne (cf. section 1.2).

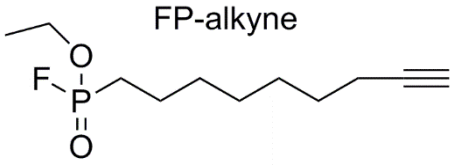

Figure 5: FP-alkyne probe. The FP-warhead targets SHs. The warhead is linked to an alkyne moiety, which can be utilized for click-chemistry to attach fluorophores or biotin in a 2-step approach. This probe is even more suitable for *in vivo* labelling due to its low molecular weight and suitable hydrophobicity.

1.1.2.2 Glycosidases and associated probes

Glycosidases (alternative names are glycoside hydrolases or glycosyl hydrolases) catalyze the hydrolysis of O- or S-glycosidic bonds. In the ExPasy database, they are listed as EC 3.2, thus they are members of the large hydrolase enzyme class (EC 3). Today, 245 sub-groups of glycosidases are known. This pinpoints for a high diversity and importance throughout all kingdoms of life. Historically, glycosidases were grouped by their mechanism or their substrate.[26] However, the most important database for glycosidases nowadays is CArbohydrate-Active EnZymes (CAZy).[27,28] Herein, glycosidases are mainly classified by their natural substrate. Uncharacterized gene loci or proteins are assigned by homology. The CAZy database discriminates more than 160 glycosidase families (GHs) and several auxiliary proteins (166 GH families, last updated on 04/12/2019). For example, carbohydrate esterases are important auxiliary proteins.[29,30] These esterases are able to cleave acetyl groups of hemicellulose (cf. section 1.3).

In this PhD thesis, a focus was put on identifying glucosidases, in particular exo-β-glucosidases. These enzymes are able to cleave terminal glucose monomers from polymers (β-1-4-connected) or cleave disaccharides into a glucose and another sugar monomer. In the CAZy database, these enzymes are mainly classified as GH3 and GH5. All of them exhibit acidic residues in their catalytic cleft (Asp/Glu) that are essential for enzyme activity, overtaking roles as nucleophiles or general acid/base catalysts.[31-33] When a substrate enters the catalytic cleft, the nucleophile attacks the anomeric carbon atom in the glucose ring which leads to cleavage of the glycosidic bond and formation of an acylal intermediate. In a second step, this intermediate is then attacked by a water molecule, subsequently releasing a free glucose monomer from the glucosidase (Fig. 6). Accordingly, the underlying mechanism displays similarities to the mechanism underlying SHs. In both cases, a covalent intermediate is formed which is then hydrolyzed by a second addition reaction with water.

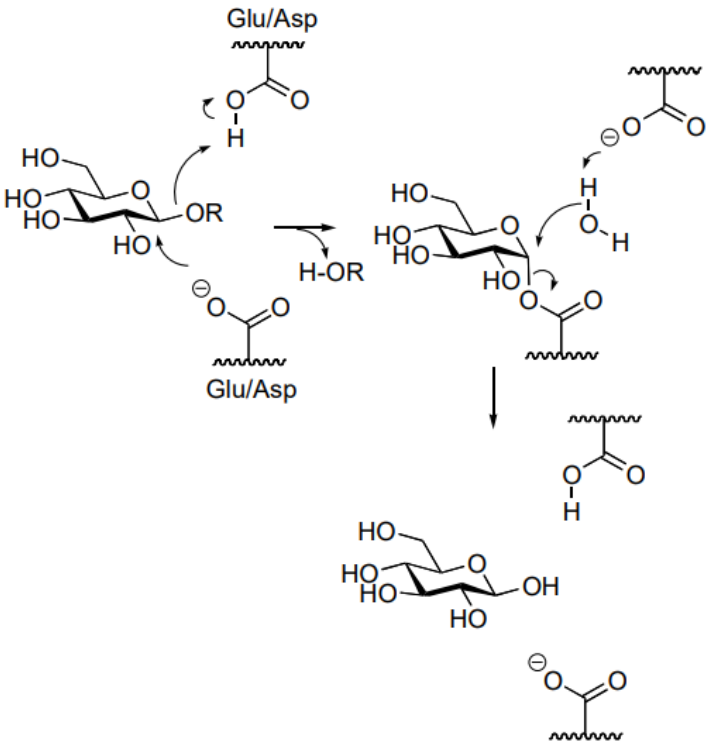

Figure 6: Catalytic mechanism underlying GH3 and GH5 glycosidases. A nucleophilic attack of a catalytic acid leads to a covalent acylal intermediate. Subsequently, the acylal is cleaved by hydrolysis (adapted from Li *et al.*).[32]

Thus, it is not surprising that covalent inhibitors utilizing this mechanism are also known. A prominent example is Cyclophellitol which was isolated in 1990 by Atsumi *et al*.[4] Cyclophellitol is a covalent β-glucosidase inhibitor from *Phellinus* sp.. Also already in 1990, the first synthesis of this natural product from L-glucose was reported. Cyclophellitol's inhibitory potency stems from its structural homology to glucopyranose.[5,32] Consequently, β-glucosidases are inhibited by Cyclophellitol via irreversible binding to one of the two essential catalytic acids by forming a stable ester instead of the acylal intermediate (Fig. 7).

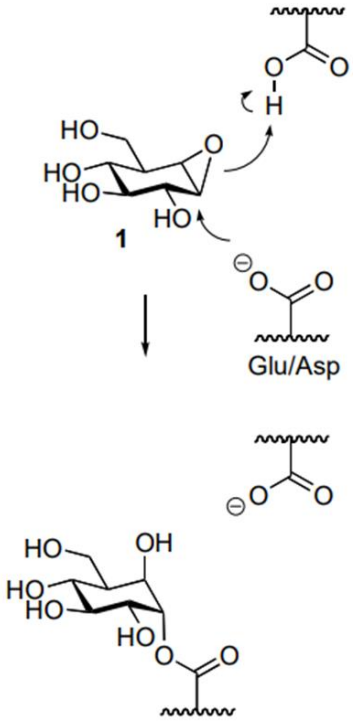

Figure 7: Inhibitory mechanism of Cyclophellitol. Cyclophellitol (**1**) binds covalently to one of the two catalytic acids and thereby forms a stable ester moiety which can no longer be hydrolyzed by water addition (adapted from Li *et al.*).[32]

In the last years, Overkleeft and co-workers explored Cyclophellitol-based glucosidase inhibitors and developed a whole suite of glycosidase ABPs based on this inhibitory motif.[33]To this end, they made several modifications to the native Cyclophellitol scaffold. For example, they synthesized derivatives in which the epoxide was replaced by an aziridine moiety or they performed stereochemical variations of the hydroxyl groups to improve their inhibitory and labelling potential or to enlarge their glycosidase target spectrum (Fig. 8).

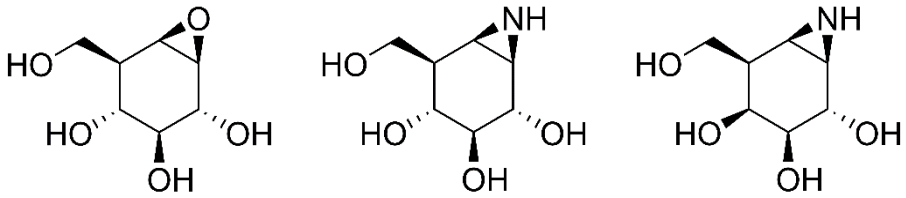

Figure 8: Structure of Cyclophellitol and specific derivatives Cyclophellitol (left) is a natural glucosidase inhibitor. Inhibitory potency was enhanced by substitution of the epoxide with an aziridne (middle). Moreover, the stereochemistry of the hydroxy groups can be altered to improve specificity against different glycosidases. For example, the right molecule is more selective for galactosidases compared to glucosidases.

Accordingly, the Overkleeft group developed many different ABPs that can be used to screen and annotate glycosidases. For example, van der Hoorn and co-workers identified more than 20 glycosidases in *Arabidopsis thaliana* using a single glycosidase probe.[31] In this PhD thesis, such ABPs were used for a glycosidase screening in *P. chrysosporium* (Fig. 9). The used glycosidase ABP was thereby configured to target

β-exo-glucosidases. As a reporter, a biotin tag was used which allows pull-down of targeted enzymes and subsequent identification by MS.

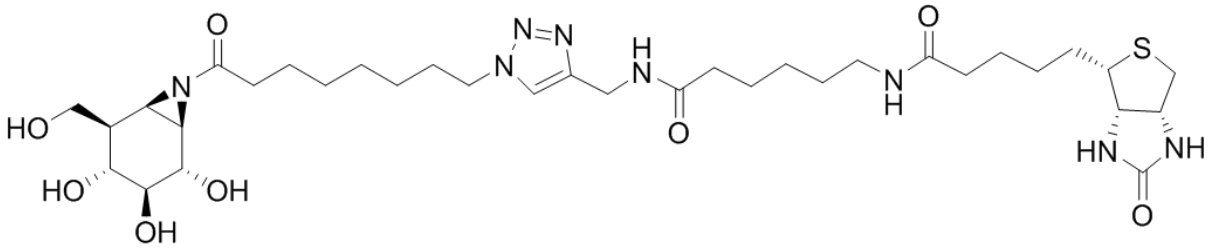

Figure 9: Exemplary structure of a glucosidase ABP based on a cyclophellitol-aziridine scaffold. The ABP displays a β-glucosidase-like warhead. The acyl-aziridine moiety improves labelling efficiency. For affinity enrichment, a biotin is attached to the probe. The probe was already used for glycosidase screening in *A. thaliana*.[31]

1.2 Activity-based Protein Profiling

ABPP is a powerful chemical proteomics approach to profile proteomes for active enzymes and can for example been used to screen for enzyme inhibitors or to annotate the function of unknown proteins.[6] To this end, covalent small molecule inhibitors frequently denoted as 'warheads' connected *via* a linker to a reporter moiety and known as ABPs are used. These ABPs label an enzyme by forming a covalent bond with an amino acid within its active center. Therefore, most synthesized probes are electrophiles that react with nucleophilic 'active' amino acid residues in the active site. Many of the used warheads are based on long-known inhibitors, for example the fluorophosphonate moiety, which inhibits active serine hydrolases (SHs). Naturally, a suitable chemical derivatization of these inhibitors may affect their binding properties and thus target spectrum and ABPs thus differ from their target selectivity: There are specific and broadband ABPs known (Fig. 10).

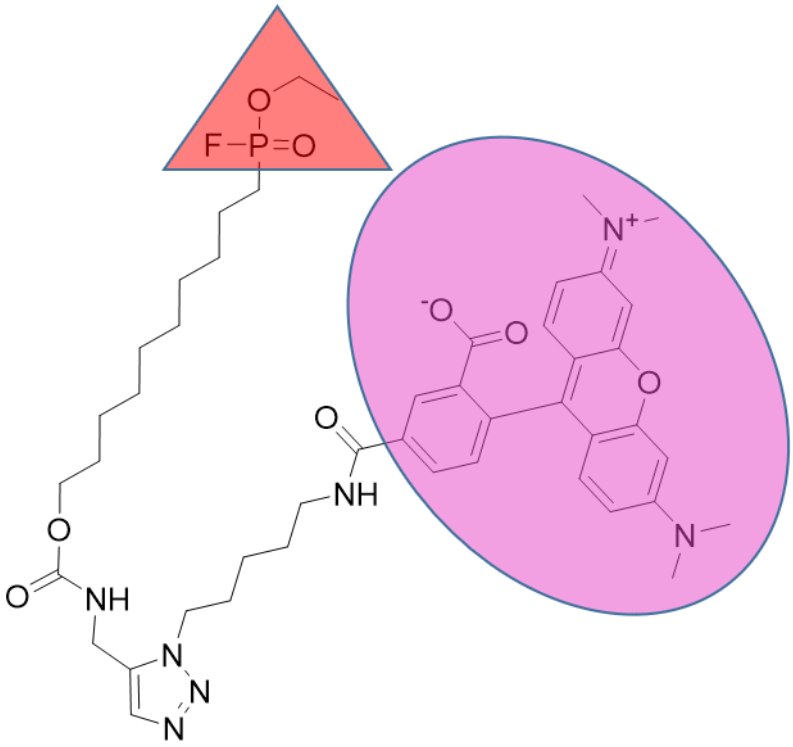

Figure 10: Structure of a FP-Rh probe. This probe was synthesized in-house. FP-Rh features a fluorophosphonate (FP)-warhead (red triangle) which targets SHs. The warhead is connected to a Rhodamine (Rh, pink circle) residue by a carbon-triazole linker which is utilized as a reporter group.

Besides the warheads, an ABP also features a linker and a reporter moiety. The linker is often an inert carbon chain (e.g. a polyethylene glycol residue). Nevertheless, the linker has important properties as it is important to assure the solubility or bioavailability of the probe (e.g. for passing biological membranes). In addition, it serves to prevent steric hindrance between the warhead and the reporter group, thus improving labelling potency. Finally, ABPs furthermore possess a reporter group for monitoring probe labelling. This can be a fluorophore which can be used to directly visualize enzyme activity *via* a gel-based analysis. A use of various ABPs with different fluorophores targeting similar enzymes or enzyme families can even be used to determine target specificity. However, an even more powerful tool is an ABP that carries an affinity tag like biotin instead of a fluorophore. These probes can be utilized to enrich labelled proteins and to identify them by MS.

The first ABP was reported in 1999 by Liu *et al.*[6,7] Its warhead is a derivative of Diisofluorophosphonate that was linked to a carbon chain and a biotin moiety for affinity enrichment. This probe was named FP-biotin and was a milestone in the development of ABPP as this single probe is highly versatile and can be used to screen for SHs under many conditions, e.g. from crude extracts of different cell lines, tissues or even complete organisms in a straightforward and simple manner. Moreover, this seminal

study also pointed out a particular strength of ABPP: ABPP does not 'simply' quantify protein expression levels but it quantifies enzyme activity, which makes this approach complementary to other methodologies that are able to measure protein abundance.

Since this original publication, ABPP has strongly emerged.[34-36] In the last two decades, many alternative ABPs, workflows and the combination of ABPP with MS approaches (cf. section 1.3.2) have led to new applications in the field of molecular and chemical biology. One of the main improvements was thereby the introduction of an alkyne or azide moiety as a reporter group. These groups can be used in 'click chemistry' approaches and facilitate *in vivo* ABPP, i.e. the use of ABPP in living systems. This is achieved by a 2-step ABPP methodology. As fluorophores and other reporter tags such as biotin are very bulky groups with low membrane permeability, most ABPs cannot be used directly in living systems. ABPs with the two possible click moieties are however much smaller and can more easily pass membranes and thus allow *in vivo* ABPP. After in vivo labelling, labelled enzymes can then be detected by a second step (i.e. 2-step ABPP) in which a reporter moiety is attached to the labelled enzyme by a biorthogonal chemical reaction such as a Cu(I)-catalyzed Huisgen's azide-alkyne cycloaddition (Fig. 11).

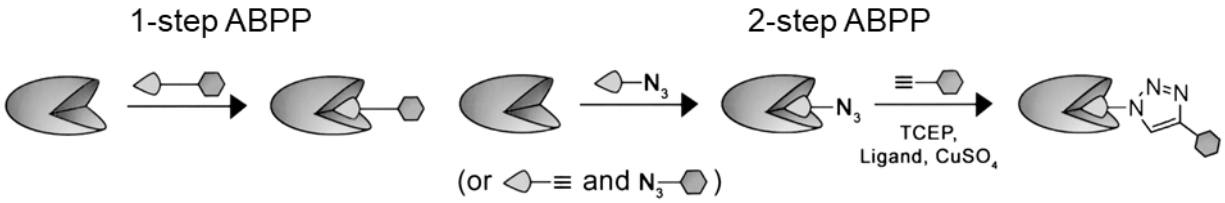

Figure 11: Schematic illustration of 1-step and 2-step ABPP. In 1-step ABPP, ABPs directly carry the used reporter group. Accordingly, labelled proteins are directly identified by the reporter group (hexagon) after labelling. In contrast, 2-step ABPP utilizes smaller probes. These probes consist of the warhead (triangle) and an alkyne or azide moiety as a small reporter group. After labelling, these reporter groups are modified with the final reporter, e.g. via a click reaction, for downstream analysis. TCEP: Tris(2-carboxyethyl)phosphine, Ligand: Tris[(1-benzyl-1H-1,2,3-triazol-4-yl)methyl]amine) (adapted by Speers *et al.*).[36]

Besides comparative ABPP in which ABPs are used to display enzymatic activity states of different physiological states, competitive ABPP is another application that allows to screen for small molecule inhibitors (competitors) of enzymes directly in a complex proteome background.[37-39] Moreover, the use of a characterized inhibitor in a competitive ABPP can be used to validate protein identifications from an ABPP approach as well as to identify off-targets and cross-reactivity of an ABP. In brief, pre-treatment of a sample or tissue with a competitor will outcompete labelling from an ABP as competitors will occupy the binding sites of the ABPs. Accordingly, a comparison of the band patterns and their intensities after application of a

characterized (i.e. target-specific) inhibitor can validate a labelled enzyme as a member of a distinct enzyme family or reveal ABP off-targets.

Finally, workflows for an efficient combination of MS-based target identification and ABPP have been developed in the last years (cf. section1 .3.2).[40,41] To this end, one methodological approach was the development of so-called 'trifunctional' ABPs.[25] These probes consist of a warhead and two reporter groups, most frequently a fluorophore for visual analysis in a gel after labelling and a second tag, e.g. an alkyne or azide moiety, for protein enrichment and thus MS analysis after click chemistry-mediated attachment of a biotin moiety.

1.3 Protein Mass Spectrometry

Mass spectrometry (MS) has evolved into an irreplaceable tool to identify and characterize proteins, either from 'pure' compounds after protein purifications or from proteomes.

MS-based protein identifications can thereby be achieved from native proteins (top-down approach) or after a controlled protein digest that delivers unique peptides for analysis (bottom-up approach).[42-44] As the bottom-up approach enables an easy implementation of high-throughput (HTP)-methods, it is by far the most used approach today. Major advances in this approach were for example done by Fenn and Tanaka (Nobel Prize 2002).[45-48] They introduced electro spray ionization (ESI) to analyze biological macromolecules. Another milestone of protein MS was the invention of the 'orbitrap' detector and online coupling to liquid chromatography (LC)-systems by Makarov and co-workers,[49] which facilitated the analysis of complex protein samples by a prior LC-separation as a second separation dimension as well as an improved analysis by a high mass precision. Although the technical advances in the development of orbitrap detectors or coupled LC systems is still ongoing, these technical advances turned ESI-Orbitrap-protein analysis into an accessible, useful and affordable tool for many molecular biology research applications.[50,51] The broad availability of MS data led to the need of efficient methodologies for computer-based analysis of the hundreds of thousands MS spectra that accrue during MS analysis. This resulted in the new field of algorithm-based protein MS analysis.[52-55] Besides many other methods, Mann and Cox developed a user friendly algorithm for data analysis that significantly simplified protein MS analysis from sample preparation to protein identification up to a level that MS analyses can now be prepared without a detailed knowledge of each methodical

step. All these developments finally enabled to analyze full proteomes of an organism in a straight-forward fashion. Indeed, the field of proteomics is nowadays strongly dominated by MS-based analyses.

To identify proteins by MS (in bottom-up approaches), their peptides and fragments have to match to *in silico* derived MS spectra. To this end, two main features of the MS spectra are used: First, mass accuracy on the peptide level (MS^1) and second, fragmentation patterns of the peptides (MS^2, Fig. 12).

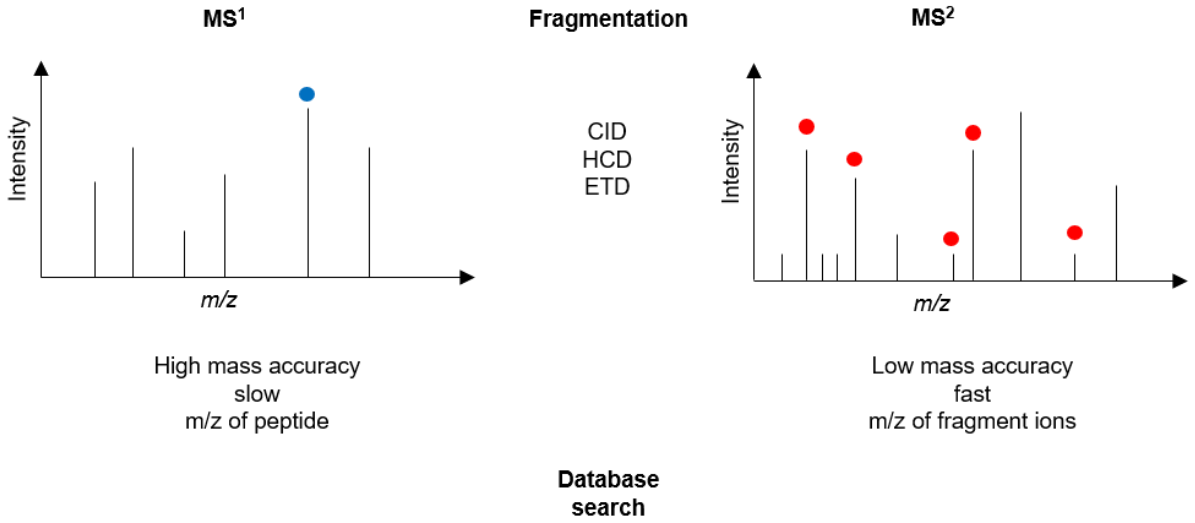

Figure 12: Schematic overview of peptide identification by MS. Peptides are ionized by ESI and enter the MS. On the MS^1-level, the peptide *m/z* is measured with high mass accuracy. A distinct peptide is picked for MS^2 (blue dot). Subsequently, peptides are fragmented (by indicated methods) into specific fragment ions (red dots). Spectra of fragment ions are compared to *in silico* generated fragment patterns (database search). Comparison of these patterns leads to a score which represents the accuracy of the peptide sequence. By involving further parameters like MS^1 signal intensity, retention time and other computational methods, more information, for example on post-translational modifications or relative peptide quantification, is gathered.

Protein MS is and remains a highly dynamic field and new recent developments such as methodologies to efficiently measure post-translational modifications (PTMs), protein localization or involvements of proteins in protein-protein interactions continuously arise.[43,44]

1.3.1 Full proteome analysis

One of the most often used protein MS analyses is to identify as many proteins as possible from a single multiprotein sample. This method is named full proteome analysis. To this end, a protein sample is for example gained by cell or tissue lysis and subsequent protein precipitation. Such pre-purified proteins are then subjected to MS sample preparation which mainly consists of protein digestion and desalting. MS spectra of the samples are then acquired, allowing proteins identification *via* suitable algorithms. Finally, the resulting protein identifications are statistically evaluated, allowing (in certain cases) to obtain relative protein abundances in a statistically significant manner. For example, in 2008 Godoy *et al.* reported the first identification of the entire yeast proteome. [56-60] Other research groups determined the complete proteomes of human cell lines. Along these lines, about 10 years ago, the human proteome project was launched, aiming to characterize all of the more than 20,000 gene products. With these data in hand, one can for example better investigate the effect of bioactive natural products. The depth of the analysis can be improved by sample preparation methods like fractionation or enrichment of specific PTMs.[61,62] Moreover, an annotation of identified proteins with its function or localization enables the elucidation of compound-affected cellular processes or pathways. From a clinical point view, such analyses may also be valuable for studying drug side-effects or characterizing new drugs.[23]

1.3.2 Protein MS analysis of ABPP-derived samples

Sample preparation is an important step for a successful protein MS analysis. There exist two main workflows for preparing ABP-labelled proteins for MS analysis.

The first approach is known as ‘in-gel-digestion’ (IGD).[63,64] In this approach, ABP-labelled proteins are first separated by gel-electrophoresis. Bands of interest are then cut-out from the gel and the corresponding gel sections are washed, followed by addition of a protease, for example trypsin, to initiate sample digestion. The resulting peptides dissociate from the gel matrix and can then be analyzed by MS after a desalting of the sample.

Another method is the ‘on-bead-digest’ (OBD).[35,65] Here, samples are not separated in a gel but bead-captured proteins (e.g. via a biotin-modified ABP and an avidin-coated bead) are directly digested on the beads and subsequently analyzed.

Both methods have their advantages and drawbacks. Pre-separation by gel-electrophoresis leads to a less complex sample, which facilitates protein identification. However, IGD also leads to less concentrated samples, making the identification of low abundant proteins difficult. For OBD analysis, proteins have to be captured on beads, for example by biotin-streptavidin interactions. This introduces intrinsic biases as biotin is an endogenous co-factor of proteins. Moreover, OBD produces massive digestion side products (peptides derived from streptavidin) that can interfere with protein identification.[6] Today, these disadvantages of OBD are becoming less relevant by instrumentation improvements such as higher spectral resolution, throughput and sensitivity, which all lead to a higher accuracy of protein identification. Thus, OBD is nowadays for most applications the preferred method.

1.4 *Phanerochaete chrysosporium* and wood degradation

P. chrysosporium is a fungus that belongs to the basidiomycotica (subkingdom dikarya or 'higher fungi').[66,67] As all basidiomycota, *P. chrysosporium* forms hyphae. Macroscopically, *P. chrysosporium* forms crust-like fruit bodies. Furthermore, *P. chrysosporium* is a saprophyte, i.e. it metabolizes decayed organic matter.

Many members of the genus *Phanerochaete* are able to degrade wood and other dead plant biomass.[68,69] Accordingly, *P. chrysosporium* are classified as white-rot fungi; these are fungi that are able to completely breakdown dead organic matter such as wood via lignin, cellulose and hemicellulose metabolization. In contrast, soft- or brown-rot fungi such as for example *Aspergillus* can only metabolize cellulose and hemicellulose. In contrast, *P. chrysosporium* can degrade lignin to carbon dioxide. To this end, *Phanerochaete* expresses lytic polysaccharide monooxygenases (LPMOs) and other ligninases.[67] These essential lignin breakdown enzymes have been thoroughly characterized in the last years.[70,71] In addition to lignin-degradation, *P. chrysosporium* is also able to degrade other wood polymers like cellulose and hemicellulose.[72,73] In contrast to cellulose that is a simple polymer of β-1,4-connected glucose monomers, Hemicellulose is a much more complex heteropolymer and consists of different sugar monomers and branches. Hemicellulose contains sugars such as xylose and arabinose as well as pentoses, galactose and mannose. Moreover, it was shown that hydroxyl groups of different sugars are acetylated to protect hemicellulose against hydrolysis (Fig. 13).

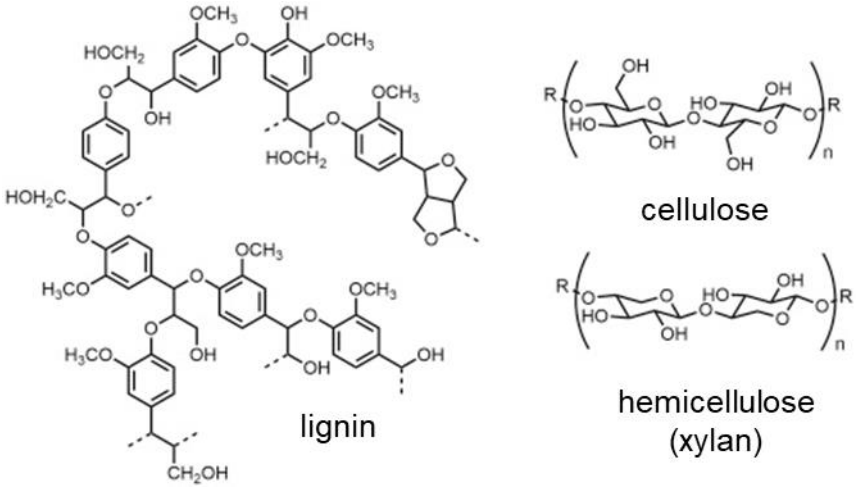

Figure 13: Polymers of wood. Wood consists of lignin, cellulose and hemicellulose. Lignin is a polymer of phenol derivatives. In contrast, cellulose and hemicellulose are built from different sugar monomers. Cellulose is chemically less complex as it is built from glucose monomers which are 1-4 β-linked. Hemicellulose however has a much higher complexity and consists of different sugars, various forms of glycosidic linkages, branches and hydroxyl group acetylations (not shown here, adapted by Kazmi *et al.*).[74]

To degrade cellulose and hemicellulose polymers by glycosidases, these acetylations have first to be removed. Overall, a full wood degradation requires a combined attack from different enzyme classes.[75,76]

P. chryspsorium is also a thermophilic fungus.[66] Its growth optimum is about 40 °C. However, it is able to grow in the range from 20 °C up to 60 °C. Thus, its enzymes reveal heat stability. In 2004, Martinez and co-workers published the full genome of *P. chrysosporium strain RP78*.[77] Today, the genome and corresponding proteome is curated by the Joint Genome Institute (JGI).[78] The availability of genome and proteome sequences are essential for using MS approaches. Additionally, homology analyses indicate the presence of numerous interesting gene products for (Hemi-)cellulose degradation in *P. chrysosporium*. However, only a handful of such enzymes are characterized so far.

The ability of *P. chrysosporium* to completely breakdown wood and its heat stability turns *P. chrysosporium* into a promising organism for identifying biotechnologically useful enzymes.[79] For example, *P. chrysosporium* was shown to be able to metabolize polycyclic aromatic hydrocarbons.[80] In this PhD work, wood degrading hydrolases of *P. chrysosporium* were therefore investigated, using an ABPP approach as such hydrolases could be promising candidates for biotechnological applications, e.g. in the paper industries or for bioethanol production.[81,82]

2 Aim

This work aims to demonstrate the generic applicability of MS-driven methodologies for basic chemical biology research. To this end, two different topics will be addressed. In the first part of the thesis, the bioactivity of Zelkovamycin in eukaryotic cells will be investigated. In the second part, a hydrolase screening of *P. chrysosporium* via the MS-based chemical proteomics methodology ABPP will be performed.

Zelkovamycin, which was recently shown to be member of the argyrin family, is a moderate antibiotic. Recent studies by Krahn however showed that it also displays a bioactivity in human cancer cell lines. In the present thesis, the bioactivity of Zelkovamycin in different human cancer cell lines should therefore be studied. To this end, unbiased MS-analysis in conjunction with other biochemical and biological methodologies should be used to characterize Zelkovamycin's bioactivity in human cancer cell lines. Moreover, insights into the underlying structure-activity relationships (SAR) should be obtained.

In the second part of this work, a hydrolase-screening of *P. chrysosporium* should be performed. Due to the ability of *P. chrysosporium* to completely degrade wood in conjunction with its heat stability, this organism is a promising source for identifying novel hydrolases for biotechnological applications. To elucidate these promising enzymes, the chemical proteomics methodology ABPP in combination with subsequent MS-analysis should be used. Of note, until now, the use of ABPP approaches for identifying enzymes for biotechnology is a rather novel approach and with fungi, ABPP has been used so far only once.

3 Material and Methods

Chemicals, consumables, devices and software are listed in the appendix (appendix section 8.4).

3.1 Buffer composition

Table 1: Composition of buffers.

Buffer/Medium	Composition
Blotting buffer	100 mL 10× SDS-running buffer 200 mL MS-MeOH 700 mL MS-H_2O
Colloidal Coomassie	100 g ammonium sulfate 20 mL 5% Coomasie G-250 30 mL 85% ortho-phosphoric acid 20 mL EtOH *ad* 1000 mL MS-H_2O
MOPS, 20×	MOPS 104.6 g TrisBase 60.6 g SDS 10.0 g EDTA*2•H_2O 3.8 g *ad* 500 mL MS-H_2O
PBS, 10×	1.6 M NaCl 30 mM Na_2HPO_4 10.6 mM KH_2PO_4 pH 7.4 *ad* 1000 mL MS-H_2O
SDS-running bufffer, 10×	TrisBase 30 g SDS 1 g Glycin 144 g *ad* 1000 mLMS-H_2O
Sypro Ruby fixing buffer	10% MeOH 7% acetic acid *ad* 1000 mLMS-H_2O
Sypro Ruby washing bufer	50% MeOH *ad* 1000 mL MS-H_2O
TBS, 10×	Tris-Base 24.2 g NaCl 87.7 g add 800 mL MS-H_2O adjust pH to 7.5 with 37% HCl *ad* 1000 mL MS-H_2O

3.2 Kits

3.2.1 Activity assays

Lactate activity assay	Abnova, #KA3776 Version 02
Pyruvate Dehydrogenase activity assay	Sigma-Aldrich®, #MK183
Phosphofructokinase activity assay	Sigma-Aldrich®, #MAK093

MitoTox™ Complete OXPHOS Activity Assay Kit Abcam, #ab110419

3.2.2 Western blot

SuperSignal™ West Femto Maximum Sensitivity Substrate
Thermo Fisher, #34094

SuperSignal™ West Pico PLUS Chemiluminescent Substrate
Thermo Fisher, #34557

3.3 Organisms

3.3.1 Cell lines

HeLa and SH-SY5Y cell lines were a gift from AG Ehrmann (University of Duisburg-Essen).

3.3.2 Fungi

P. chrysosporium and *R. emersonii* were obtained from the AG Begerow (Ruhr-University, Bochum) and were cultured by the AG Siebers (University of Duisburg-Essen).

3.4 Culturing methods

3.4.1 Culturing of cancer cell lines

HeLa cells were cultured using Dulbecco's Modified Eagle's Medium (DMEM) at 37 °C (5% CO_2). DMEM was supplemented with 10% fetal bovine serum (FBS) and 1% Penicillin/Streptomycin (Pen/Strep). Cells were splitted every two to three days and discarded after a maximum of 25 passages.

SH-SY5Y cells were cultured in DMEM/F12 at 37 °C (5% CO_2). DMEM/F12 was supplemented with 10% FBS and 1% Pen/Strep. Cells were splitted every three to four days and discarded after a maximum of 15 passages.

For some assays, cells were seeded one day before execution of the assay. In these cases, cells were seeded at a confluency of about 80%. Before the grown cells were further treated, they were washed twice with Phosphate-buffered saline (PBS).

To elucidate the effects of Zelkovamycin towards glucose-deprived (low glucose medium) cells, the corresponding cells were seeded in low glucose DMEM and grown for at least 16 h.

3.4.2 Culturing of fungi

P. chrysosporium was cultured by Christian Schmerling (AG Siebers, University of Duisburg-Essen). In brief, MYP-agar dishes (50 µg/mL Chloramphenicol) were inoculated with *P. chrysosporium* glycerol stocks and grown for two days at 37 °C. These cultures were maintained for a maximum of two weeks at RT. From these agar dishes, *P. chrysosporium* was inoculated into the indicated liquid media (supplemented with 50 µg/mL Chloramphenicol). Fungi were grown in minimal medium (containing different carbon sources) or MYP-medium for five days at 37 °C (shaking at 180 rpm). Minimal medium was supplemented with 40 g/L wood chips, Avicel 1% (microcrystalline cellulose, particle size = 50 µm) or 5 g/L Avocel (macroscopic cellulose fibers). The used wood chips and Avocel were autoclaved and dried before addition.

3.4.3 Secretome purification

To remove fungal cell bodies and carbon substrates prior to labelling, cultures were decanted into fresh tubes. The cell culture medium was centrifuged 15 min at full speed. The supernatant was transferred into a 20 mL syringe (attached to a small injection needle) and filtrated by 0.2 µm filtration membranes to remove residual cell bodies or carbon substrates. Finally, 2, 5 or 50 mL aliquots of purified secretomes were freeze-dried. The resulting ‘secretome-powder’ was stored at -20 °C until analysis. However, for initial experiments secretomes were purified by molecular weight cut-off filters (MWCO). In brief, 2 mL of *P. chrysosporium* cell culture supernatant (prepared as described above without freeze-drying) was transferred into 5 kDa cut-off devices and centrifuged for 20 minutes at 14,000 ×g. Secretome-concentrates were washed at least three times with 500 µL of 50 mM Na_2HPO_4 (pH 8).

3.5 Biochemical assays

3.5.1 Cell viability assay

In order to elucidate cell viability, HeLa (1.4×10^4 cells/well) or SH-SY5Y (1.6×10^4 cells/well) cells were seeded in 96-well plates and cultured overnight (37 °C, 5% CO_2). Cells were treated with indicated compounds. After indicated time points, 25 µL of MTT reagent (Blue Tetrazolium Bromide, 5 mg/mL in PBS) were added to each well and incubated for 3 h. Subsequently, culture medium and MTT were added. For cell lysis, 100 µL of 20% SDS (1:1 Dimethylformamide/Water, pH 4.7) were added and incubated for at least 3 h. Lastly, the absorbance of the reduced MTT reagent (blue/purple) was

quantified using a microplate reader via measurement of absorption at a wavelength of 570 nm. Raw data were transformed and analyzed as described in section 3.8.2.

3.5.2 Extracellular acidification

Cells were cultured as described above (3.5.1) and treated with indicated compounds. Extracellular acidification was determined via UV absorbance measurements at a Tecan Spark 10 M using default settings at the maximum of the pH indicator phenol red, i.e. 550 nm. As a reference, absorbance at 425 nm was also measured. The ratio of 550/425 nm was calculated for further analysis. Raw data were transformed and analyzed as in section 3.8.2.

3.5.3 Lactate activity assay

Extracellular lactate levels were quantified using a Lactate activity assay kit (Abnova, #KA3776 Version 02). To this end, HeLa and SH-SY5Y cells (0.1× 10^6 cells/well) were seeded in 12-well plates and cultured overnight. Cells were treated with indicated compounds. After indicated time points,100 µL of cell culture medium was transferred to fresh tubes and snap frozen. Aliquots were stored at -20 °C. Cell culture medium samples were diluted 100× with water. Lactate concentration was measured according to the manufacturer's instructions using fluorescence detection (Ex530/Em585 nm) at a Tecan Spark 10 M plate reader. Raw data were transformed and analyzed as described in section 3.8.2.

3.5.4 Pyruvate Dehydrogenase activity assay

For biochemical activity determinations of the mitochondrial Pyruvate Dehydrogenase (PDH), SH-SY5Y cells (0.3× 10^6 cells/well) were cultured in 6-well plates as described above. After indicated time-points, cells were detached by a cell scraper using 500 µL of PBS (+ 1× Protease-Inhibitor). Cells were transferred to fresh tubes, lyzed by sonication and samples were prepared and measured as described in the manufacturer's instructions (Sigma-Aldrich®, #MK183). The resulting raw data were transformed and analyzed as described in section 3.8.2.

3.5.5 Phosphofructokinase activity assay

In order to elucidate glycolytic activity in HeLa cells, Phosphofructokinase (PFK) activity was measured by a colorimetric assay kit (Sigma-Aldrich®, #MAK093). To this end, HeLa cells (0.3× 10^6) were cultured in 6-well microplates as described before. After indicated time-points, cells were detached by a cell scraper using 500 µL of PBS (+ 1× Protease-Inhibitor). Cells were transferred to fresh tubes, lyzed by sonication and

samples were prepared and measured with the help of the PFK assay kit as described in the manufacturer's instructions. The resulting raw data were transformed and analyzed as described in section 3.8.2.

3.5.6 OXPHOS-activity assay

The effect of Zelkovamycin vs. specific OXPHOS complexes was tested using an OXPHOS activity assay kit (Abcam, #ab110419). The assay was performed according to the manufacturer's instructions. Zelkovamycin was used in 2-fold dilution series starting at 200 µM down to 0.39 µM, resulting in 9 samples with different concentrations. As positive controls, manufacturer's instructions recommended complex inhibitors were used. The resulting read-outs were quantified using a Tecan Spark 10 M microplate reader as recommended by manufacturer's instructions and analyzed as described in section 3.8.2.

3.5.7 Oxygen consumption rate

Oxygen consumption rates of different cancer cell lines were measured using an extracellular flux analyzer (SeaHorse XFe96). These assays were performed by Felix Vogel (University Hospital Essen, AG Roesch) using the following conditions.

To functionally and physiologically analyze the effect of the drug on mitochondrial metabolism, real time metabolic analyses of the oxygen consumption rate (OCR) and extracellular acidification rate (ECAR) were performed on a SeaHorse XFe96 extracellular flux analyzer (Agilent Technologies). In brief, cell number optimization experiments were first performed to determine appropriate cell densities as required for the experimental conditions. Based on this, 15,000 WM3734 cells, 15,000 HeLa cells or 50,000 SH-SY5Y cells were seeded per well of a XFe96 V3 PS tissue culture microplate one day prior to the experiment and incubated overnight at 37 °C in presence of 5% CO_2. The cell culture medium was then replaced by Agilent Seahorse XF Base Medium supplemented with iso-osmolar concentrations of glucose, sodium pyruvate, and glutamine 1 h before assay read-out. At least 4-6 replicates (wells) were used per concentration or experimental condition. During the real time analysis, 3 baseline measurements were followed after the application of the drugs Zelkovamycin, argyrin B, ΔMeO-Zelkovamycin or reduced-Zelkovamycin and their direct effect on mitochondrial metabolism was documented over 18 measurements (≈ 108 min.). Finally, FCCP was applied to determine the maximal respiratory capacity of the cells (RRC) after incubation with the mentioned drugs and the effect on mitochondrial

metabolism was analyzed by 3 measurements. For data normalization to the actual cell numbers per well, cells were fixed overnight with 4% paraformaldehyde in PBS and stained with 4′,6-diamidino-2-phenylindole (DAPI). Fluorescence was measured on a Tecan Spark microplate reader. Data analysis and normalization to DAPI fluorescence was performed using the Seahorse XF Mito Fuel Flex Test Report Generator in the Wave Software (Agilent Technologies, Version 2.4.0.60).

3.5.8 Bradford assay

Protein concentrations were determined using a modified Bradford assay (Roti® Nanoquant) according to the manufacturer's instructions. In brief, lysates or secretomes were diluted 40- or 100-fold in de-ionized water. An aliquot of 50 µL of a 40- or 100-fold dilution was measured two times independently. Therefore, 50 µL of the dilution were transferred into 96-well plates. Subsequently, each sample was further diluted by addition of 200 µL of 1× Roti-Nanoquant (manufacturer' reagent) and the resulting absorbance was measured at 590 and 450 nm. Protein concentrations of the samples were obtained by correlation with a BSA standard solutions after also measured at 590 and 450 nm. To this end, the ratio of 590/450 nm of BSA standard solutions were fitted by a linear equation. The calculated equation was used to interpolate protein concentrations of unknown samples.

3.5.9 Glycosidase and esterase activity

The corresponding assays were performed by Christian Schmerling (AG Siebers, University of Duisburg-Essen). In brief, for glycosidase activity quantification, 3,5-Dinitrosalicylsäure (DNSA) was utilized as a chromogenic substrate. Carboxymethyl cellulose solution (0.5%) was incubated with secretomes of *P. chrysosporium*. Subsequently, the DNSA reagent was added and the reducing end concentration was determined by measurement of the absorbance at 540 nm. These values were correlated with the measurements from a glucose standard solution.

In order to analyze esterase activity, *para*-nitrophenol acetate (pNPAc) was used as an artificial chromogenic substrate, which is commonly used for activity determinations of acetyl-xylan esterases.[83] Purified protein was incubated with pNPAc and the release of para-Nitrophenol was continuously measured at 410 nm ($e = 1200\ M^{-1}\ cm^{-1}$). Initial reaction velocities were taken and used to calculate the specific activity for the reaction. Optimal activity was observed at 40°C and pH 7.

3.6 Activity-based protein profiling

3.6.1 Gel-based analysis of *P. chrysosporium* secretomes

For gel-based analysis, 2 mL of freeze-dried secretomes (section 3.4.3) were diluted in 100 µL of 50 mM Na_2HPO_4 buffer (pH 8) for FP labelling or 50 mM NaOAc buffer (pH 5) for glycosidase labelling. The protein concentrations of the different samples were determined by a Bradford assay (section 3.5.8) and samples were diluted to a concentration of 15 µg in 100 µL of the indicated buffer. ABPs were used at a concentration of 2 µM. Labelling was performed at 37 °C for 1 h. When indicated, labelling was competed with inhibitors at the given concentrations for 30 min at 37 °C. FP-alkyne labelled proteins were clicked to the Tri-azide tag using the following conditions: The following compounds were added in the given order: 2 µL 0.5 mM Tri-azide tag, 2 µL 5 mM Tris(benzyltriazolylmethyl)amine (TBTA), 2 µL 100 mM Tris(2-carboxyethyl)phosphine (TCEP) and 2 µL 50 mM $CuSO_4$. The resulting solutions were mixed and incubated for 1 h at RT in the dark. The reaction was stopped by adding 3× volume of 4× LDS (100 mM Dithiothreitol (DTT)) and samples were heated to 70 °C for 15 minutes. An equivalent of 2-5 µg was loaded onto a 11% SDS gel and proteins were separated for 1.5 h at 120 V/55 mA. Labelled proteins were visualized by a Typhoon FLA 9000 imager. For FP labelling, the Cy3-channel (532 nm) and for glycosidase labelling, the Cy2-channel (473 nm) were used. Images were edited to enhance contrast using Adobe Photoshop. Gels were stained by colloidal Coomassie overnight and destained using 10% acetic acid for at least 30 min. Gels were visualized using the Intas GelDoc (exposure 15 – 30 ms) system.

3.6.2 Large scale labelling for target identification

To identify targets of FP and glycosidase probes, secretomes were labelled on a large scale. To this end, 50 mL of freeze-dried secretomes (described in 3.4.3) were diluted in 2 mL of indicated buffers (section 3.6.1) and the resulting protein concentrations of the samples were determined by a Bradford assay (section 3.5.8). Samples were diluted to 400 µg protein in 2 mL of indicated buffers. Labelling with FP or glycosidase probe was performed as described above (section 3.6.1) via adapting the volumes of the different reagents to a reaction volume of 2 mL.

After labelling, proteins were precipitated. For FP-treated samples, proteins were precipitated with ¼ volumes of trichloroacetic acid (TCA) at 4 °C overnight, while for glycosidase probe-treated samples, proteins were precipitated by addition of 4× volumes MeOH at -20 °C overnight. The resulting suspensions were centrifuged for 15

min at 4 °C at full speed and supernatants were aspirated. Protein pellets were washed with acetone or MeOH for 10 min at -20 °C and were centrifuged as before. Protein pellets were resuspended in 8 mL 0.2% SDS and 100 µL of pre-equilibrated avidin beads (50 µL bead-slurry per sample) were added and the resulting samples were incubated for 1 h while slowly rotating. The samples were centrifuged at 400× g for 3 min and the supernatant was discarded. For washing, 10 mL 0.2% SDS was added to each sample and incubated for 10 min while slowly rotating. The supernatant was aspirated again and this overall washing procedure was repeated five times. The beads were transferred to low-binding tubes. A small aliquot (about 10 µL) of the beads was boiled at 70 °C for 15 min in 2× LDS and subjected to SDS-gel and Western Blot analysis to control a proper affinity enrichment (section 3.6.3). Finally, the samples were washed three times with MS water to remove residual SDS and the dried bead-pellets were stored at 4 °C.

3.6.3 Western Blot analysis

To check labelling with biotinylated probes, labelled proteins were visualized using Streptavidin-Horseradish Peroxidase (HRP). Accordingly, proteins were blotted onto a nitrocellulose membrane after gel electrophoresis. To this end, the nitrocellulose membrane was prior activated with MeOH for at least 5 minutes and all components of the western blot cassette were equilibrated wit SDS running buffer for at least 5 minutes. The gel and the western blot cassette were assembled and placed into the blotting chamber. Proteins were blotted at 110 V/500 mA and the blotting buffer solution was cooled using an ice-pack. The nitrocellulose membrane was washed three times with 25 mL TBS-T (1×TBS + 2% Tween-20) for 10 minutes and blotted proteins were blocked by 3% BSA (in TBS-T) overnight at 4 °C or for 1 h at RT. The membrane was washed three times with 25 mL TBS-T for 10 minutes. For staining, 25 mL TBS-T with Streptavidin-HRP (1:10000) were added to the membrane and incubated for 1 h at RT. The membrane was washed three times with 25 mL TBS-T for 10 minutes. Biotinylated proteins were visualized by chemiluminescence using SuperSignal™ West Pico PLUS Chemiluminescent Substrate and SuperSignal™ West Femto Maximum Sensitivity Substrate according to the manufacturer's instructions. Chemiluminescence was read-out using an Amersham AI600 imager (GE Healthcare).

3.6.4 Growth time-dependent labelling

For analysis of growth time-dependent secretome labelling, *P. chrysosporium* was cultured up to 12 days. Each day an aliquot of 5 mL was taken out from the culture and secretomes were prepared as described in section 3.4.3. The corresponding secretomes were labelled as described in section 3.6.1.

3.6.5 Temperature-dependent labelling

To evaluate the heat stability of the investigated esterases and glycosidases, pre-heated secretomes were subjected to labelling (section 3.6.1). To this end, 2 mL aliquots of secretomes were prepared as described in 3.4.3. These secretomes were diluted in 100 µL of the corresponding buffers and heated for 15 min at indicated temperatures (20 – 80 °C). The samples were then cooled on ice and labelled as described in section 3.6.1.

3.6.6 On substrate labelling

To profile proteins via ABPP that were directly attached to oak wood chips, the following workflow was established: Oak wood chips (3 g from cultures grown for 5 days) were taken out from the culture and washed two times with 10 mL pure minimal medium. The wood chips were transferred into fresh tubes and covered with 3 mL of the corresponding buffers for esterase or glycosidase labelling. Labelling efficiency was determined as described before (section 3.6.1). To detach labelled proteins from the oak wood chips, the chips were heated up in 1 mL 1% SDS at 60 °C for 30 min. This treatment did not affect the integrity of residual fungal cells (validated by Christian Schmerling, AG Siebers, University of Duisburg-Essen) to prevent contamination of the samples with cellular proteins from the fungi. The samples were precipitated by addition of 4× volumes of MeOH (-20 °C, overnight). The resulting suspensions were centrifuged for 30 min at full speed (4 °C). The supernatants were discarded and the pellets were washed with ice-cold MeOH again. The protein pellets were solved in 30 µL 2× LDS (+100 mM DTT, heating up to 70 °C for 15 min). For further sample purifications, the solutions were shortly centrifuged and the supernatants were transferred to fresh tubes. The samples were subjected to gel electrophoresis analysis and visualized by a fluorescence scanner as described before (section 3.6.1). Equal protein loading was confirmed by the sensitive Sypro Ruby staining according to the manufacturer's instructions (rapid protocol).

3.7 Mass Spectrometry

3.7.1 In solution digest

To evaluate Zelkovamycin-induced proteome changes, cells were treated with 20 µM Zelkovamycin for 16 h at 37 °C. The cells were washed twice with PBS and harvested in 500 µL PBS using a cell scraper. The cells were lyzed by sonication (Bioruptor, 15 min, 1 min pulse, 30 sec pause, high voltage in ice water) and the resulting lysates were centrifuged for 30 min at 4 °C (full speed). The supernatants were transferred to fresh tubes and the protein concentrations of each sample were determined by a Bradford assay (section 3.5.8). An equivalent of 15 µg protein was taken for each sample and was precipitated by addition of 4× volumes of acetone overnight. Samples were spun for 30 min at full speed (4 °C) and the supernatant was discarded. To remove residual acetone, the protein pellet was air-dried for about 10 min. The protein pellet was resuspended in 25 µL 8 M Urea.

For secretome analysis of *P. chrysosporium*, an aliquot of 5 µL from a volume of 5 mL of the cell culture supernatant was subjected to a Bradford assay (section 3.5.8). An equivalent of 15 µg proteins was taken from the cell culture and precipitated by addition with ¼ volumes of TCA at 4 °C overnight. The resulting protein pellet was resuspended in 25 µL 8 M Urea (in 50 mM ammonium bicarbonate, ABC).

The samples were next treated with DTT for disulfide bond reduction. To this end, DTT was added to a final concentration of 5 mM and the resulting samples were incubated for 30 min at RT (shaking at 1000 rpm). The reduced samples were alkylated by adding iodoacetamide (IAM) to a final concentration of 20 mM and incubated for 30 min at 37 °C in the dark while shaking at 1000 rpm. The alkylation reaction was quenched by adding DTT to a final concentration of 25 mM. Proteins were pre-digested using Lys-C in a ratio of 1:30 (Lys-C:Protein) for at least 1 h. For the Trypsin digest, the resulting solution was diluted to 1 M Urea by adding 50 mM ABC. Trypsin was subsequently added in a ratio of 1:30 (Trypsin:Protein). The samples were digested overnight at 37 °C (shaking at 1000 rpm). After a minimum of 16 h, the samples were acidified by addition formic acid (FA) to a final concentration of 5% which stops the digestion reaction. The resulting samples were subjected to stage-tipping and prepared for MS analysis as described before.[55] Finally, dried peptide samples were diluted by addition of 10 µL 0.1% FA and 3 µL of these solutions were injected into the LC-MS/MS system.

3.7.2 On bead digest

To identify biotin-labelled proteins, samples were prepared for MS analysis after large scale labelling (section 3.6.2) via an on bead digest. To this end, 100 µL of 0.8 M Urea (in 50 mM ABC) were added to the dried beads. DTT was added to a final concentration of 5 mM for disulfide bond reduction in the samples and the samples were incubated for 30 min at 37 °C while shaking at 1500 rpm. The reduced samples were alkylated by adding IAM to a final concentration of 10 mM. The resulting suspensions were incubated for 30 min at 37 °C in the dark while shaking at 1500 rpm. The alkylation reactions were quenched by adding DTT to a final concentration of 10 mM. 1 µg of Trypsin were added to each sample and the resulting suspensions were shaken overnight at 37 °C at 1150 rpm. After a minimal period of 16 h, the samples were centrifuged for 5 min at 650 ×g to separate the beads from the peptide-containing supernatants. 80 µL of the peptide-containing supernatants were transferred to fresh tubes and the samples were acidified by adding 80 µL of 1% FA solution. The residual supernatants of the bead samples were also acidified by addition of 40 µL 1% FA and the resulting suspension was shaken for 5 min at 1150 rpm. The beads suspensions were centrifuged as described above and 60 µL of the peptide-containing supernatants were transferred and combined with first peptide-containing supernatants, resulting in 140 µL peptide solution for each sample. These peptide solutions were further filtered by glass microfiber stage-tips (2× disc, poresize: 1.2 µM). To this end, the glass microfiber stage-tips were pre-equilibrated with 0.5% FA. The peptide-containing supernatants were loaded onto the tips and centrifuged for 5 min at 100 ×g. The flow-throughs were subjected to stage-tipping for desalting as described before.[55] The resulting dried peptides were redissolved by addition of 15 µL 0.1% FA of which 5 µL were injected into the LC-MS/MS system.

3.7.3 MS Settings

Samples were separated online using ultra high pressure liquid chromatography (UHPLC) systems directly coupled to the mass spectrometers. The solvents used for UHPLC were of UHPLC grade (formerly Sigma, now Honeywell). Solvent A was 0.1% formic acid (FA) in water. Solvent B (Easy nLC 1000) was 0.1% FA in ACN or 0.1% FA in 80% ACN (Easy nLC 1200).

In this work, either an Orbitrap ELITE (with Tune Plus v2.7.) or an Orbitrap Fusion LUMOS (with Tune v3.3) mass spectrometer was used (both Thermo Fisher Scientific).

3.7.3.1 ELITE LC-MS/MS system

The Orbitrap Elite instrument was coupled online to an EASY-nLC 1000 UHPLC operating in the on-column mode (no trap column). Samples were measured as reported in Grosse-Holz *et al*.[84] Briefly, peptides were loaded onto the analytical column (fused silica capillary inner diameter = 75 µm × variable length, with an integrated PicoFrit emitter (New Objective) and packed in-house with Reprosil-Pur 120 C18-AQ 1.9 µm resin (Dr. Maisch)). Loading pressure was set to not exceed 980 bar which resulted in a flow of 0.5 – 0.8 µL/min (depending on the column length). The analytical column was encased by a column oven (Sonation) and the temperature during LC-MS data acquisition was set to 45 °C or 49°C. The analytical column was attached to a nanospray flex ion source (Thermo Fisher Scientific). For peptide separation the following gradient was run for 140 min at a flow rate of 300 nL/min (gradient: start with 7% B; gradient 7% to 35% B in 120 min; gradient 35% to 80% B in 10 min and 80% B for 10 min).

XCalibur software (version 2.2. SP1.48) was used to control the LC-MS runs. Ionization was set to positive mode. Precursors were scanned in the Orbitrap analyzer (FTMS; Fourier Transform Mass Spectrometry) in the scan range of *m/z* 300–1800 and at a resolution of 60,000. Polysiloxane (*m/z* = 445.120025) was set as internal lock mass. Fragment ions were acquired in data-dependent manner using a variable scan range at a rapid scan rate mode in the ion trap (ITMS) analyzer. The ionization potential was set to 1.8 kV. A full precursor ion scan (1.0×10^6 ions or 50 ms) was followed by 15 fragment ion scans (1.0×10^4 ions or 50 ms). Threshold for tandem MS (MS2) selection was set to 500 counts. Peptides were fragmented using collision induced dissociation (CID, normalized collision energy (CE) 35). Dynamic exclusion was turned on, with exclusion duration 60 s (max. 500 members). Charge states had to be > 1 to be fragmented. Furthermore, ion injection time prediction, preview mode for FTMS, monoisotopic precursor selection and charge state screening were enabled.

3.7.3.2 LUMOS LC-MS/MS system

The Orbitrap Fusion Lumos instrument was coupled online to an EASY-nLC 1200 UHPLC operating in the on-column mode (no trap column). System maximum pressure was set to 1000 bar. Analytical columns were generated in the same way as described for the Elite LC-MS-system. Briefly, peptides were loaded onto the analytical column (fused silica capillary inner diameter = 75 µm × variable length, with an integrated PicoFrit emitter (New Objective) and packed in-house with Reprosil-Pur 120 C18-AQ

1.9 µm resin (Dr. Maisch)). Loading pressure was set to not exceed 980 bar which resulted in a flow of 0.5 – 0.8 µL/min (depending on the column length). The analytical column was encased by a column oven (Sonation) and the temperature during LC-MS data acquisition was set to 45 °C or 49°C. The analytical column was attached to a nanospray flex ion source (Thermo Fisher Scientific). For peptide separation the following gradient was run for 105 min at a flow rate of 300 nL/min (gradient: start with 9% B; gradient 9% to 44% B in 90 min; gradient 44% to 100% B in 10 min and 100% B for 5 min).

XCalibur software (version 4.3.) was used to control the LC-MS runs. Ionization was set to positive mode. Precursors were scanned in the Orbitrap analyzer (FTMS; Fourier Transform Mass Spectrometry) in the scan range of *m/z* 375–1500 and at a resolution of 240,000 for a maximum of 50 ms (AGC target was set to “standard”). Quadrupole isolation was enabled. Polysiloxane (*m/z* = 445.120025) was set as internal lock mass. Fragment ions were acquired in data-dependent manner with a maximum cycle time of 3 s between two master scans. Fragment ions were detected using ITMS and the scan rate was set to ‘Turbo’. Intensity threshold for fragmentation was set to 5000 counts. Peptides were fragmented with higher-energy collisional dissociation (HCD, nCE 30) and were excluded for fragmentation for 120 s with a mass tolerance of ±10 ppm. Charge states had to be 2-7 to be fragmented. Fragment ions were isolated using quadrupole (isolation window of 1.6 *m/z*) and normalized AGC target was set to 300% or a maximum of 60 ms.

3.8 Data Analysis

3.8.1 MS data analysis

Raw spectra were analyzed using MaxQuant (different versions, cf. 8.4.5.4) section algorithm with default settings. Moreover, label-free quantification (LFQ) and match between runs (MBR) were set on. For statistical analysis of identified proteins, proteingroups.txt was loaded into Perseus (different versions, cf. 8.4.5.4). All data sets were prepared as follows: Data sets were filtered for contaminants, reverse peptides and peptides only identified by modified peptides. Subsequently, LFQ intensities were log_2-transformed and samples were annotated depending on their grouping. Depending on the experiment, data were further filtered for 2 out of 3 or 3 out of 4 valid values in at least one group (treatment). For full proteome or secretome analyses, missing values were imputed (default settings). Significance of protein fold-changes were tested by permutation-based t-tests (FDR = 0.05, s0 = 0.1, 250 randomizations).

For enrichment analyses, ‘Fisher exact test’ were used. To this end, proteins were annotated using GO and KEGG terms. Categorical enrichment was tested against significant regulated proteins. The corresponding enrichment threshold was set to Benjamini-Hochberg FDR = 0.02 and only top ten enriched annotation terms were reported (depending on enrichment factor).

3.8.2 Statistical evaluation

Raw data of biochemical assays were analyzed using EXCEL and GraphPad PRISM. Each sample was measured at least in triplicates. When indicated, data was normalized to DMSO (control). The resulting mean values and error bars (indicating standard deviation or standard error of the mean) were calculated and are plotted in the figures. To elucidate the significance of measurements, two-sided t-tests were performed. Significance was quantified by the p-value and annotated with asterisks (*). P-value < 0.05 = *, < 0.01 = **, < 0.001 = ***, < 0.0001 = ****. For calculation of IC_{50}-values, results (response) were analyzed using a non-linear fit (normalized response vs. log concentrations, four parameters). To this end, the indicated concentrations were log-transformed and plotted against results. Constraints were set when indicated. These analyses delivered the IC_{50}, regression (R^2) and 95% confidence interval (CI 95%) which are reported.

For visualization of MS data, final data from Perseus was exported to GraphPad PRISM. Data were not further manipulated. For target identification experiments, all enriched proteins were plotted against their numerical order and the threshold for enrichment was set to 2 (log_2, 4× fold-enrichment). To identify specific targets from competitive experiments, log_2 fold-enrichments of increased protein signals were exported to GraphPad PRISM and visualized as described above.

4 Results

4.1 Elucidation of Zelkovamycin's bioactivity

In order to elucidate the bioactivity of Zelkovamycin in human cancer cell lines, we started to test its impact on HeLa cell proliferation. First results of Krahn revealed a time-dependent color change of the pH-indicator phenol red in the HeLa cell culture medium after application of Zelkovamycin. In addition, Zelkovamycin application led to a slight loss of cell viability of different cancer lines.[12] To gain more insights, the investigations started by repeating and quantifying these preliminary assays. Subsequently, the Zelkovamycin-induced global proteome alterations were determined by MS-based proteomics, followed by various biochemical and biological assays to better characterize the molecular mode-of-action of Zelkovamycin.

4.1.1 Zelkovamycin leads to extracellular acidification by increased lactate production

Treatment of HeLa cells with Zelkovamycin resulted in an acidification of the cell culture medium in preliminary experiments. To corroborate this finding, the experiment was repeated and acidification was quantified by measurement of the absorbance of the pH indicator phenol red that is supplemented in the cell culture medium. Antimycin A (AMA) and Carbonylcyanid-m-chlorphenylhydrazone (CCCP), which are known inhibitors of oxidative phosphorylation (OXPHOS) and lead to extracellular medium acidification, served as positive controls (Fig. 14).[85]

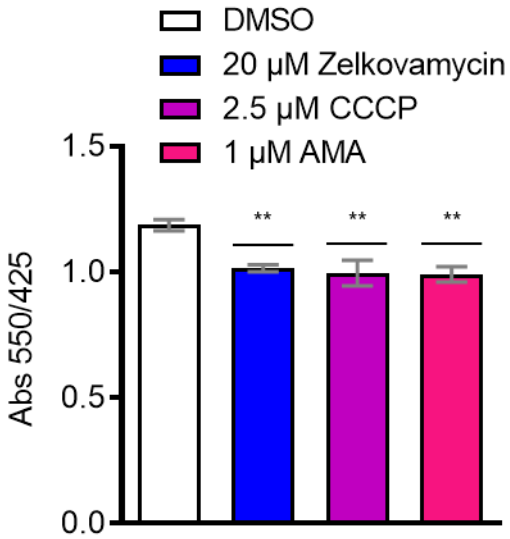

Figure 14: Zelkovamycin leads to color change of the pH indicator phenol red. Neutral absorbance maximum of phenol red (550 nm) was measured against acidic absorbance maximum (425 nm) in the presence of Zelkovamycin or known OXPHOS inhibitors. Cells were treated with indicated compounds for 48 h. Error bars indicate standard deviation from three replicates. ** p-value < 0.01.

Zelkovamycin significantly increased acidification of the cell culture medium. Moreover, this observation could be mimicked by known OXPHOS inhibitors. Next, the molecular mechanism behind acidification was investigated. A well-established mechanism is a higher cellular lactate production that is subsequently secreted from the cells.[86,87] Indeed, OXPHOS inhibitors such as AMA or CCCP impair mitochondrial function. To overcome energy deprivation, AMA or CCCP treated cells respond by metabolizing pyruvate to lactate, leading to increased intracellular lactate levels. Finally, lactate is pumped into the extracellular space to avoid intracellular dysfunction by acidification. To confirm that the observed, extracellular acidification was caused by lactate excretion, extracellular lactate levels were determined using an L-Lactate assay kit (Fig. 15).

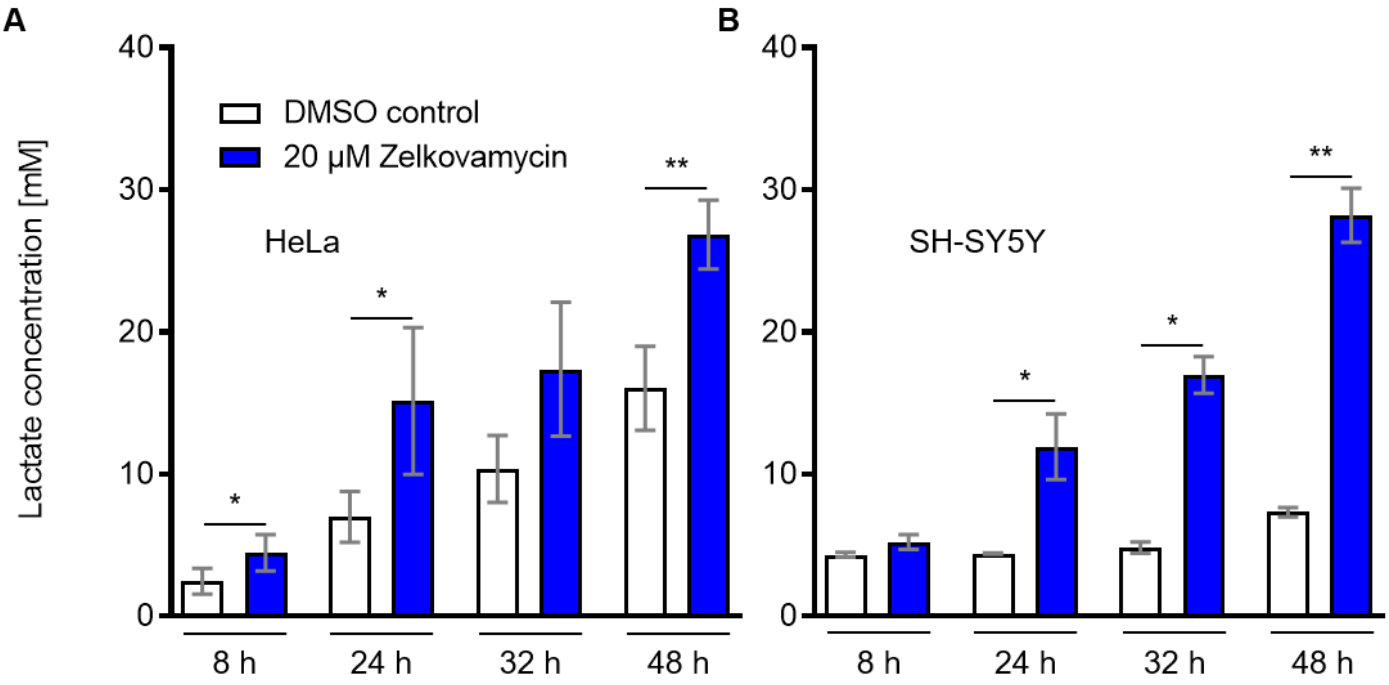

Figure 15: Zelkovamycin increases extracellular lactate concentrations in a time-dependent manner. Cells were treated with Zelkovamycin. After indicated time points, lactate concentrations in cell culture medium were measured. Error bars indicate standard deviation from three replicates. * p-value < 0.05, ** p-value < 0.01.

Zelkovamycin increased extracellular lactate levels in a time-dependent manner in HeLa cells (Fig. 15A). An even stronger effect was observed in SH-SY5Y cells (Fig. 15B). In contrast to the visceral HeLa cells that mainly use glycolysis to satisfy their energy demands, these cells are of neural origin and rely stronger on OXPHOS,[88] suggesting that the extent of increased extracellular lactate levels may rely on the cell's metabolic state.

4.1.2 Increased extracellular lactate correlate with mitochondrial dysfunction

To unravel a potential molecular mechanism underlying Zelkovamycin-induced lactate production, an unbiased MS-analysis was performed. To this end, HeLa cells were treated with 20 µM Zelkovamycin for 16 h (Fig. 16).

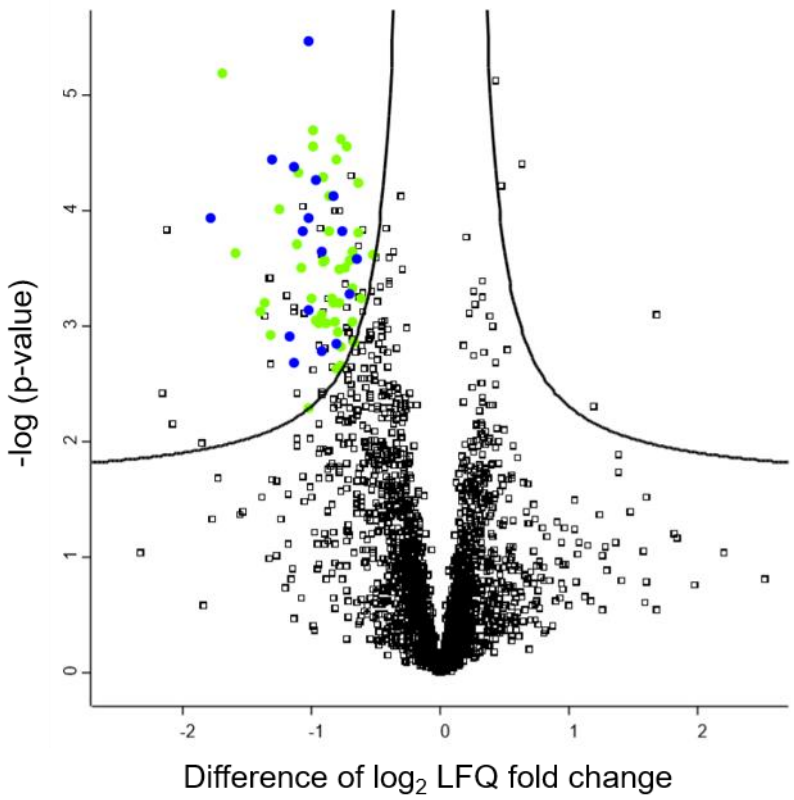

Figure 16: Zelkovamycin leads to a lower abundance of mitochondrial proteins. HeLa cells were treated with Zelkovamycin (20 µM) for 16 h and the resulting protein fold-change was analyzed by MS. Mitochondrial proteins (green circles) were less abundant. Particularly, proteins that are part of the electron transport chain (blue circles) were strongly reduced. The y-axis indicates the corresponding p-values (FDR = 0.01), while the x-axis indicates log_2 LFQ fold-changes of detected proteins.

Treatment of HeLa cells with Zelkovamycin resulted in a lower abundance of mitochondrial proteins (green). In particular, protein abundances of OXPHOS complex subunits (blue) were decreased. These less abundant proteins were then annotated by GO and KEGG terms for a functional enrichment analysis (Fig. 17).

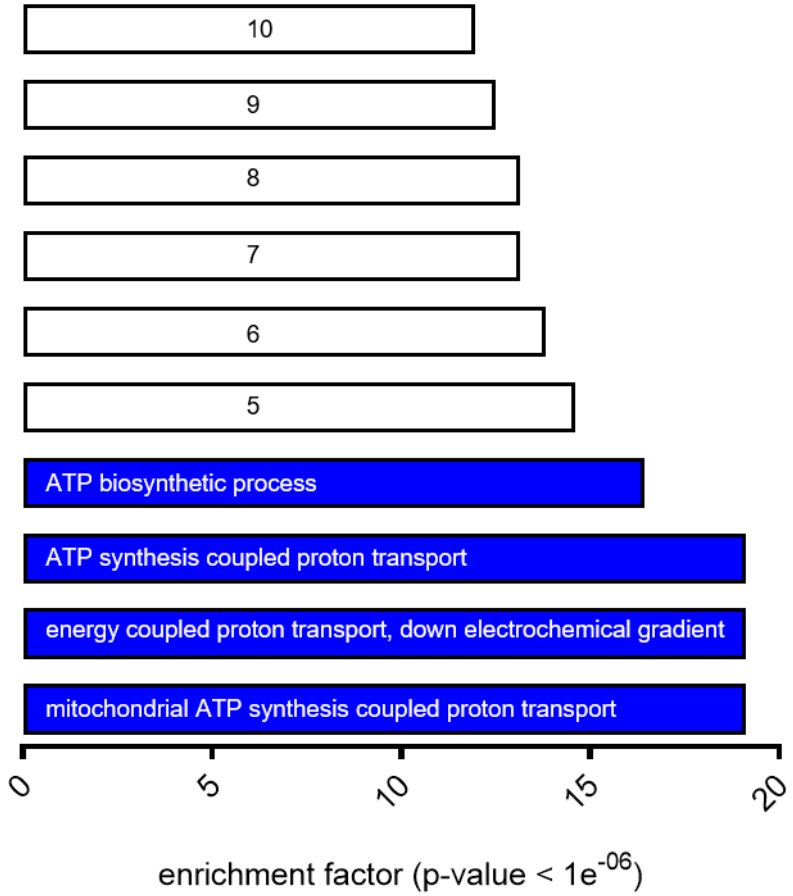

Figure 17: Zelkovamycin mostly affects ATP biosynthetic processes. Less abundant proteins were annotated by GO and KEGG terms and subjected to enrichment analysis (Perseus). Plotted are the ten most enriched GO and KEGG terms. The corresponding enrichment factor (x-axis) was calculated by over-representation of specific terms against its approximate occurrence in the GO or KEGG database. Significance threshold was set to Benjamini-Hochberg FDR < $1e^{-06}$. 5: purine ribonucleoside triphosphate biosynthetic process, 6: purine nucleoside triphosphate biosynthetic process, 7: monovalent inorganic cation transmembrane transporter activity, 8: Cardiac muscle contraction, 9: ribonucleoside triphosphate biosynthetic process,10: hydrogen ion transmembrane transporter activity.

The enrichment analysis revealed that Zelkovamycin mainly decreases the abundance of proteins that function in the electron transport chain (blue) which is utilized for adenosine triphosphate (ATP) production, indicated by a high enrichment factor. Thus, Zelkovamycin probably introduces mitochondrial dysfunction.

To confirm these results, the activity of key enzymes of cytosolic glycolysis and mitochondrial respiration were evaluated.[89,90] To this end, the activity of Phosphofructokinase (PFK, cytosolic) and Pyruvate Dehydrogenase (PDH, mitochondrial) was measured (Fig. 18).

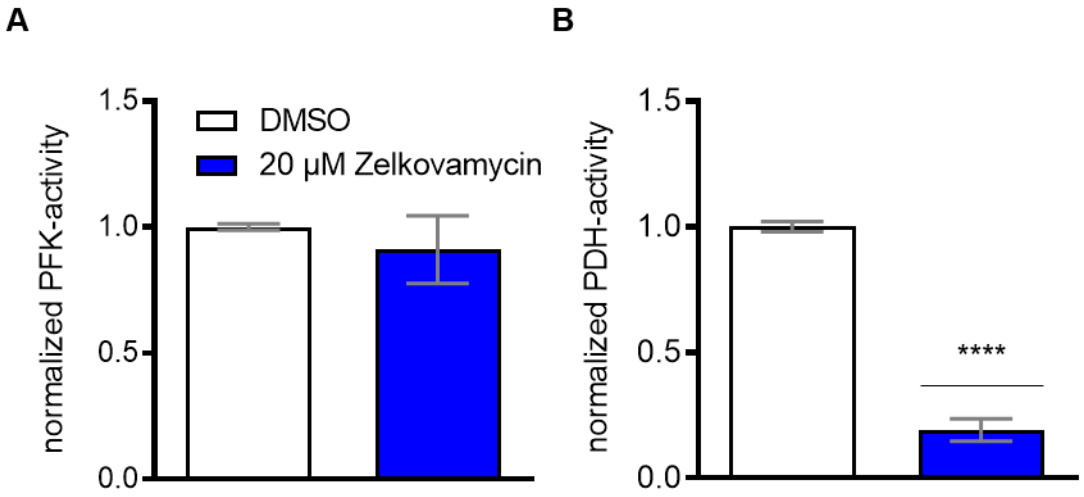

Figure 18: Zelkovamycin does not affect PDH activity but PFK activity. SH-SY5Y cells were treated with Zelkovamycin for 24 h and PFK and PDH activities were determined. (A) PDH activity of SH-SY5Y lysates treated with Zelkovamycin. (B) PDH activity of HeLa lysates treated with Zelkovamycin. Error bars indicate standard deviation from three replicates. **** p-value < 0.0001.

These assays revealed that Zelkovamycin did not affect cytosolic glycolysis (Fig. 18A) in SH-SY5Y cells, while PDH activity in HeLa cells was significantly about five-fold decreased (Fig. 18B). These results corroborate that Zelkovamycin indeed leads to mitochondrial dysfunction.

4.1.3 Glucose-deprived cells are more sensitive towards Zelkovamycin

The MS data as well as the observed decreased PDH activity indicate Zelkovamycin-induced mitochondrial dysfunction. Accordingly, Zelkovamycin-treated cells should become more dependent on glycolysis and glucose deprivation should thus display a harmful effect on cells in presence of Zelkovamycin. To test if this is the case, the cell viability of glucose-deprived HeLa and SH-SY5Y cells was elucidated (Fig. 19).

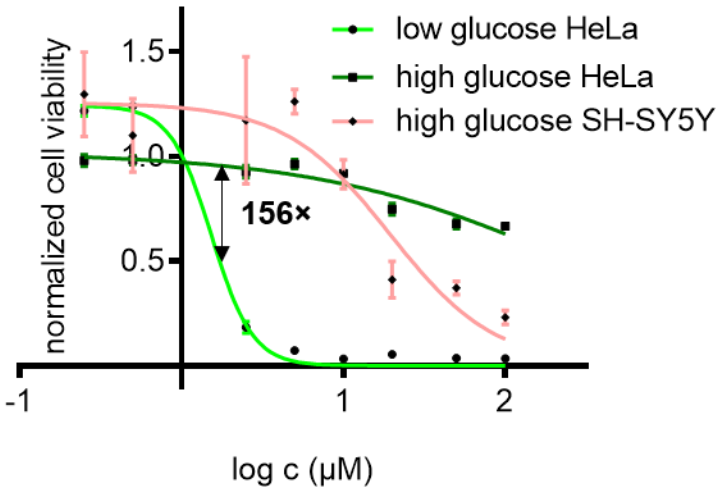

low glucose HeLa: **IC_{50} = 1.531 µM**
CI 95% = 1.190 - 1.970 µM
R^2 = 0.9923

high glucose HeLa: **IC_{50} = 238.7 µM**
CI 95% = 141.7 - 402.2 µM
R^2 = 0.8808

high glucose SH-SY5Y: **IC_{50} = 19.47 µM**
CI 95% = 12.79 - 29.62 µM
R^2 = 0.8361

Figure 19: Glucose-deprived HeLa cells are more sensitive to Zelkovamycin treatment. Cells grown in high or low glucose medium were treated with 0.25 – 200 µM Zelkovamycin for 48 h. The resulting cell viability was measured by an MTT assay and normalized cell viability was plotted against the log of Zelkovamycin concentration to calculate the corresponding IC_{50}. Error bars indicate the standard deviation from three replicates. CI 95% indicates 95% confidence interval of IC_{50}.

As expected, HeLa cells grown in low glucose medium were much less viable and a 156-fold reduction of cell viability compared to HeLa cells grown high glucose medium was observed. The same assay however could not be repeated with SH-SY5Y cells that, due to their dependence on OXPHOS, did not grow in a low glucose medium.

4.1.4 Zelkovamycin directly targets OXPHOS

MS analysis revealed that OXPHOS proteins are much less abundant after Zelkovamycin treatment, indicating a switch towards glycolysis because of mitochondrial metabolic dysfunction. Such an effect could for example be caused by a direct impairment of mitochondrial energy production via the OXPHOS system. To test this hypothesis, oxygen consumption rates (OCR) of HeLa and SH-SY5Y cells after Zelkovamycin treatment were determined by Felix Vogel (AG Roesch, University Hospital Essen) using the so called ‘Seahorse assay system’ (Fig. 20 and 21).

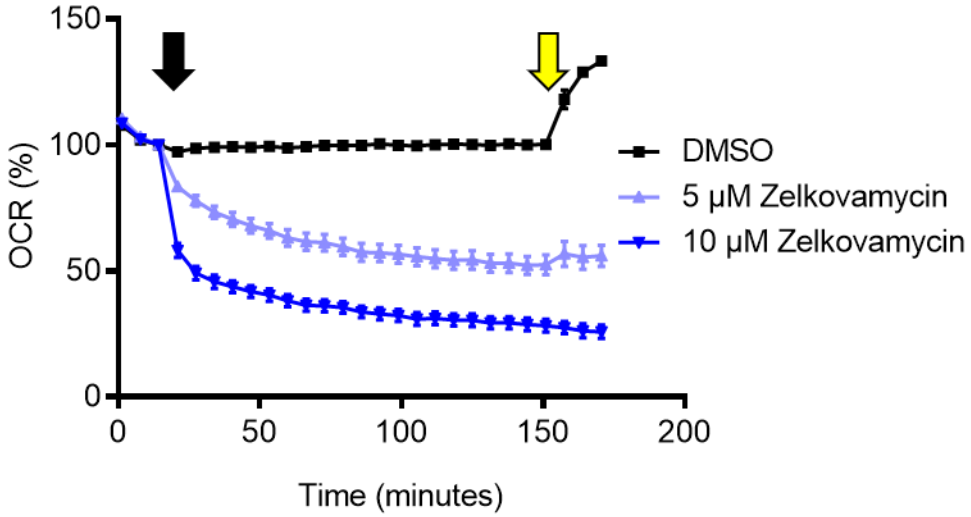

Figure 20: Zelkovamycin directly impairs mitochondrial OCR. HeLa cells were treated with Zelkovamycin (black arrow) and the resulting OCR was measured for about 120 min. To elucidate the maximal respiratory capacity in presence of Zelkovamycin, the cells were treated with FCCP (yellow arrow) after 150 min. The measured OCR was normalized to DMSO (control). Error bars indicate the standard error of the mean from at least six replicates. This assay was performed by Felix Vogel (AG Roesch, University Hospital Essen).

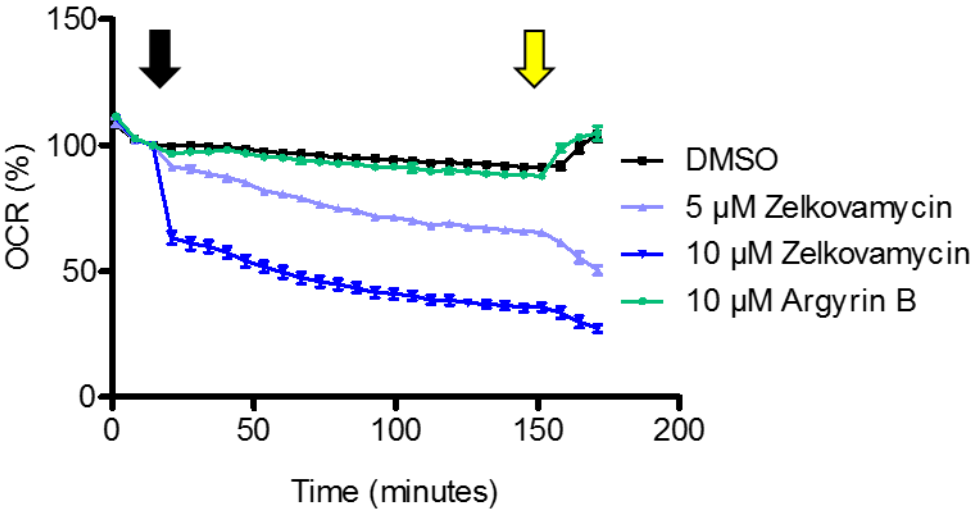

Figure 21: Zelkovamycin directly impairs mitochondrial OCR. SH-SY5Y cells were treated with Zelkovamycin (or argyrin B, black arrow) and the resulting OCR was measured for about 120 min. To elucidate maximal respiratory capacity in presence of Zelkovamycin or Argyrin B, the cells were treated with FCCP (yellow arrow) after 150 min. The measured OCR was normalized to DMSO (control). Error bars indicate standard error of the mean from at least six replicates. The assay was performed by Felix Vogel (AG Roesch, University Hospital Essen).

This analysis revealed that Zelkovamycin directly decreased the OCR in HeLa and SH-SY5Y cells in a concentration-dependent manner. Of note, OCR could not be recovered by addition of FCCP which is used to induce reserve respiratory capacity (RRC) of mitochondria. In contrast, argyrin B which targets a mitochondrial protein did not decrease OXPHOS in SH-SY5Y cells.

4.1.5 Zelkovamycin leads to decreased cell viability in OXPHOS-dependent skin cancer cells

Zelkovamycin thus leads to a loss of cell viability most likely by OXPHOS inhibition. In addition, these effects were stronger in cells such as SH-SY5Y cell that have higher energy demands. An alternative OXPHOS-dependent cell line is WM3734 which are skin cancer cells.[91,92] Accordingly, the effect of Zelkovamycin on these cells was also tested by Felix Vogel (AG Roesch, University Hospital Essen, Fig. 22).

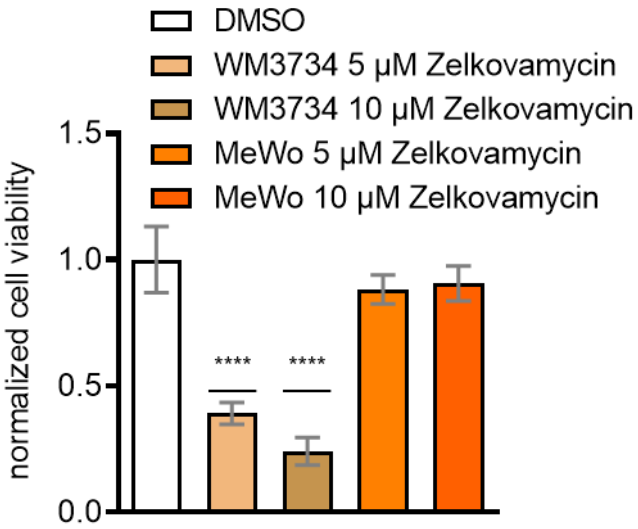

Figure 22: Zelkovamycin leads to loss of cell viability in an OXPHOS-dependent skin cancer cell line. Two skin cancer cell lines, WM3734 that is OXPHOS-dependent as well as non-OXPHOS-dependent MeWo cells were treated with Zelkovamycin and the resulting cell viability was measured by an MTT assay after Zelkovamycin application at the indicated concentrations for 72 h. Error bars indicate standard deviation from six replicates. **** p-value < 0.001. The assay was performed by Felix Vogel (AG Roesch, University Hospital Essen).

The cell viability of WM3734 cells decreased by more than 50% after 72 h treatment with 5 or 10 µM Zelkovamycin, respectively. Interestingly, the cell viability of related, non-OXPHOS-dependent skin cancer cells (MeWo) was not affected, thus again corroborating that Zelkovamycin may act via OXPHOS inhibition.

Preliminary results of Krahn indicate only slight loss of cell viability in visceral cell lines. In order to confirm these results, the cell viability of HeLa and SH-SY5Y cells as well as an enlarged set of visceral cancer cell lines was tested (Fig. 23).

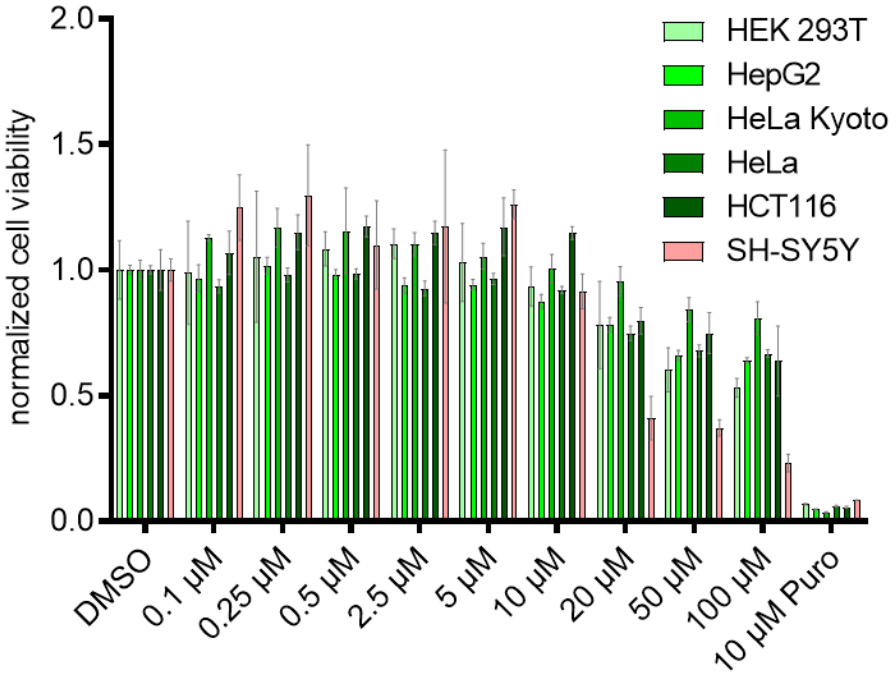

Figure 23: Visceral cancer cell lines are slightly sensitive towards Zelkovamycin, while neuronal cells are more sensitive. Cells were treated with Zelkovamycin at indicated concentrations for 48 h. Cell viability was measured by an MTT-assay. Puromycin (Puro) was used as a positive control. Error bars indicate standard deviation from three replicates.

Zelkovamycin treatment of different cancer cell lines resulted in a slight effect on cell viability for most cell lines. However, SH-SY5Y again revealed a higher vulnerability, corroborating previous results that Zelkovamycin is more harmful for OXPHOS-dependent cancer cell lines.

Analysis of OCR in WM3734 cells confirmed the observations made with the HeLa and SH-SY5Y cells. Again, Zelkovamycin treatment led to a breakdown of OCR that could also not be recovered by addition of FCCP. Of note, argyrin B which also targets mitochondria and is a member of the argyrin family, does not affect OCR in WM3734 cells nor does it impair RCC induction by FCCP (performed by Felix Vogel, AG Roesch, University Hospital Essen, Fig. 24).

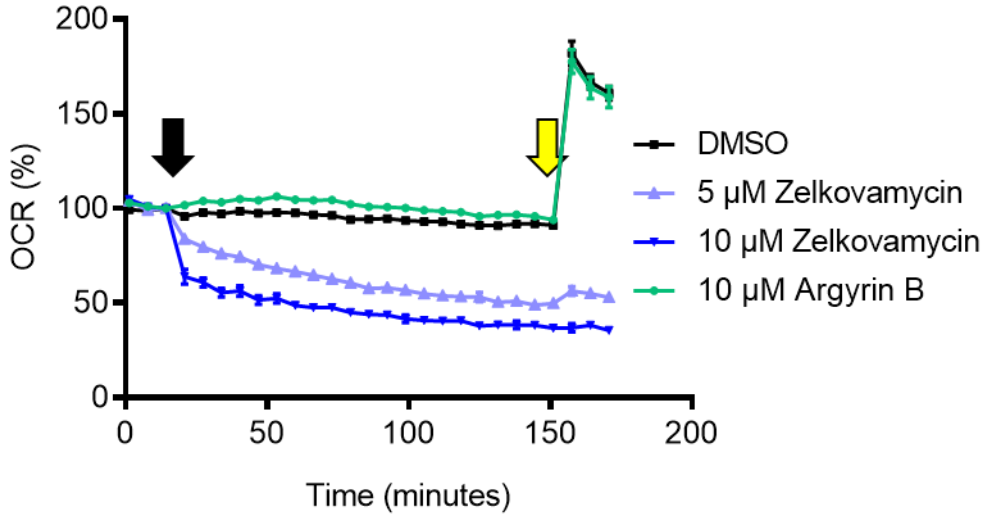

Figure 24: Zelkovamycin directly impairs OCR in OXPHOS-dependent skin cancer cells. WM3734 cells were treated with Zelkovamycin (or argyrin B, black arrow) and the resulting OCR was measured for about 120 min. To elucidate maximal respiratory capacity in presence of Zelkovamycin or Argyrin B, the cells were treated with FCCP (yellow arrow) after 150 min. The measured OCR was normalized to DMSO (control). Error bars indicate the standard error of the mean from at least six replicates. The assay was performed by Felix Vogel (AG Roesch, University Hospital Essen).

Analysis of OCR in WM3734 cells after treatment with Zelkovamycin confirmed that WM3734 cells had a considerable loss of cell viability after treatment with Zelkovamycin. Again, argyrin B had no effect on OCR.

Finally, the general OCR was tested after application of Zelkovamycin. To this end, WM3734 cells were treated with 1 µM Zelkovamycin for 16 h and OCR was tested using standard settings (performed by Felix Vogel, AG Roesch, University Hospital Essen, Fig. 25). This assay enables calculation of several OCR parameters (Tab. 2).[85]

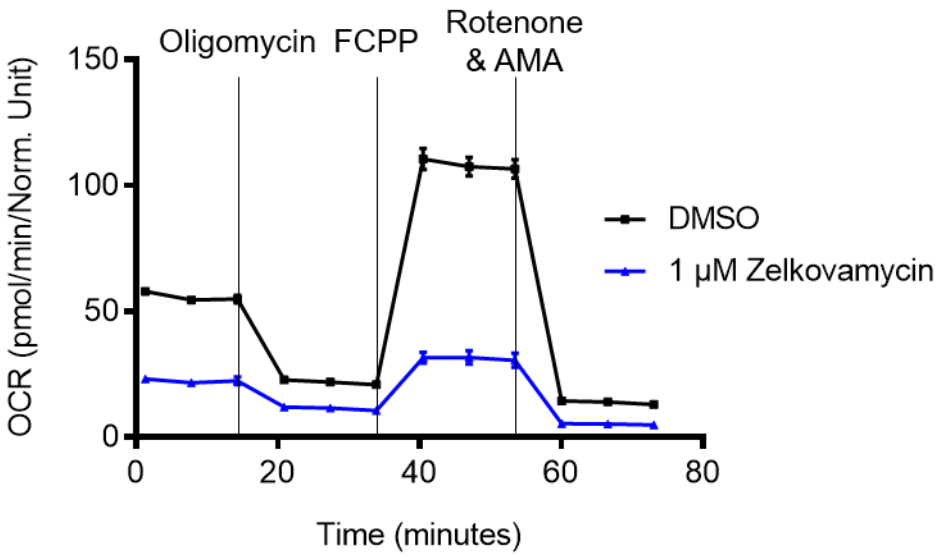

Figure 25: Zelkovamycin reduces basal OCR in WM3734 cells. WM3734 cells were treated with Zelkovamycin for 16 h and OCR was measured for about 70 min. To elucidate different parameters of OCR, cells were treated with indicated compounds. OCR was normalized and error bars indicate standard error of the mean from at least nine replicates. The assay was performed by Felix Vogel (AG Roesch, University Hospital Essen).

Table 2: Calculations of OCR parameter.

	WM3734 DMSO 16h		WM3734 16h 1µM Zelkovamycin	
Parameter	**OCR**	**St Dev**	**OCR**	**St Dev**
Basal	30,26	2,78	13,35	0,54
Proton Leak	5,44	0,62	4,31	0,44
Maximal Respiration	72,84	7,98	20,39	0,35
Spare Respiratory Capacity	42,59	5,50	7,04	0,27
Non Mitochondrial Oxygen Consumption	10,47	1,47	5,74	0,54
ATP Production	24,82	2,27	9,05	0,15
Coupling Efficiency (%)	82,02%	1,04%	67,79%	2,03%
Spare Respiratory Capacity (%)	240,55%	10,29%	152,80%	3,91%
Acute Response				

Indeed, Zelkovamycin decreased basal OCR. Moreover, it decreased the response to known OPXHOS-inhibitors. Notably, the calculation of OCR parameters indicated that the spare respiratory capacity (marked in red) is mostly affected by Zelkovamycin treatment.

Overall, Zelkovamycin thus displays unique properties that are not shared by other members of the argyrin family.

4.1.6 Structure-Activity Relationships

So far, our results indicate that Zelkovamycin inhibits OPXHOS. Moreover, argyrin B that inhibits elongation factor G1 and thus a mitochondrial protein does not affect

OXPHOS. This indicates that a distinct structure-activity relationship may underlie the observed OXPHOS inhibition. To figure out which residues of Zelkovamycin are essential for its bioactivity, a SAR analysis was performed with two additional Zelkovamycin derivatives. These were two compounds that either lacked the 4-methoxy moiety (ΔMeO Zelko.) or possessed a reduced 2-methyl-dehydro threonine (red. Zelko.) moiety. Most argyrins harbour a 4-methoxy tryptophan moiety, while the 2-methyl-dehyro threonine is a unique structural feature of Zelkovamycin. To evaluate the impact of these structural changes on bioactivity, OCR measurements and the determination of extracellular lactate levels were next performed (Fig. 26).

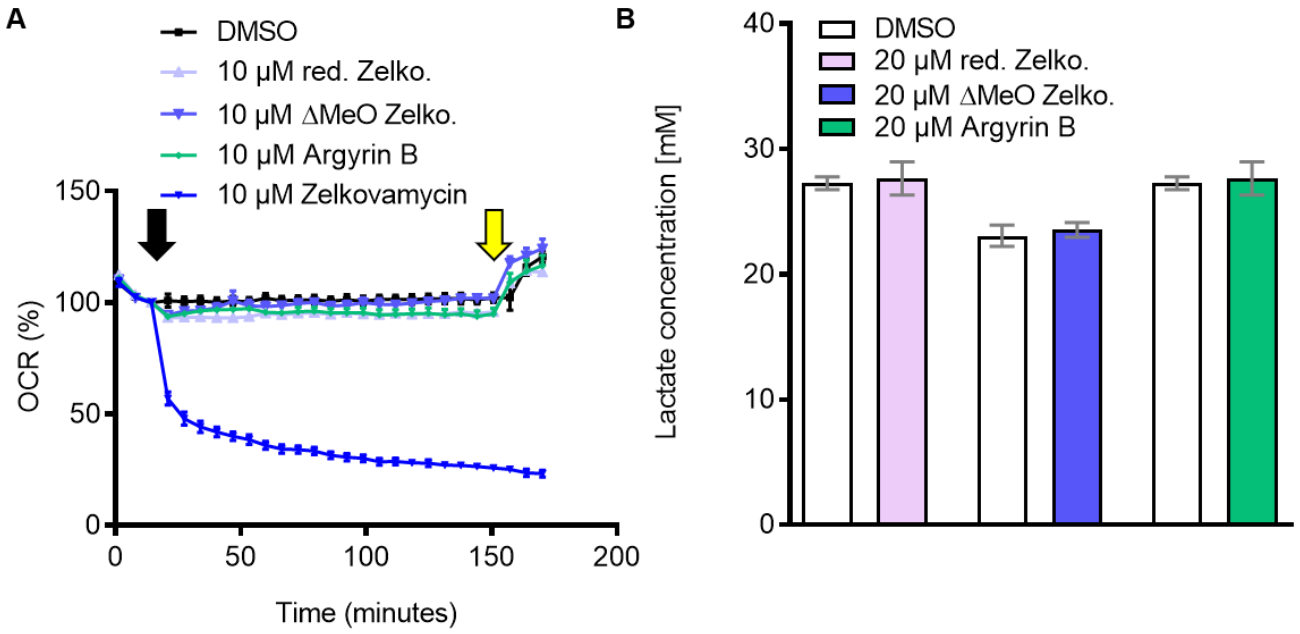

Figure 26: OCR measurements and lactate level determinations with Zelkovamycin analogues. (A) OCR after application of Zelkovamycin, Zelkovamycin derivatives and argyrin B at the indicated concentrations in HeLa cells. (B) Extracellular lactate levels after a 48 h treatment of HeLa cells with the two Zelkovamycin analogues or argyrin B at the indicated concentrations. Error bars indicate standard deviation from at least three replicates.

Neither the Zelkovamycin derivatives nor argyrin B affected OCR or extracellular lactate levels at the tested concentrations, indicating that the OXPHOS inhibitory properties of Zelkovamycin are strongly structure-dependent and most probably rely on the 4-methoxy tryptophan and the 2-methyl-dehydro threonine moiety.

4.1.7 Zelkovamycin inhibits OPXHOS complex II

To determine the exact molecular target of Zelkovamycin, the inhibitory effects of Zelkovamycin treatment vs. all five OXPHOS complexes were next determined. To this end, a spectrophotometric assay kit (cf. section 8) was used according to the manufacturer's instructions, leading to the results depicted in Tab. 3.

Table 3: Summary of inhibitory effects of Zelkovamycin vs. the different OXPHOS complexes. IC_{50} values of Zelkovamycin were determined via a commercially available spectrophotometric assay kit. To this end, a Zelkovamycin 2-fold dilution series starting from 200 µM was prepared and measured. Of note, CI 95% could not be calculated because the measured values did not follow the standard regression curve.

OXPHOS complex	IC_{50}	Linear regression (R^2)
I	70.48 µM	0.9002
II	24.46 µM	0.8036
II+III	> 200 µM	-
IV	> 200 µM	-
V	> 200 µM	-

In these assays, Zelkovamycin did not affect the activity of complexes III – V. However, Zelkovamycin displayed a slight inhibitory activity against complex I and an even higher inhibitory activity against complex II (Fig. 27).

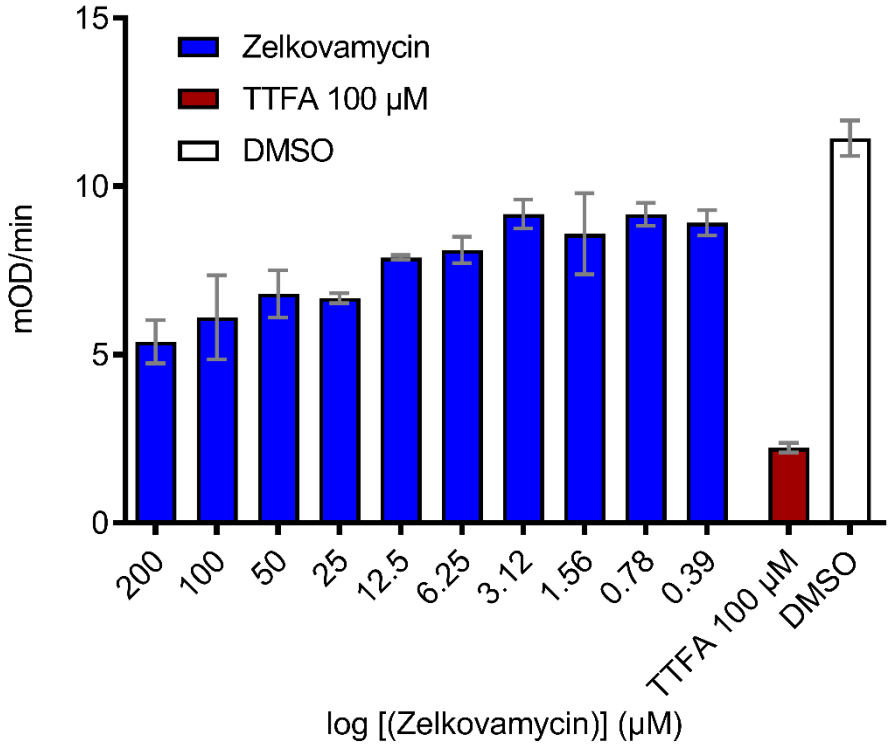

Figure 27: Zelkovamycin moderately decreases OXPHOS complex II activity. OXPHOS complex II activity was measured using a commercially available spectrophotometric assay kit according to the manufacturer's instructions. Zelkovamycin was used in two-fold serial dilution starting from 200 µM. As a positive control, 100 µM TTFA was applied. Error bars indicate standard deviation from three replicates.

These measurements revealed a moderate inhibitory effect of Zelkovamycin against complex II. However, the resulting values were atypic, thus not allowing an IC_{50}

determination. Re-analysis of the assay revealed that Zelkovamycin interfered with the photometric dye 2,6-Dichlorphenolindophenol (DCPIP) that is utilized to quantify complex II activity (appendix Fig. 40). Therefore, the assay was repeated with a longer time interval > 30 min which leads to a steady state that can be measured more reliably (Fig. 28).

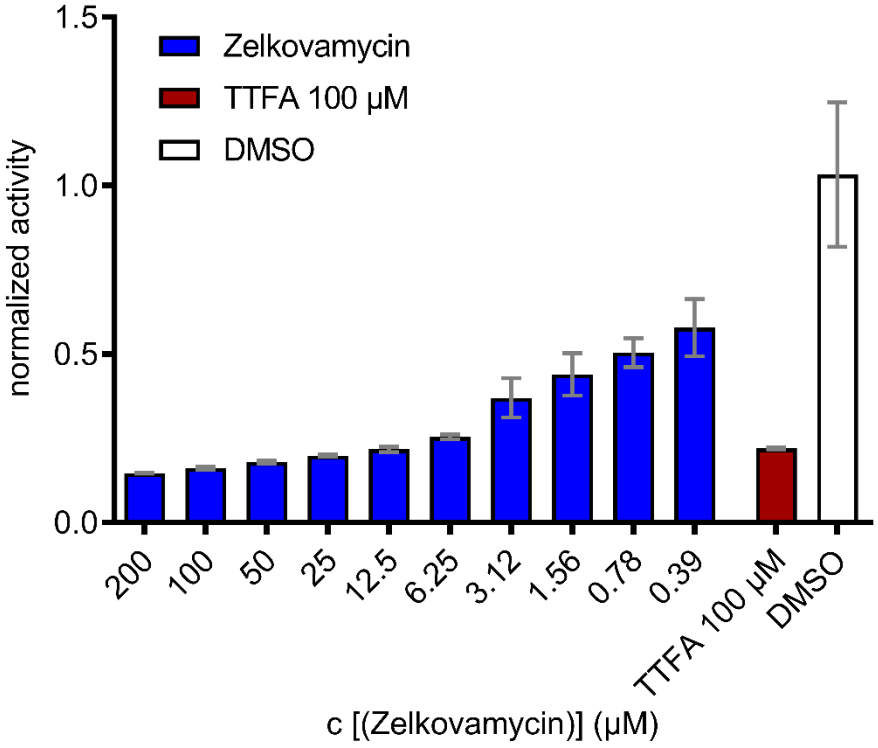

Figure 28: Zelkovamycin decreases OXPHOS complex II activity in an elongated kinetic measurement. OXPHOS complex II activity was measured via a commercially available spectrophotometric assay kit using longer measurement times. To this end, the absorbance of the read-out dye was measured after 24 h incubation with the indicated concentrations of Zelkovamycin and was normalized against DMSO. This measurement represents OXPHOS complex II activity in a steady state. As a positive control, TTFA was applied. Error bars indicate standard deviation from three replicates.

These measurements revealed that Zelkovamycin is an efficient inhibitor of complex II, although an exact calculation of an IC_{50} was not possible. Of note, the inhibitory effects of TTFA did not increase with the changed experimental conditions.

4.2 Hydrolase screening in *P. chrysosporium*

The second part of this thesis is devoted to a hydrolase screening in the thermophilic fungus *P. chrysosporium* which is a promising source organism for identifying biotechnological useful biocatalysts.

4.2.1 Workflow optimization

In order to perform the envisaged hydrolase screening by ABPP, the first step was to optimize the standard ABPP workflow for a secretome analysis of *P. chrysosporium*. To this end, the optimal secretome concentration as well as best pull-down method had to be elucidated. These experiments were part of the Bachelor thesis of Leonard Sewald ("Investigation of hydrolases in thermophilic fungi by ABPP and mass spectrometry", 2019, AG Kaiser, University of Duisburg-Essen) which were performed under my supervision. In the following section, the elucidation of the optimized workflow is briefly summarized:

A sample preparation workflow for MS analysis of *P. chrysosporium* secretomes was already reported previously.[73] In this study, the MS samples were obtained from a *P. chrysosporium* culture medium via a filtration step by cloth towels followed by a subsequent concentration by molecular weight cut-off filters (MWCOs). The such obtained secretome was then separated by gel electrophoresis.[73]

To enable a more direct ABPP approach, a workflow without gel electrophoresis and concentration of the cell culture medium was however required. Microfiltration and lyophilization of the cell culture medium were therefore tested as an alternative approach for sample preparation. Accordingly, a gel-based ABPP analysis using FP-Rh with secretomes prepared either after filtering with MWCOs was compared to the sample preparation *via* microfiltration and lyophilization of the cell culture medium.

This gel-based ABPP analysis revealed that both approaches resulted in a similar labelling efficiency. However, microfiltration and freeze-drying did not remove small proteins, salts or metabolites. Additionally, the freeze-dried powder was dissolvable in probe-specific buffers without further manipulations and the underlying preparation of the secretome was much faster than with the MWCO concentration method. Indeed, the required large sample amounts for target identification approaches could be obtained via lyophilization of ca. 50 mL culture medium overnight, while smaller sample sizes for gel-based analysis were prepared within 2-3 h. Besides the time factor, lyophilization was also much more cost-effective and required less consumables.

Moreover, specific optimizations such as the impact of the pH value on labelling efficiency were also evaluated (Fig. 29).

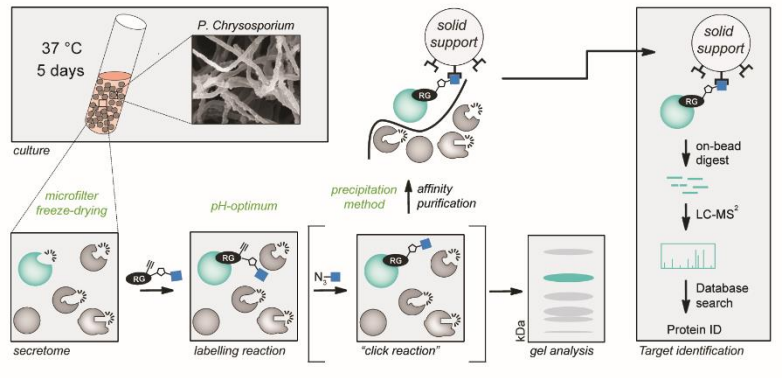

Figure 29: Schematic overview of the optimized ABPP workflow for fungal secretomes. The ABPP workflow was optimized along a standard operation protocol. Four main steps were optimized (green). Secretomes were purified by microfilters and concentrated by freeze-drying. Labelling was further optimized by evaluating different pH buffers for specific ABPs. Finally, different precipitation methods were tested to improve the affinity purification step. This resulted in the establishment of a methanol-chloroform precipitation step.

4.2.2 Gel-based analysis of different carbon sources

After optimization of the workflow, a comparative ABPP of *P. chrysosporium* using the fluorescent SH probe FP-Rh was performed via a gel-based analysis. To this end, *P. chrysosporium* cultures were grown on different carbon sources and the resulting secretome alterations were profiled by ABPP. As carbon sources, MYP, wood, Avicel and Avocel were used. These experiments revealed a carbon source-specific labelling pattern (Fig. 30).

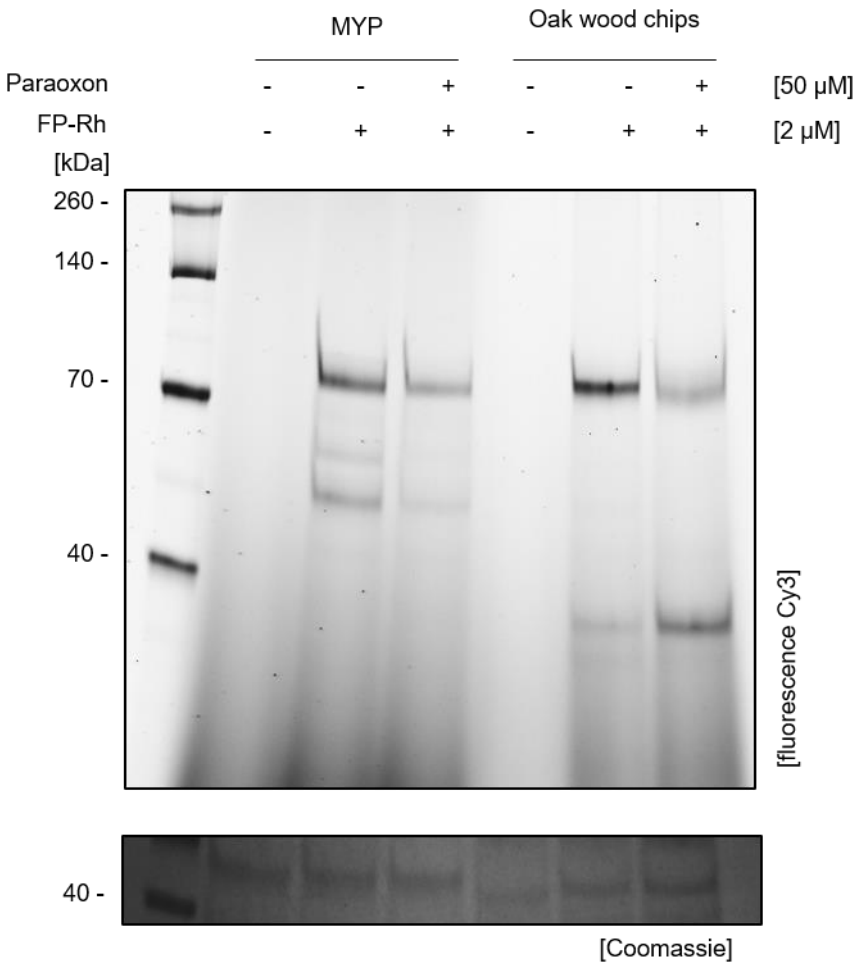

Figure 30: FP labels distinct enzymes in secretomes of *P. chrysosporium*. Exemplary gel of a FP labelling approach. Freeze-dried secretomes were pre-treated with Paraoxon for 30 min at 37 °C where indicated and labelled with FP-Rh for 1 h at 37 °C. Proteins were separated by SDS page and the resulting labelling pattern was visualized by a fluorescence scanner.

FP-Rh distinctly labelled several bands in MYP and wood secretomes. In MYP secretomes, at least three bands were obtained, of which two were efficiently competed by Paraoxon pretreatment. Labelling of wood secretomes revealed two strong bands that were both competed by Paraoxon pretreatment. However, no labelling was observed in Avicel or Avocel secretomes, perhaps as a consequence of problems during workup. Altogether, these results indicate that MYP and wood secretomes contain active SHs.

4.2.3 Full secretome analysis of *P. chrysosporium*

In order to gain insights into which proteins were present in the isolated secretomes, a full secretome analysis was next performed. To this end, *P. chrysosporium* cultures were again grown on different carbon sources in the cell culture medium, followed by a standard full proteome analysis (Fig. 31).

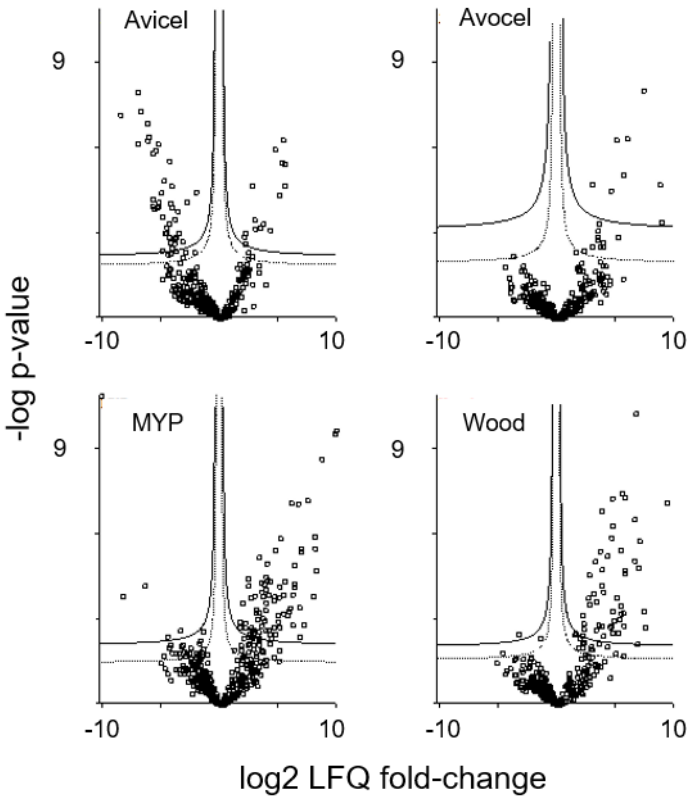

Figure 31: The protein constitution of the secretome depends on carbon source supplementation. *P. chrysosporium* was grown for 5 days in medium supplemented with different carbon sources. The resulting secretomes were analyzed by MS and the results were depicted in a 'Hawaii-plot' which indicates significantly less or more abundant proteins compared to the average abundance of each protein in the whole data set. Dashed line indicates FDR = 0.05, continuous line indicates FDR = 0.01. s0 was set to 0.1, n = 4.

Overall, this procedure led to the identification of 381 proteins, of which 318 were significantly changed in their abundance based on an ANOVA-test (FDR = 0.05) between all groups. Identified proteins were screened for secretion signal peptides using SignalP. This sequence analysis revealed that at least 179 proteins carried a signal peptide for secretion. To gain insights into the function of the differently abundant proteins, the ten most abundant proteins (FDR ≤ 0.01, carbon source vs. average abundance in whole dataset) were annotated and ranked by their $\log_2$ fold-change (Tab. 4 - 7).

Table 4: Ten most abundant proteins in the MYP-derived secretome. Most abundant proteins were ranked by their log_2 fold-change and annotated using the JGI database or Uniprot.

Protein ID	log_2 fold-change	Annotation
Q06326	9.874	Ligninase
P06181	9.778	Ligninase
6811	8.656	Ligninase
138738	8.047	Endonuclease/Phosphatase
8470	8.031	Endopeptidase
126189	7.418	Endopeptidase
8292	6.868	-
3589	6.861	Ligninase
8468	6.592	Endopeptidase
4127	6.051	Glycoside hydrolase superfamily

Table 5: Ten most abundant proteins in the wood-derived secretome. Most abundant proteins were ranked by their log2 fold-change and annotated using the JGI database or Uniprot.

Protein ID	log_2 fold-change	Annotation
41123	9.314	GH61
41563	6.947	GH61
8466	6.698	GH12
4690	6.563	GH61
122129	5.668	GH61
9257	5.504	GH3
128306	4.654	catalase
134658	4.647	Beta-glucosidase
134956	4.555	Catalase
3097	3.694	CBM, SGNH hydrolase-type esterase domain

Table 6: Ten most abundant proteins in the Avicel-derived secretome. Most abundant proteins were ranked by their log_2 fold-change and annotated using JGI database or Uniprot.

Protein ID	log_2 fold-change	Annotation
134492	5.481	Hsp20/alpha crystallin family, HS20-like chaperone
137138	5.463	histidine phosphatase superfamily, acid phosphatase activity
133830	5.320	Hsp20/alpha crystallin family, HS20-like chaperone
138453	5.237	aspartic type endopeptidase activity
36045	5.016	GH3 (glucosidase, xylosidase, glucanase), hydrolase activity
137747	4.631	Hsp20/alpha crystallin family, HS20-like chaperone
6357	4.253	6-phosphogluconate dehydrogenase, pentose-phosphate shunt, metabolic process, oxidoreductase, NADp binding
4525	3.627	
127435	2.870	ATP binding, hydrolase activity, Vsp4 c terminal, TonB-box, cell division protein 48
4889	2.681	Hsp20/alpha crystallin family, HS20-like chaperone

Table 7: Eight most abundant proteins in the Avocel-derived secretome. Most abundant proteins were ranked by their log_2 fold-change and annotated using JGI database or Uniprot.

Protein ID	log_2 fold-change	Annotation
131262	8.844	aspartic-type endopeptidase activity
8737	8.707	
8739	7.294	
3855	5.926	serine carboxypeptidase, S10
8740	5.609	
7064	4.975	RNA binding, endoribonuclease activity
8738	4.520	
4988	2.945	aspartic-type endopeptidase activity

Interestingly, the culturing of *P. chrysosporium* in the MYP medium led to an enhanced secretion of four ligninases, while the culturing in medium supplemented with oak wood chips revealed four lytic polysaccharide monooxygenases (LPMOs = ligninases, GH61 now classified as AA9) and three enzymes with cellulolytic activity as the most abundant proteins. However, the results from a growth on pure cellulose (Avicel: microcrystalline cellulose or Avocel: macroscopic cellulose fibers) led to results that are much more difficult to interpret. For example, avicel revealed three proteins with a Hsp20/alpha crystalline family annotation as the most abundant proteins; these are however normally intracellular proteins. Again, these results may result from problems during sample workup, more particularly the separation of the secretome from the Avicel or Avocel matrix.

This MS analysis revealed that different carbon sources result in differentially secreted proteins and may thus serve as a knowledge database to better explore the relationship between substrate availability and protein expression. However, such a detailed analysis was not the aim of this project. Nevertheless, even a simple analysis can demonstrate the potential of this database. For example, the most significantly (-log p-value = 9.40903, based on the ANOVA test) altered protein was the protein with the ID 138266. This protein is annotated to harbor a BNR/Asp-box repeat which is commonly found in glycosyl hydrolases.[93] Moreover, a blast analysis revealed that the amino acid sequence is similar to a glycosidase of *Phanerochaete carnosa* (Fig. 32).

glycoside hydrolase family 74 protein [Phanerochaete carnosa HHB-10118-sp]

Sequence ID: XP_007390431.1 Length: 842 Number of Matches: 1

See 1 more title(s)

Range 1: 5 to 742 GenPept Graphics ▼ Next Match ▲ Previous Match

Score	Expect	Method	Identities	Positives	Gaps
977 bits(2526)	0.0	Compositional matrix adjust.	492/745(66%)	589/745(79%)	27/745(3%)

```
Query  16   SVVSATVAPAAVAAPSISTQSYTWKNVKIGGGGGFTPGIVFNPSQKGLAFLRTDIGGVYK  75
            +  SA  A +   A ++S+Q+YTWKNVKIGGGGGF P IVFNPSQ+GLA+ RTDIGG YK
Sbjct  5    TAFSALAASSVPFAHAVSSQAYTWKNVKIGGGGGFVPSIVFNPSQQGLAYARTDIGGAYK  64

Query  76   LNPDDSWTPLLDFADNDHWDYWGSDAIATDPVDPQRLYIAAGMYTNFWDPNNGTILISKD  135
            LN DD+WTPLLDF DN  W+YWG DA+ATDPVDP RLY+A GMYTN WDPNNG +LIS D
Sbjct  65   LNSDDTWTPLLDFVDNARWNYWGVDALATDPVDPDRLYLATGMYTNSWDPNNGQVLISTD  124

Query  136  QGKTFTESPLPFKVGGNMPGRGVGERLAVDPHSNNILLFGARSGNGLWKSTDFGATWSKV  195
            QG+TFT SPLPFKVGGNMPGRG+GERLAVDP+SNN+L FGARSGNGLWKSTD+G +W+KV
Sbjct  125  QGQTFTPSPLPFKVGGNMPGRGMGERLAVDPNSNNVLFFGARSGNGLWKSTDYGQSWAKV  184

Query  196  TSLPDSGTYAPDPTDSSGINSDKTGVTFVTFDSTSGAAGAATPRIFVGVASVGSPNIFRS  255
            +SLPD GTY PDPTD+SG NSDK GV+FVTFDSTSG++G ATPRIFVGVA+  S N+F S
Sbjct  185  SSLPDVGTYVPDPTDTSGYNSDKIGVSFVTFDSTSGSSGNATPRIFVGVATNTSSNLFMS  244

Query  256  DDAGETWTAIQGTNSSWMAHKGVLSPKEGVLYLSTSDGVGPNDGSIGAVYKYDIASETIT  315
            +DAG TW+A+ GTNSSWMAHKGVLSP E  LY+STSDG GP DG++GAVYKY+I S T+
Sbjct  245  NDAGSTWSALPGTNSSWMAHKGVLSPAEKALYISTSDGAGPYDGTLGAVYKYNITSGTME  304

Query  316  NISPVSGSDLFFGFGGLAVDVQRPGTVMVAALNCWWPDGQVWRTTDGGSTWSPLWAWEAY  375
            NI+PVSGS+L+FGFGGLAVD+Q PGTVMVAALNCWWPDGQV+R+TDGG+TW+ LW W +Y
Sbjct  305  NITPVSGSNLYFGFGGLAVDLQNPGTVMVAALNCWWPDGQVFRSTDGGNTWTSLWDWASY  364

Query  376  PSLYKYYTYDDSLAPWIGPDYTNPDIVQQIGWWMEALVIDPFDSNHWLYGTGETVYGGHD  435
            P++ +YYTYDDSLAPW+GPD T   IV QIGW MEAL IDPFDSNHWLYGTG T+YGGHD
Sbjct  365  PTMNRYYTYDDSLAPWLGPDGTADSIVTQIGWMMEALAIDPFDSNHWLYGTGATIYGGHD  424

Query  436  LLNWDTTHNITLKSLADGIEEDAVQGLISPPAGPPLLSAVGDNGGFVHFDLLKAPTAAAR  495
            LL WDT  N+TL+SLADGIEE + Q L+SPP GP LLS V D  GF H +L +AP+  A
Sbjct  425  LLKWDTVRNVTLESLADGIEETSAQALLSPPTGPTLLSGVLDEEGFAHTNLDQAPS--AE  482

Query  496  FNPVWTTNVD-LDFAGNVPSTIVRIGNSNG----EFALSTDAGNTWSQNIGGTSNVNSGK  550
            F P   T V  LD+AGN P T+VR+GN +     + A+S DAGNTW+ + G  S V+ GK
Sbjct  483  FAPATGTGVTGLDYAGNDPQTVVRVGNGDSTDGPQAAISNDAGNTWALDYGSPSGVSGGK  542

Query  551  IALSANGTNILWSSGNAGVLLSQ------------AGGAFAPN---DNVFYAAAGPKFFV  595
            +A+SA+G  +LWSS   GV +SQ             AG A A +   D++FYA +G +F++
Sbjct  543  VAISASGDTVLWSSSANGVQVSQYTNAFSVVSSLPAGAAIASDKKIDSIFYAGSGNQFYL  602

Query  596  STDGGKTFTTAAGTLGGSTSPVKVAVNPKTSGDVWVSTDKGLFHSTNSGASFSAVSGITQ  655
            STDGGKTFT  A TLG S+S   V  NP  +GDVWVSTD GLFHS N+G SFSAVSG++Q
Sbjct  603  STDGGKTFTKQA-TLGTSSSTSTVIANPGVTGDVWVSTDTGLFHSINNGTSFSAVSGVSQ  661

Query  656  AWAIALGAPESTNAYPAVFAAANVAAGSGGGIGYYRSDNGGKNWVKINDAAHGFGSISSN  715
            AW+I+ GAP ST  YPA+FA A+++    G +GY+RSD+ G NWV+INDAAHGFGS S+N
Sbjct  662  AWSISFGAPASTGGYPALFAIADIS----GVVGYFRSDDAGTNWVQINDAAHGFGSASAN  717

Query  716  VLTADPRVYSRVYIGTNGRGIFYGE  740
            V+  DPR+Y R Y+GTNGRGIFYG+
Sbjct  718  VIAGDPRIYGRAYVGTNGRGIFYGD  742
```

Figure 32: BLASTp result of protein 138266. The protein sequence of protein 138266 was annotated with the JGI *Phanerochaete chrysosporium* database and subsequently blasted (NCBI database, default settings). Accordingly, query corresponds to protein 138266, Sbjct is the amino acid sequence of the most similar protein. – indicates gaps, while + indicate similar but not identical amino acids.

This analysis revealed that protein 138266 shares 66 % identity with a protein annotated as GH74 from another species of *Phanerochaete*. This glycosidase hydrolase family consists of xyloglucanases.

4.2.4 Target identification of serine hydrolases

After the ABPP workflow was optimized for *P. chrysosporium* and a full secretome analysis was successfully performed, this workflow was applied to identify SHs in the

secretome of *P. chrysosporium*. Accordingly, a large scale ABPP experiment with a FP-tri probe was next performed. *P. chrysosporium* was grown either in MYP medium or on oak wood chips as the carbon source and labelled with FP-tri. Before enriched proteins were analyzed by MS, the efficiency of the affinity purification was confirmed by a gel-based analysis (Fig. 33).

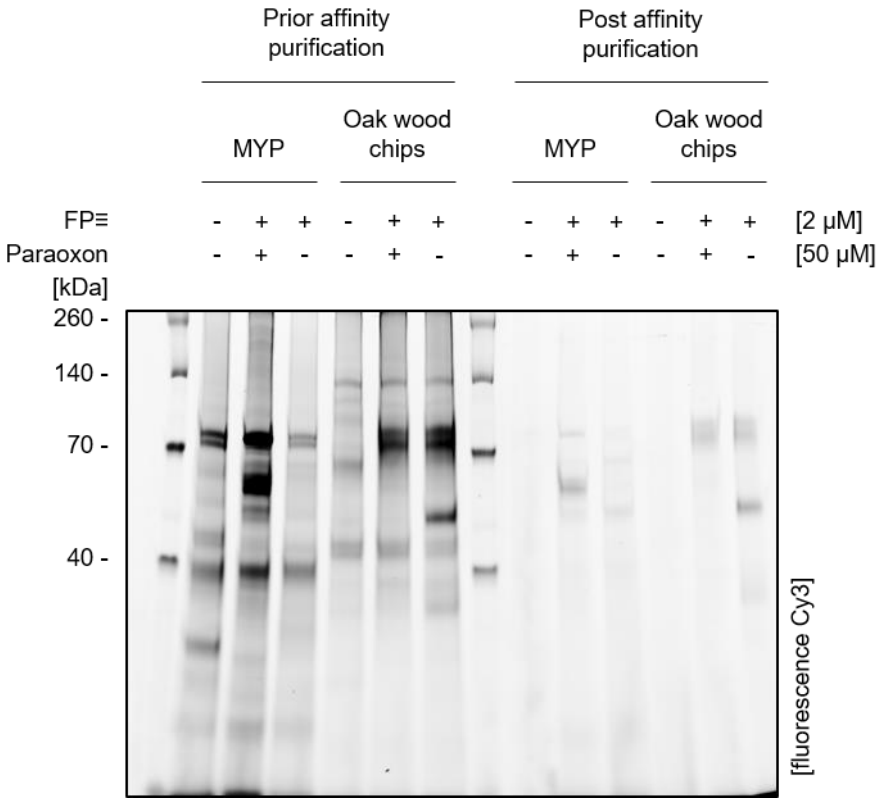

Figure 33: Gel-based control of FP target enrichment Secretomes were labelled with FP-alkyne and subsequently a N3-biotin-Cy3 was coupled to FP-alkyne using click-chemistry. This results in the probe FP-tri which harbors a biotin and Cy3 tag as reporters. Targets of FP-tri were separated by gel electrophoresis and visualized by a fluorescence scanner. To confirm the efficiency of the affinity purification step, samples prior and post affinity enrichment were compared.

The fluorescence scan revealed labelling of one distinct band at about 40 kDa in the MYP secretome and two prominent bands in the wood secretome, at about 70 and 50 kDa, previous to affinity enrichment. After affinity enrichment, however, a band could be identified only in samples from the wood secretomes; this band could be competed by Paraoxon and has a molecular weight of about 50 kDa. In contrast, the MYP secretome did not reveal any labelling after the affinity enrichment step.

Indeed, the ABPP analysis of the MYP medium-derived secretome did not result in the identification of any SHs via the standard workflow. In contrast, the corresponding workflow used on the secretomes grown on oak wood chips revealed 21 enriched targets, of which five were more than 2-fold (on a $\log_2$-scale) enriched compared to the

DMSO control. Their identity as SHs was further confirmed by precompetition with Paraoxon (Fig. 34).

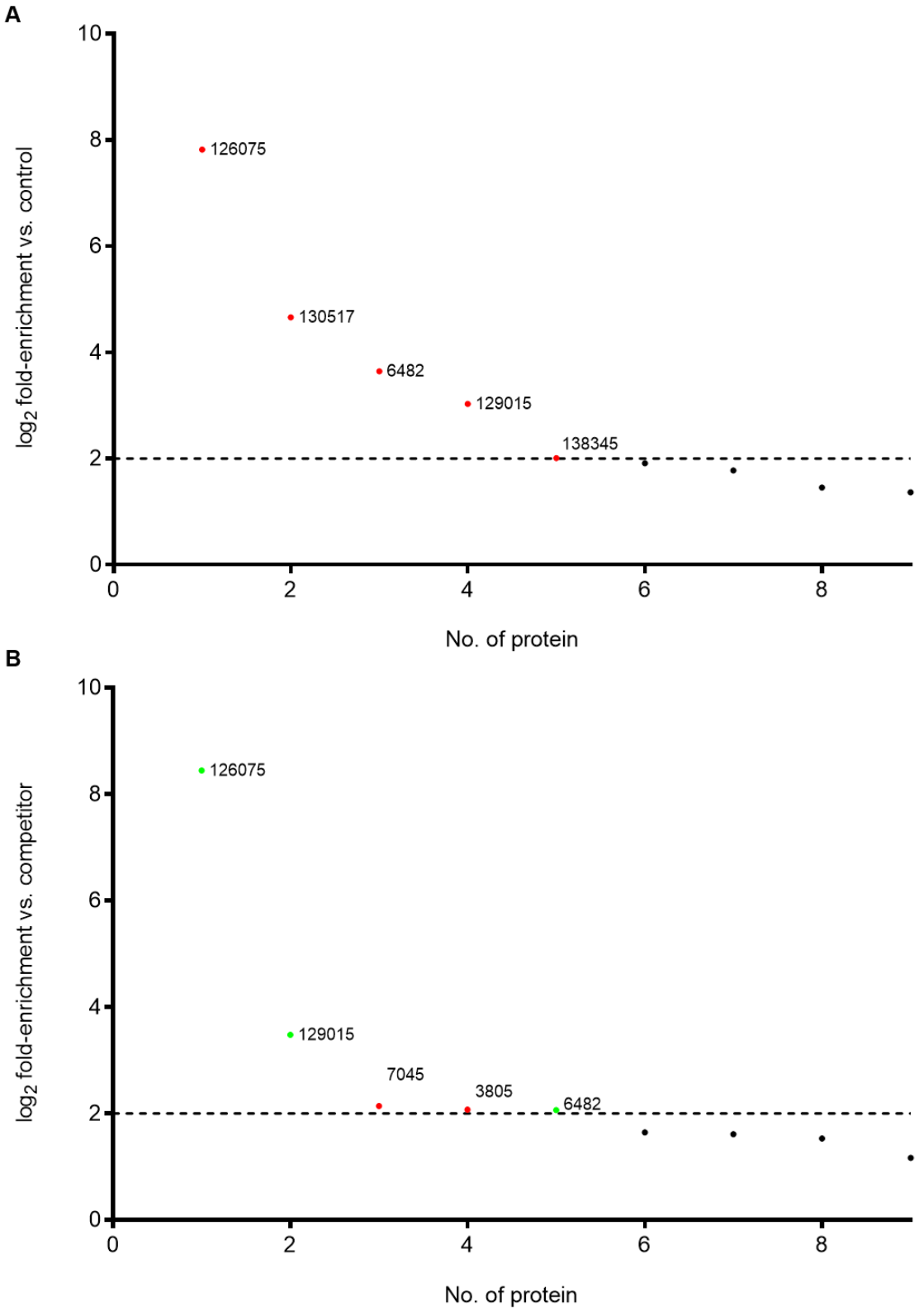

Figure 34: ABPP profiling of oak wood chip-derived secretomes with FP-biotin. (A) SHs of oak wood chip-derived secretomes of *P. chrysosporium* were labelled using FP-biotin and identified by MS. Five proteins were identified with log_2-fold enrichments > 1 (red). (B) Results of a competition experiment with Paraoxon as a competitor. Labelling of three proteins (green) was competed by pre-incubation with paraoxon. Threshold was set to $log_2 \geq 2$ (4-fold enrichment, indicated by the dashed line).

The analysis of the ABPP approach revealed five probe-enriched proteins. Among them, the Protein with the ID 126075 displayed the highest fold-enrichment (8× $\log_2$), thus it was roughly 250-times more abundant (measured in LFQ intensities) than the DMSO control. The competitive ABPP with Paraoxon confirmed that at least three of them were SHs. The corresponding data is summarized in Tab. 8.

Table 8: Overview of the results from the two ABPP experiments. Five proteins were enriched by FP-biotin ABPP. Three of them were confirmed as SHs by a subsequent competitive ABPP approach with paraoxon. These three proteins were annotated using JGI. A potential extracellular localization was predicted by using SignalP.

Protein ID	Mol. weight [kDa]	Score	Localization	Annotations
126075	35.586	91.228	extracellular	Esterase, CBM1, serine active site
6482	44.293	146.45	extracellular	Structural homolog of AXE1
129015	38.877	45.355	extracellular	Acetyl xylan esterase

The identified proteins were subsequently annotated using the Joint Genome Institute (JGI) database. This sequence-based annotation revealed that two of the three targets as annotated esterases: The protein with the ID 126075 is an esterase with a carbohydrate binding module (CBM) and the protein with the ID 129015 is annotated as an acetyl xylan esterase. The protein with the ID 6482 was not annotated, but a homology analysis with the HHpred database (performed by Christian Schmerling, AG Siebers, University of Duisburg-Essen) predicted this protein as a structural homolog of *Trichoderma reseii* acetyl xylan esterase (AXE1). The molecular weights of all three proteins are between 35 to 45 kDa which was in line with molecular weights indicated by the gel and fluorescence analysis (Fig. 33). Importantly, all identified esterases also possessed a secretion signal peptide for extracellular localization.

In order to confirm the most enriched protein (ID 126075) as a target of FP, the protein was overexpressed by Christian Schmerling (AG Siebers, University of Duisburg-Essen) in *Kluyveromyces lactis* (*K. lactis*). This protein was then labelled with FP-Rh in absence or presence of paraoxon. In addition, a commercially available acetyl xylan esterase (synthetic acetyl xylan esterase) as well as three *K. lactis* clones were also profiled with FP-Rh (Fig. 35).

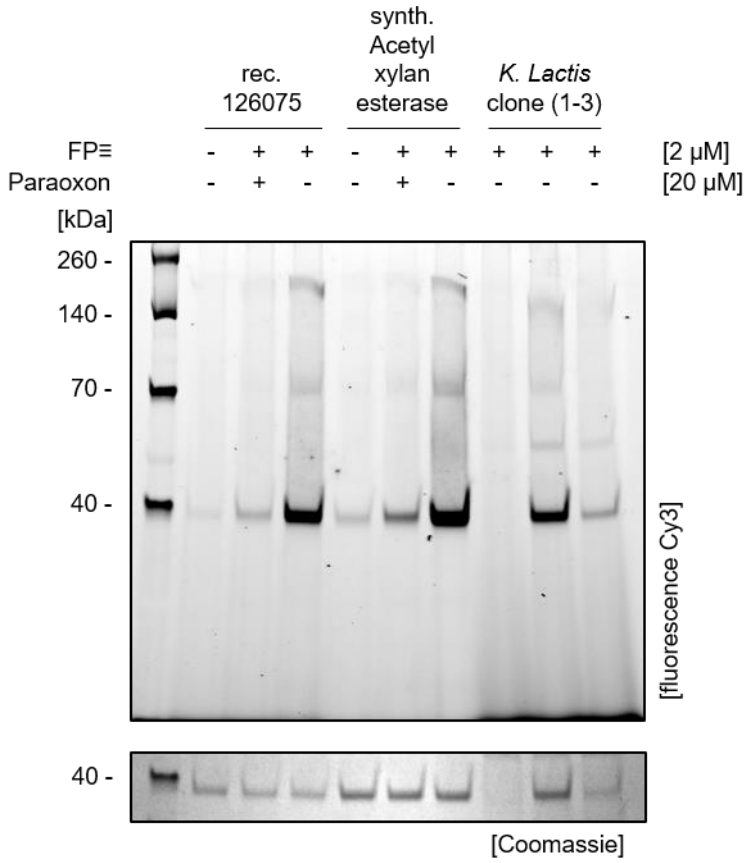

Figure 35: FP-Rh labels acetyl xylan esterases. A competitive ABPP approach with the FP-Rh ABP and the recombinantly expressed protein ID 126075 was performed. As a competitor, Paraoxon was used. These experiments were complemented by a corresponding competitive ABPP approach with a commercially available acetyl xylan esterase (acetyl xylan esterase from *Orpinomyces sp*., Megazyme) and three *K. lactis* clones used for overexpression of protein ID 126075 were performed. Coomassie staining indicated loading levels of protein ID 126075 or the purchased acetyl xylan esterase.

These experiments confirmed that protein ID 126075 could be labelled by FP-Rh and that this labelling could be competed by preincubation with Paraoxon. The same behavior was observed for a commercially available acetyl xylan esterase, i.e. acetyl xylan esterase from *Orpinomyces sp*. Finally, labelling of various *K. lactis* clones showed that FP-Rh also labelled the active protein 126075 in another organism. Of note, clone 1 did not express this protein and was therefore also not labelled. Clone 2 had the highest expression levels and was thus most strongly labelled, while clone 3 expressed the desired protein in much lower levels. Altogether, these experiments revealed that ABPP in the presence of oak wood chips can be used to identify interesting, potentially in wood degradation involved enzymes in *P. chrysosporium.* Finally, esterase activity was proven by spectrophotometric pNPAc-assay (performed by Christian Schmerling, AG Siebers, University of Duisburg-Essen, Fig. 36)

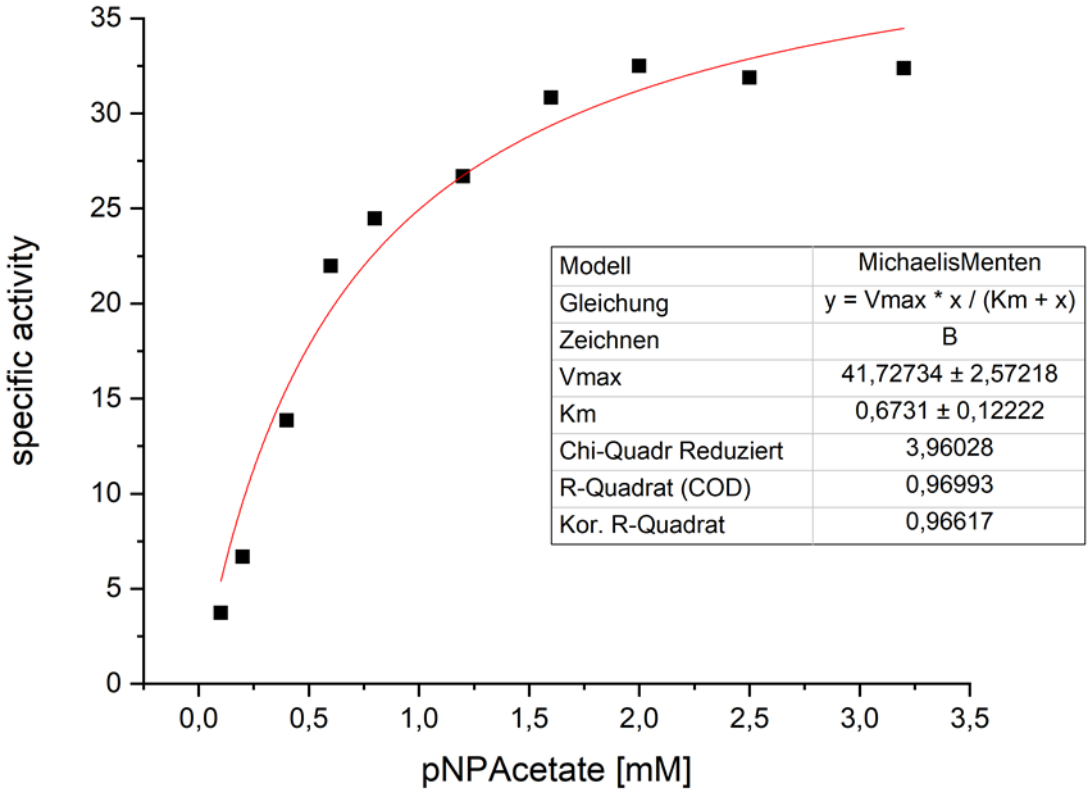

Figure 36: Esterase activity of recombinantly produced protein 126075. The esterase activity was determined by a pNPAc-assay (Christian Schmerling, AG Siebers, cf. section 3.5.9). K_m and V_{max} were calculated using a Michaelis-Menten-model. The specific activity is reported in U/mg.

Indeed, protein 126075 revealed a Michaelis-Menten-like kinetics with the substrate pNPAc, a common substrate to quantify esterase activity. The K_m of protein 126075 was 0.67 mM.

Overall, these data demonstrated that ABPP can be used to identify active esterases in the secretomes of *P. chrysosporium*.

4.2.5 Target identification of glycosidases

After this demonstration, the corresponding approach was extended to glycosidases that were profiled in an analog manner. However, the corresponding protocol was slightly adapted to consider the low acid stability of the glucosidase probe JJB111 (cf. section 3.6.2). Again, affinity enrichment was checked before targets of JJB111 were identified by MS. To this end, a small aliquot of the samples before and after affinity enrichment was subjected to gel electrophoresis and western blotting. Targets of JJB111 were visualized using Streptavidin-HRP, which binds to the biotin moiety of JJB111 (cf. section 3.6.3, Fig. 37).

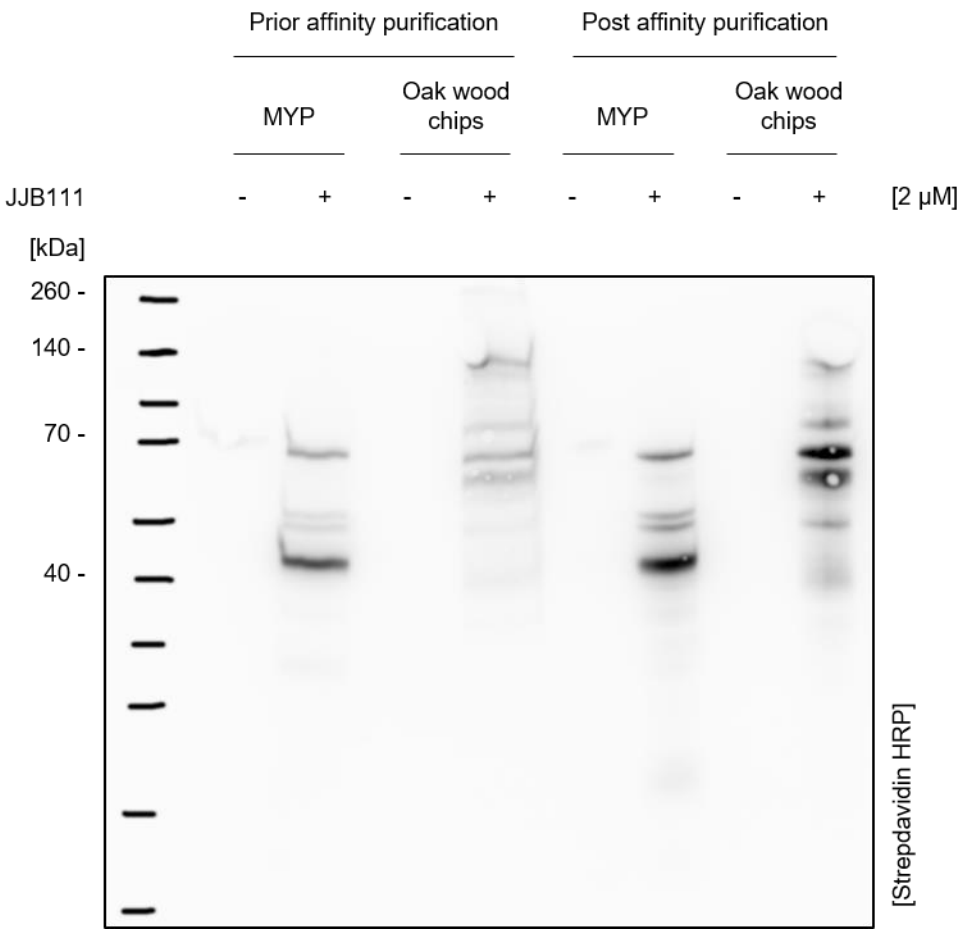

Figure 37: Gel-based control of JJB111 target enrichment Secretomes were labelled with JJB111. Targets of JJB111 were separated by gel electrophoresis and subsequently analyzed by Western Blot. Therefore, Streptavidin-HRP was utilized. To check purification, samples prior and post affinity enrichment were compared.

The Western blot analysis revealed that labelling with JJB111 resulted in four distinct bands in the MYP secretome with molecular weights between 40 to 70 kDa. The intensity of the bands was enhanced after affinity purification. The corresponding labelling of wood secretome resulted in five bands before affinity enrichment with molecular weights from 50 to 140 kDa. After affinity enrichment, the band intensity was enhanced and one band at about 50 kDa became additionally visible.

JJB111 is configured to target β-glucosidases as the stereochemistry of the hydroxyl groups of the warhead of JJB111 mimics a glucose molecule.[31-33] However, binding to glucosidases is irreversible, due to the aziridine moiety in the molecule (cf. section 1.1.2.2). Using this probe in secretomes derived from wood medium, nine proteins were enriched in an ABPP approach, of which six were more than 2-fold $\log_2$-enriched. Of them, the labelling of three proteins could be competed with KY371, a generic glucosidase inhibitor, which features the same warhead as JJB111 without a biotin tag (cf. appendix 8.4.1), thus confirming them as specific JJB111 targets (Fig. 38).

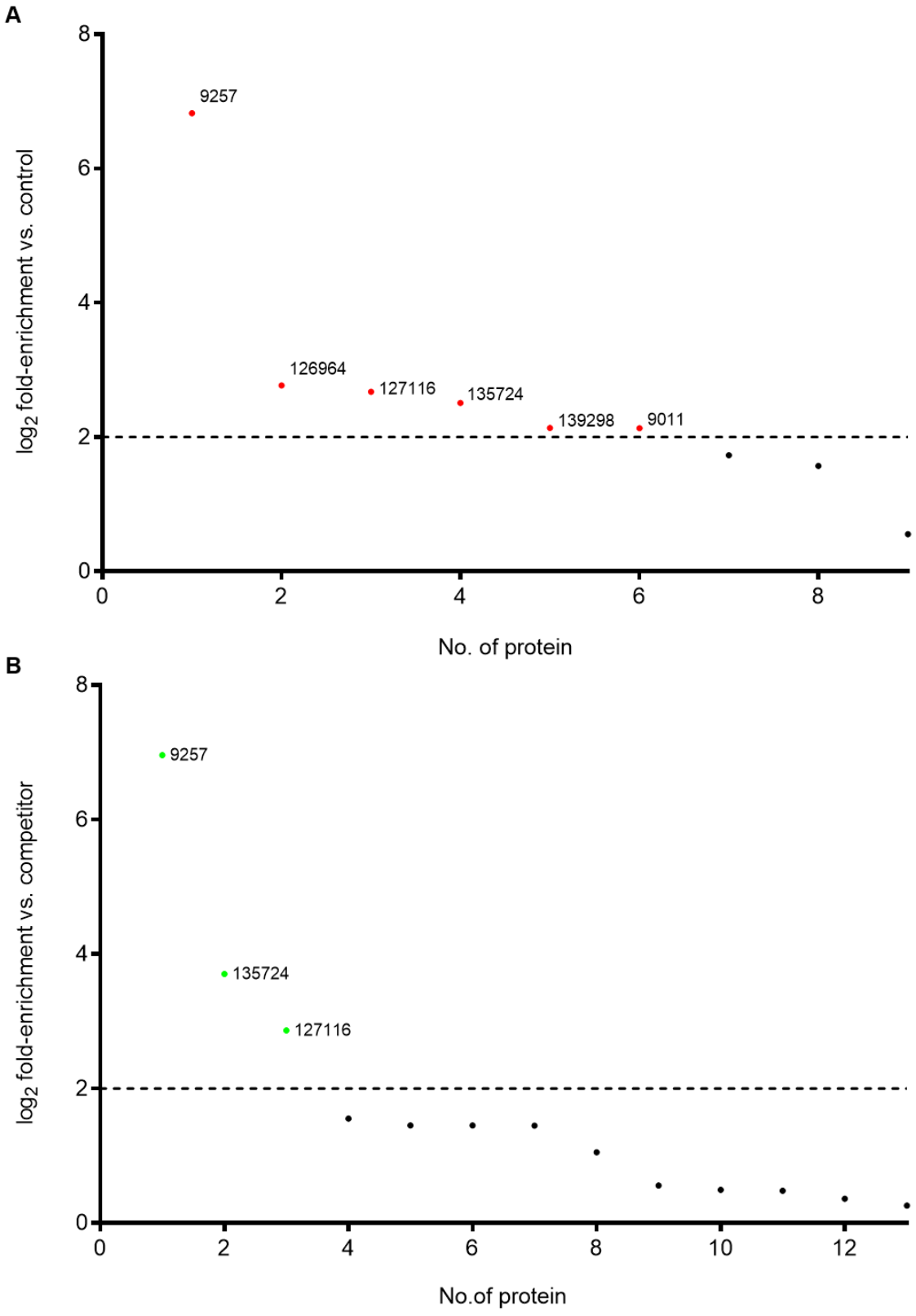

Figure 38: ABPP and competitive ABPP with the glycosidase probe JJB111. (A) A glycosidase profiling with the glucosidase probe JJB111 was performed with secretomes of *P. chrysosporium*, resulting in the identification of 5 proteins (red). (B) To validate them as specific targets of JJB111, a competitive ABPP experiment with JJB111 and the glucosidase-specific inhibitor (KY371) was next performed, confirming three specific targets (green) of JJB111. Threshold was set to $\log_2 \geq 2$ (4-fold enrichment, indicated by dashed line).

A subsequent annotation of these three identified proteins classified them as either GH3 (protein ID 9257) or GH5 (protein ID 135724) glucosidases. Interestingly, despite the fact that protein 127116 was labelled with JJB111 and competed with KY371, this protein was annotated as an Armadillo/beta-catenin-like repeat protein and thus is most probably an off-target. A further analysis revealed that all identified proteins had a molecular weight between 46 to 84 kDa, consistent with Western blot analysis, and harbor an extracellular localization sequence (Tab. 9).

Table 9: Annotation of KY371-competitve JJB111 targets. Proteins were annotated using JGI. Additionally, the presence of extracellular localization sequences was tested by using SignalP.

Protein ID	Mol. weight [kDa]	Score	Localization	Annotations
9257	83.846	22.538	extracellular	Glycoside hydrolase, GH 3
127116	55.691	323.31	extracellular	Armadillo/beta-catenin-like repeat
135724	46.551	41.301	extracellular	Glycoside hydrolase, GH 5

In contrast to the SH ABPP profiling, the corresponding glycosidase ABPP profiling in secretomes of *P. chrysosporium* grown in MYP medium revealed twelve enriched proteins, of which ten were more than 2-fold log_2-enriched. Of note, the identified proteins were thereby mostly unique. Only protein ID 135724 was found in both secretomes. Interestingly, the corresponding log_2 fold-enrichment was thereby even higher in the secretome of *P. chrysosporium* grown in MYP medium (up to 12× log_2) compared to the corresponding from oak wood chips (Fig. 39).

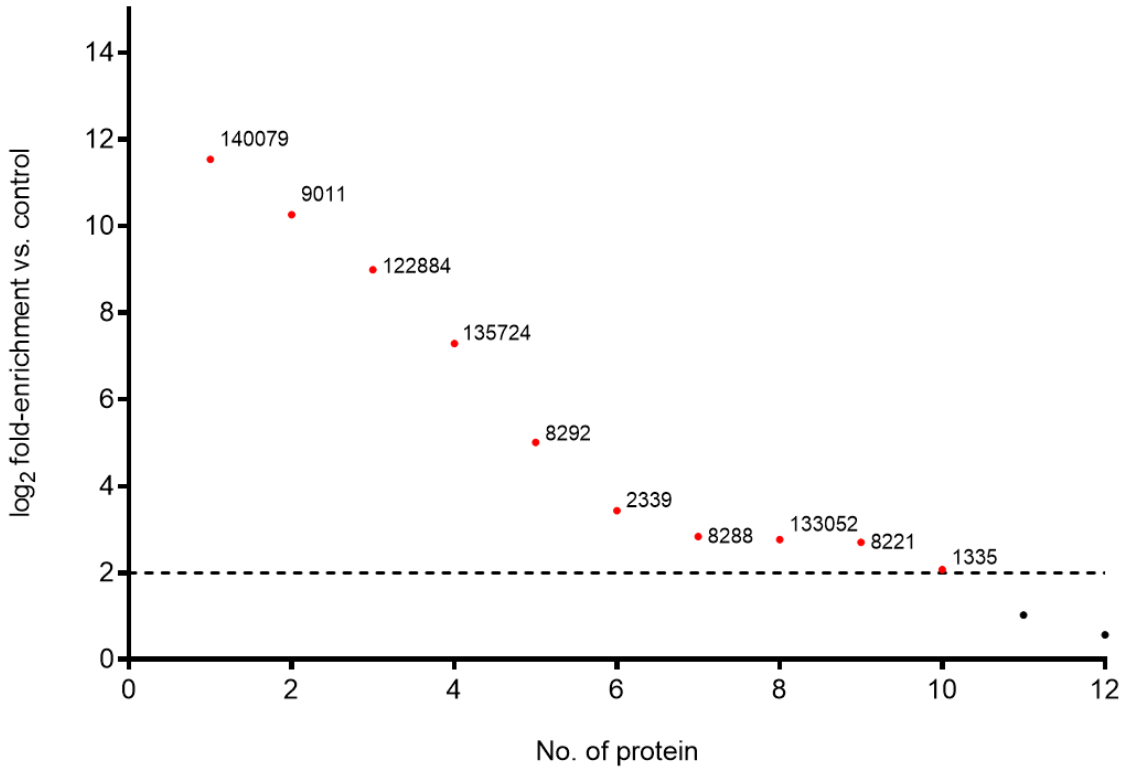

Figure 39: The glucosidase probe JJB111 targets ten proteins in secretomes derived from the MYP medium. The corresponding ABPP approach with JJB111 was also performed on secretomes derived from *P. chrysosporium* grown in MYP medium. Ten proteins (red) with a log_2-fold >2 were identified.

The resulting protein annotations of these ten proteins revealed five glycosidases belonging to GH5, GH 6 and GH 30 families. Their corresponding molecular weights ranged from 14 to 91 kDa (Tab. 7).

Table 10: Annotation of JJB111 ABPP targets in secretomes of *P. chrysosporium* grown on MYP medium. The identified proteins were annotated using JGI. Additionally, the presence of an extracellular localization sequence was tested by using SignalP.

Protein ID	Mol. weight [kDa]	Score	Localization	Annotations
140079	75.377	323.31	extracellular	Six-hairpin glycosidase superfamily
9011	58.843	323.31	extracellular	Glycoside hydrolase, GH 30
122884	73.002	323.31	extracellular	Glycoside hydrolase, GH 5
135724	46.55	323.31	extracellular	Glycoside hydrolase, GH 5
8292	65.736	323.31	extracellular	C-type lectin (carbohydrate binding domain)
2339	114.66	11.641		ATP-dependent DNA ligase
8288	42.92	6.82		Tetratricopeptide repeat
133052	46.293	85.957	extracellular	Glycoside hydrolase, GH 6
8221	14.747	22.585	cell wall	Cerato-platanin
1335	90.961	21.915		RNA binding domain

Interestingly, only the five identified glycosidases and protein ID 8292, a c-type lectin with a carbohydrate binding domain, were found to harbor an extracellular localization sequence. Moreover, all other proteins were found with an overall low score, suggesting that these proteins were most probably off-targets.

To confirm these results, the glucosidase activities of MYP and wood secretomes were tested in the presence of JJB70, which is a structural analogue of JJB111. It shares the same warhead but harbors a fluorophore instead of a biotin tag. The resulting glucosidase activity was determined by Christian Schmerling (AG Siebers, University of Duisburg-Essen) using a standard DNSA assay (Fig. 40).

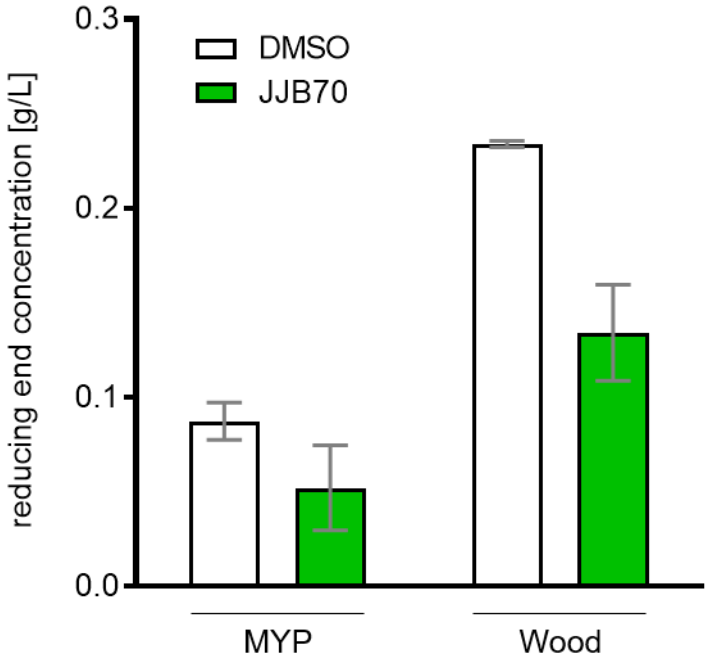

Figure 40: The Glucosidase probe JJB70 reduces glucosidase activity in wood secretomes. The glucosidase activity of secretomes of *P. chrysosporium* grown on MYP or wood medium were determined by a CMC assay either without are after pretreatment with 2 µM JJB70. Error bars indicate standard deviation from two replicates. The assay was performed by Christian Schmerling, AG Siebers.

Indeed, treatment with JJB70 reduced the glucosidase activity in wood medium. However, in MYP medium the mean difference between JJB70- or DMSO-treatment was lower, although a similar trend was observed. Moreover, basal (DMSO) glucosidase activity was lower in MYP than in wood medium. Thus, these results corroborated that JJB111/JJB70 target glucosidases in *P. chrysosporium*.

4.2.6 Secreted hydrolases are highly glycosylated

A gel-based ABPP analysis of FP- as well as JJB70- (the corresponding rhodamine-analogue of JJB111) labelled proteins revealed bands at different molecular weights than the results from the OBD analysis. As secreted proteins are however often

glycosylated, especially in fungi,[94] the corresponding labelling experiments were repeated with secretomes pre-treated with PNGase, which removes N-linked glycans (Fig. 41).

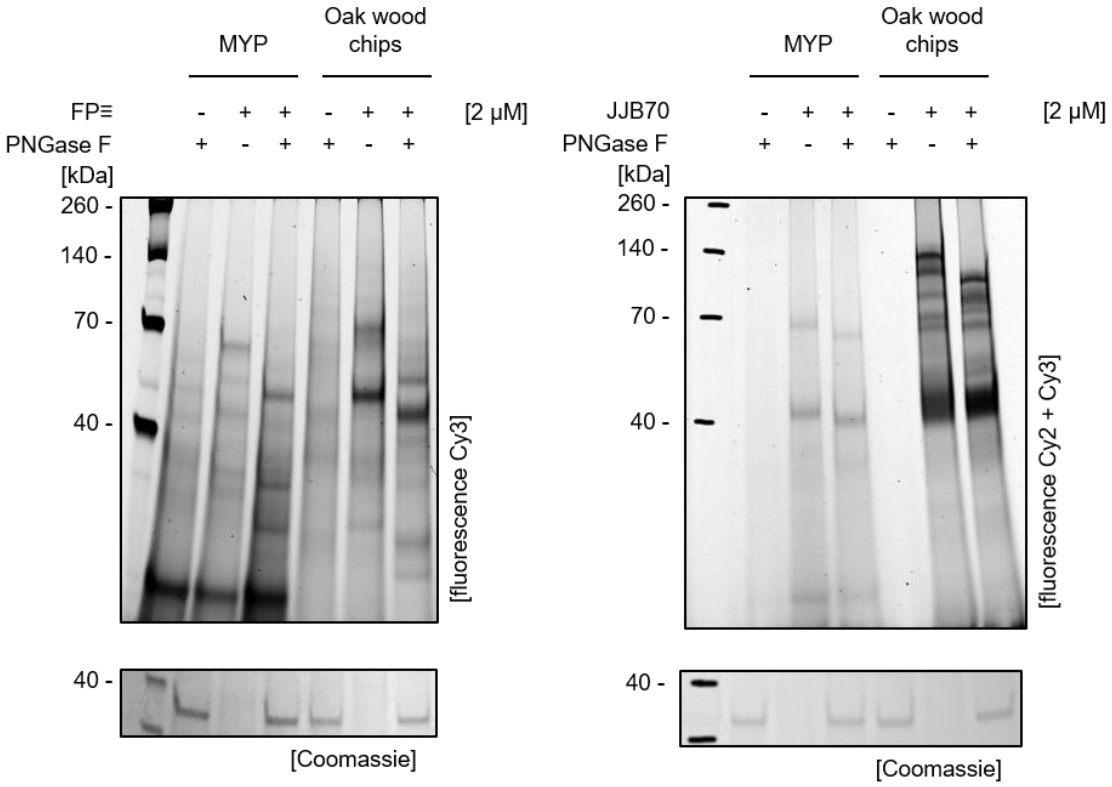

Figure 41: Secreted esterases and glycosidases are highly glycosylated. Proteins from secretomes were labelled using either FP-alkyne and rhodamine-azide or JJB70, a rhodamine analogue of JJB111 with or without pre-treatment of the corresponding secretomes with PNGase to remove N-linked protein glycosylations. Labelled and deglycosylated proteins were separated by gel electrophoresis and visualized by fluorescence. Coomassie staining indicated an equal level of PNGase in pre-treated lanes.

The pre-treatment with PNGase led to bands with strongly reduced molecular weights, thus confirming that many of the secreted proteins were glycosylated. Of interest, the glycosidases thereby appeared to be more strongly glycosylated than esterases as indicated by the higher molecular shifts after pre-treatment.

4.2.7 Heat stability of secreted hydrolases

In order to test the heat stability of the identified hydrolases, which would make them more valuable for future biotechnological applications, a gel-based ABPP after a temperature treatment of the secretomes was next performed (Fig. 42).

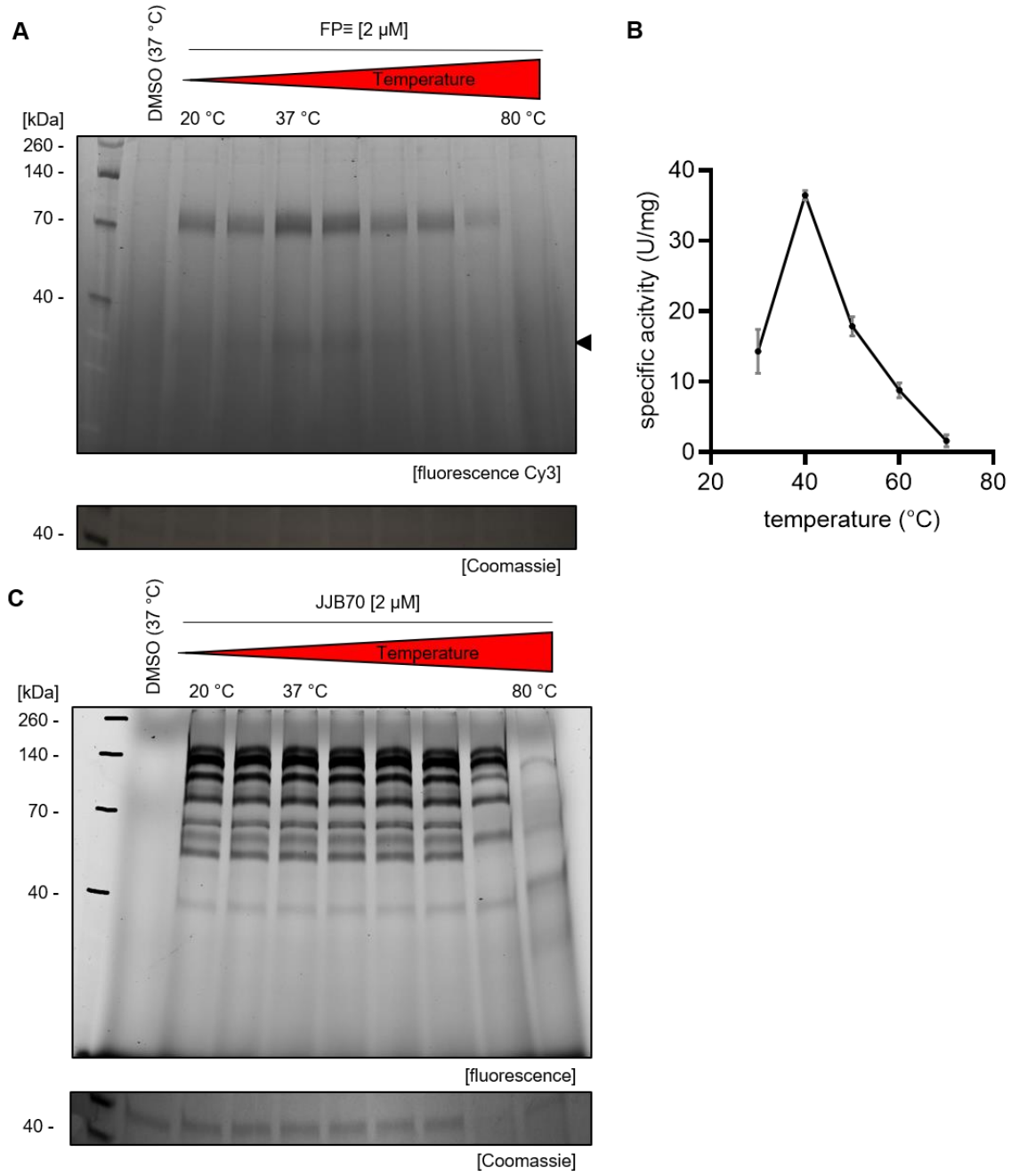

Figure 42: Temperature-dependent hydrolase labelling of wood secretomes. (A) Prior to FP-alkyne labelling, secretomes of *P. chrysosporium* were heated up to the indicated temperatures for 15 min. Labelled proteins were separated by gel electrophoresis. Triangle indicates labelling of the identified esterase (Protein 126075). (B) Esterase activity of the recombinant protein ID 126075 (triangle) was tested by Christian Schmerling, AG Siebers. To this end, the purified protein ID 126075 was heated up prior to activity determination in a biochemical assay. Error bars indicate standard deviation from three replicates. (C) The same experiment as for (A) was performed with the glycosidase probe JJB70. Labelled proteins were separated by gel electrophoresis.

For the esterases, the corresponding ABPP experiments revealed a moderate heat stability up to a maximal temperature of 60 °C. Maximal labelling was thereby observed at 37 – 40 °C (Fig. 42A). A corresponding biochemical assay with the recombinantly produced protein 126075 revealed similar results (Fig. 42B). In contrast, the labelled glycosidases were much more heat stable and were found to be active up to 60 °C.

The majority of them was even active at temperatures up to 70 °C. At 80 °C, however, all hydrolases were no longer labelled (Fig. 42C).

4.2.8 Hydrolase activity is growth time-dependent

A comparative ABPP approach allows to determine enzyme activities at different physiological conditions, e.g. after a certain growth time. To test the impact of growth time on the enzyme repertoire of *P. chrysosporium*, the enzymatic activity of the ABPP-identified esterases and glycosidases was profiled in a time-dependent manner (Fig. 43).

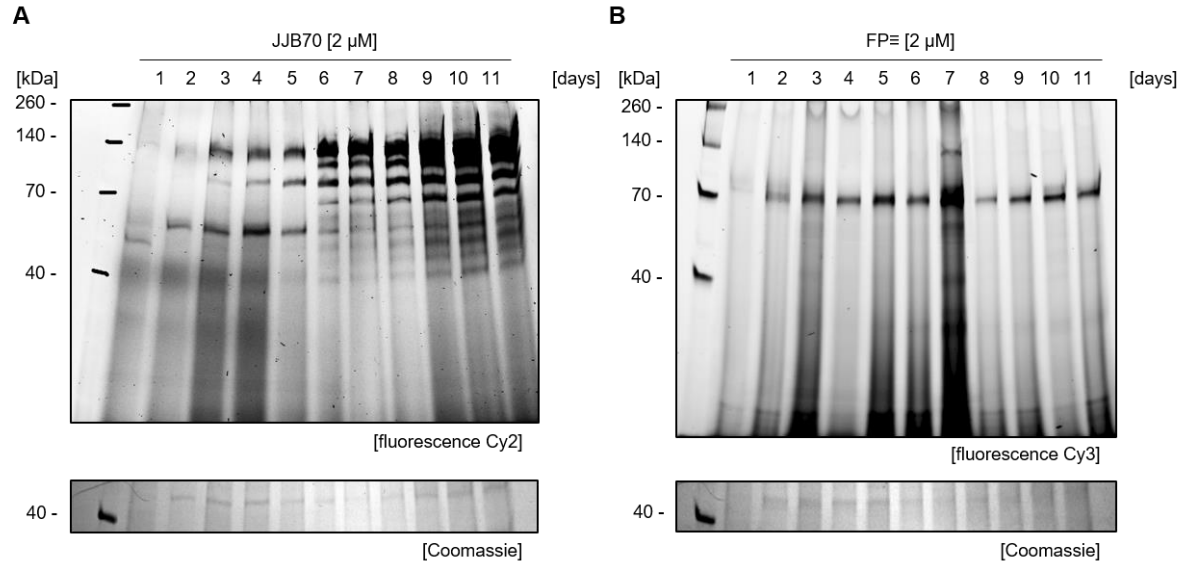

Figure 43: Growth time-dependent ABPP of hydrolases. *P. chrysosporium* was grown in presence of oak wood chips for 11 continuous days and each day, a 2 mL aliquot of the cell culture medium was sampled. The corresponding samples were freeze-dried and subjected to labelling. Labelled proteins were separated by gel electrophoresis (A) Results of the ABPP approach with the glycosidase probe JJB70. (B) Results of the ABBP approach with FP-alkyne after clicking with rhodamine azide.

The subsequent gel-based ABPP analysis revealed that esterase and glycosidase activities in oak wood chip medium were highly time-dependent. More precisely, the observed esterase activity was rather high in the beginning and relatively constant until the sixth day. However, at day seven, a maximum was reached. On day eight, a strong decrease was observed, followed by a steady increase until day eleven.

The corresponding glycosidase activities were less complex. ABPP profiling revealed a constant growth of glycosidase activities over time. At day six, additional glycosidase activities appeared that also continuously increased. Only one protein, i.e. the protein labelled at a molecular weight of ca. 60 kDa, showed a different profile. This protein reached maximal activity after four days and subsequently decreased at the next days.

4.2.9 Labelling of different thermophilic fungi

The presented results demonstrate that ABPP is a promising tool to identify and characterize proteins in secretomes of *P. chrysosporium*. After optimizing the workflow for *P. chrysosporium*, a model organism for fungal wood degradation, the workflow was tested for applicability in other secretomes of promising candidate organisms. These organisms were moderately heat stable and their genome contained various glycosidases and esterases for wood degradation (Frederick Witfeld, AG Begerow, Ruhr-University Bochum). In order to test the established workflow, gel-based ABPP was utilized with the already characterized esterase and glycosidase probes as well as workflows (Fig. 44).

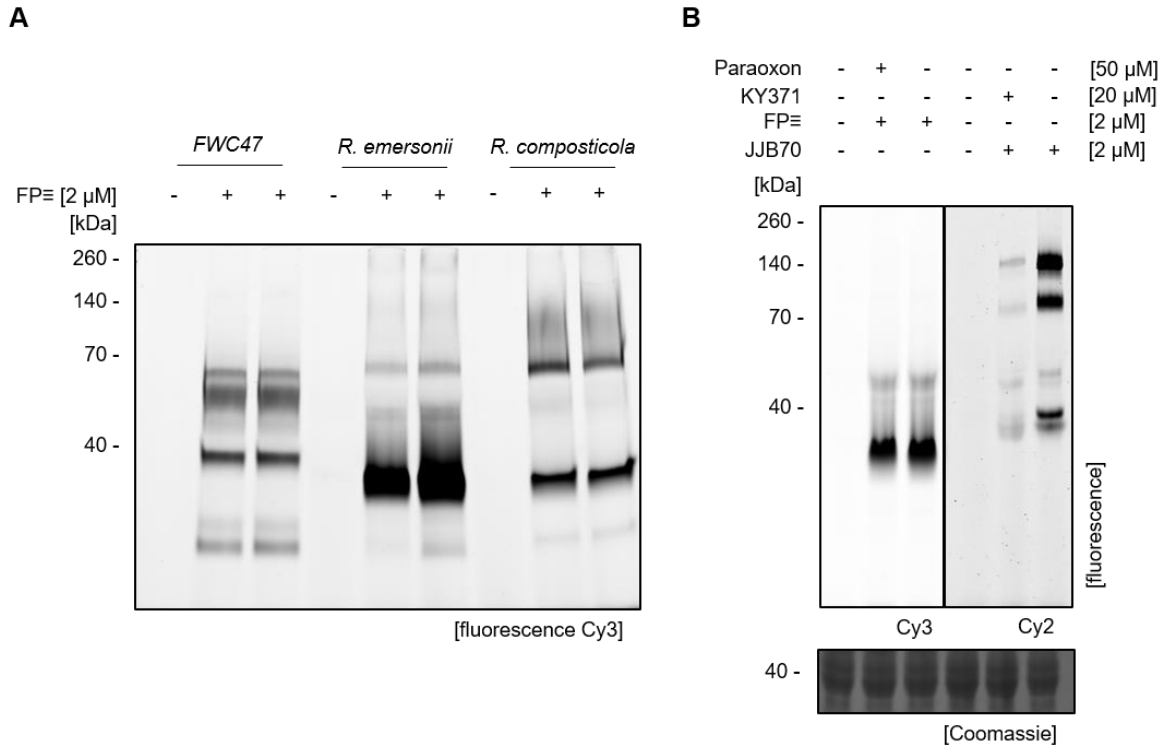

Figure 44: The established ABPP workflow is compatible with application to other thermophilic fungi. (A) Three different isolates from compost heaps were grown for 21 days in medium containing oak wood chips. Secretomes were gained as described before and labelled with FP-alkyne. A Cy3-fluorophor was tagged to FP-alkyne by click chemistry. Labelled proteins were separated by gel electrophoresis and visualized by a fluorescence scanner. (B) *Rasamsonia emersonii* (*R. emersonii*) displayed a high glycosidase activity in the CMC assay (Christian Schmerling, AG Siebers). Therefore, it was chosen for further analysis. *R. emersonii* was labelled with hydrolase probes in a competitive manner and proteins were visualized as described before. FWC47: unknown isolate, *R. composticola*: *Rasamsonia composticola*, growth optimum at 45 – 50 °C.[95]

In a first approach, FP labelling was tested. All organisms were strongly labelled by FP. In FWC47, five bands with molecular weights from 15 to 70 kDa were labelled. Both *Rasamsonia* species showed the same labelling pattern with a prominent band at about 35 kDa (Fig. 44A). As further tests indicated that *R. emersonii* had the highest glucosidase activity (Christian Schmerling, AG Siebers, University of Duisburg-Essen), this candidate was further analyzed using the glucosidase probe JJB70. Competitive

gel-based glucosidase labelling revealed several potential glucosidases while competitive FP labelling revealed that the labelled band could not be competed with paraoxon (Fig. 44B). Altogether, these findings thus indicate that the established ABPP workflow can also be applied to other fungal secretomes.

4.2.10 On-substrate labelling

As a last experiment, the scope of an ABPP approach directly on the substrates and not in the secretome was evaluated. The idea behind this approach was that secreted degradation enzymes bind to the substrate to induce their degradation. As the substrate is removed prior to secretome labelling, this may lead to a loss of potentially active enzymes. Indeed, an electron microscope image taken by Christian Schmerling (AG Siebers, University of Duisburg-Essen) indicated that certain *P. chrysosporium* cultures and thus also degrading proteins adhere directly to the oak wood chip surface.

In an attempt to determine on substrate-bound enzymes, oak wood chips grown in a *P. chrysosporium* culture were labelled with FP-alkyne as well as JJB70 and the resulting labelling was visualized by a gel-based analysis (Fig. 45).

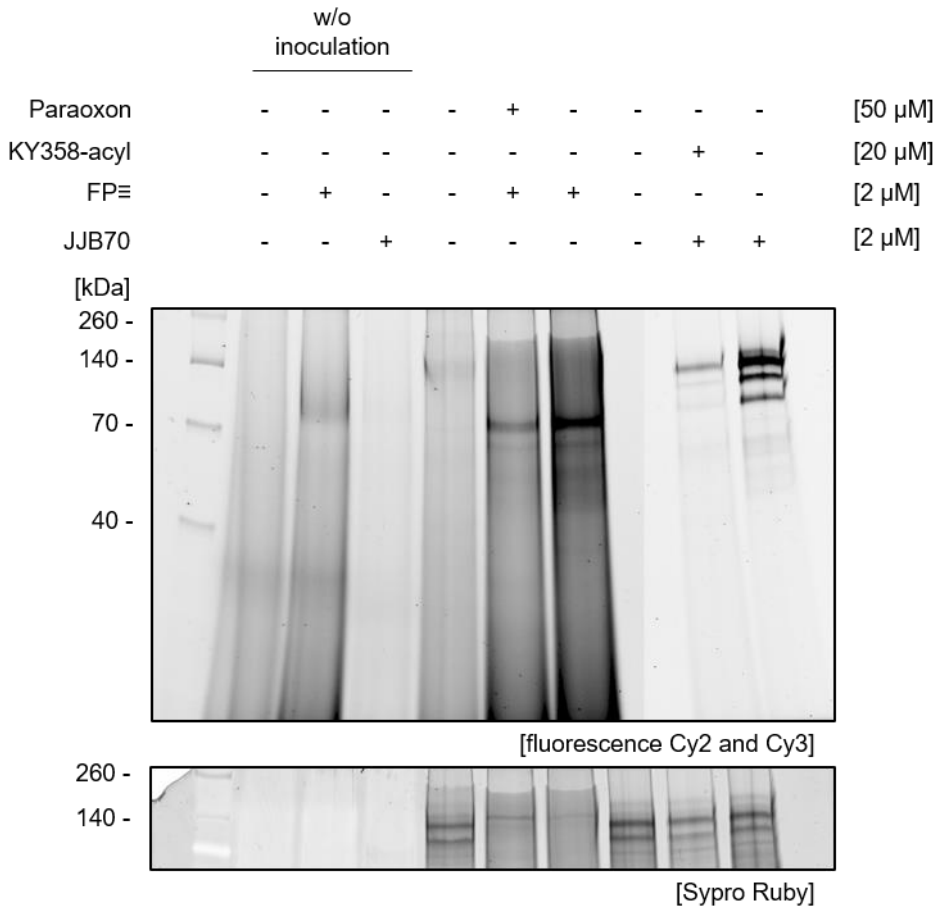

Figure 45: On-substrate labelling of hydrolases. Proteins directly attached to the oak wood chips added as a substrate to *P. chrysosporium cultures* were labelled using FP-alkyne and JJB70 in presence or absence of the competitors paraoxon or KY-358 acyl, respectively. After labelling and click chemistry with rhodamine azide in case of FP-alkyne, proteins were separated by gel electrophoresis and visualized by a fluorescence scanner. Protein loading was evaluated by Sypro Ruby staining.

These experiments revealed that on-substrate labelling also allowed to detect enzyme activities. Importantly, these active enzymes could be competed by their corresponding inhibitors, thus revealing target specificity. In addition, labelling was only detected after *P. chrysosporium* inoculation. Therefore, these experiments demonstrated that this approach can in principle be applied, although further optimizations and the determination of the corresponding labelled proteins is still required.

5 Discussion

5.1 Characterization of Zelkovamycin's bioactivity

The first part of this thesis is devoted to the characterization of the molecular mechanisms underlying Zelkovamycin's bioactivity. To this end, the work of Krahn served as starting point.[12] This work revealed that Zelkovamycin application to human cancer cells leads to an acidification of the culture medium.

In this thesis, the extracellular acidification observation was first confirmed by a cell assay using phenol red as a pH indicator, followed by the elucidation that extracellular acidification is a result of Zelkovamycin-mediated increased lactate levels (cf. section 4.1.1 and 4.1.2). The raise of extracellular lactate levels thereby indicates metabolic dysfunction which comes along with increased glycolysis. Glycolysis is a well-regulated process which can be increased by an enhanced activity of glycolytic enzymes, for example in conditions of hypoxia or impaired mitochondrial function and subsequent anaerobic metabolization of pyruvate to lactate.[87,89,96] In addition, numerous complex metabolic diseases like obesity or diabetes display this phenotype.[86] To distinguish between activated glycolysis or mitochondrial impairment, key enzymes of both metabolic pathways were next tested.[89,90,97] As the extracellular acidification phenotype could be mimicked by OXPHOS inhibitors, the first hypothesis was that Zelkovamycin also impairs mitochondrial function. Indeed, analysis of key enzymes revealed that PFK activity (glycolysis, cytosol) was not affected by Zelkovamycin treatments, while the activity of PDH (citrate cycle, mitochondrial matrix) was found to be decreased (cf. section 4.1.2). Therefore, Zelkovamycin leads to a metabolic switch towards glycolysis because of mitochondrial damage. This hypothesis was corroborated by the finding that Zelkovamycin distinctly decreases cell viability in glucose-deprived cells compared to cells grown in high glucose medium. These findings were further supported by the observed higher vulnerability of SH-SY5Y cells for Zelkovamycin treatment, as for example seen in the lower IC_{50} values in cell viability assays (cf. section 4.1.3).

In order to gain more insights into the molecular mode-of-action, proteomes of Zelkovamycin-treated cells were next analyzed. The protein levels of HeLa cells after Zelkovamycin treatment were analyzed by quantitative LFQ-based MS-analysis that revealed a decrease of numerous mitochondrial proteins. Particularly, OXPHOS complex subunits were much less abundant (cf. section 4.1.2). This finding is in

accordance with previous results showing that impairment of mitochondrial function leads to decrease of the levels of mitochondrial proteins.[98,99] These findings thus supported that Zelkovamycin impairs mitochondrial function. This phenotype may be caused by a specific inhibition of OXPHOS by Zelkovamycin. Thus, the next step was to analyze OCR after Zelkovamycin treatment. Indeed, OCR immediately dropped after application of Zelkovamycin in three different cell lines (cf. section 4.1.4). Interestingly, OCR could not be recovered by application of FCCP which is used in this type of experiments to force the RRC. Pfleger *et al.* reported that RRC mostly relies on complex II activity.[100] Accordingly, activity of Zelkovamycin against different OXPHOS complexes was tested. Zelkovamycin displayed a micromolar IC_{50} (estimated, not calculated) against complex II and slightly inhibited complex I in a micromolar range (cf. section 4.1.7). This is in line with the assumption that Zelkovamycin targets complex II as RRC was not induced by FCCP after treatment with Zelkovamycin. However, due to an interference of Zelkovamycin with the biochemical complex II assay (appendix Fig. 46), these data have to be considered with care. To show the impact of Zelkovamycin on OCR regulation also in other cell lines, WM3734 cells, a melanomal cell line dependent on OXPHOS, were treated with Zelkovamycin for 16 h and a 'classical' OCR analysis was performed (cf. section 4.1.5). The results of these experiments showed that Zelkovamycin affected already basal OCR. However, calculation of the detailed OCR parameters revealed that Zelkovamycin mostly decreased RRC, corroborating the hypothesis that Zelkovamycin most likely targets complex II. Similar effects of complex II inhibition were already reported by Pfleger *et al.*[100] In this study, the known inhibitor 3-nitro propionic acid was used to inhibit complex II activity.

Complex II is a particular element of the OPXHOS system. It has a bivalent function, since it is also part of the citrate cycle. Complex II does not function as a proton pump nor does it take part in OXPHOS supercomplex formation.[101,102] These properties illustrate that complex II activity is not essential for OXPHOS function. This corroborates our findings that Zelkovamycin does not completely abolish mitochondrial respiration like strong OXPHOS inhibitors as for example Rotenone or AMA.

Many cancer cells rely on glycolysis to fulfill their metabolic needs.[103,104] However, recent reports illustrate that some cancer cells have an OXPHOS dependency.[105] To test Zelkovamycin in this clinical background, Zelkovamycin's bioactivity was evaluated in OXPHOS-dependent cancer cell lines (cf. section 4.1.5). WM3734 skin cancer cells

possess a mutation leading to OXPHOS dependency.[91,92,106] Moreover, combined treatment of these cells with OXPHOS inhibitors leads to an increased cell death. Zelkovamycin strongly reduced cell viability of WM3734 cells. In contrast, the related, however non-OXPHOS-dependent MeWo skin cancer cells were not affected by Zelkovamycin, indicating Zelkovamycin-specific OXPHOS inhibition properties. Recent reports highlight the role of OXPHOS inhibitors in treatment of OXPHOS-dependent cancer cells.[105,107,108] Overall, these results suggest that Zelkovamycin has the potency to become an important drug in combinatorial treatment of OXPHOS-dependent cancer cells, as it simultaneously displays only low effects in other cell lines (Fig. 23).

To this end, Zelkovamycin was also evaluated in other cancer cell lines. Visceral cell lines like HeLa showed only slight global effects upon Zelkovamycin treatment. However, cells lines that mainly utilize OXPHOS for energy production, like SH-SY5Y or WM3734 were more sensitive. Nevertheless, all cell lines responded with higher extracellular lactate levels and decreased OCR, indicating a general molecular mechanism in all these cell lines. In addition, a first SAR analysis revealed that Zelkovamycin's bioactivity relied on the presence of the 4-methoxy tryptophan and 2-methyl-dehydro threonine moiety as a substitution by tryptophan or 2-methyl threonine, respectively, led to a loss of bioactivity (cf. section 4.1.6). Interestingly, argyrin B as an alternative member of the argyrin natural product family did not show similar effects as Zelkovamycin. Both compounds do not only both belong to the argyrin family[12] but also share a 4-methoxy tryptophan residue (however at a different position in the macrocycle). Interestingly, it was reported that argyrin B inhibits mitochondrial elongation factor G1 and thus an alternative mitochondrial target.[15] Hence, Zelkovamycin possess a unique bioactivity in the argyrin family. Accordingly, Zelkovamycin may represent a promising starting point to develop more potent OXPHOS inhibitors with potential applicability, e.g. in cancer therapy.

5.2 The identification of hydrolases from thermophilic fungi via ABPP

P. chrysosporium is a thermophilic fungus which is able to degrade all components of wood. To this end, it biosynthesizes a whole arsenal of different hydrolases and ligninases. Naturally, these enzymes are of potential biotechnological interest and this organism may thus represent a promising source for the identification of such enzymes. In this study, the use of ABPP for identifying such proteins from *P. chrysosporium* was described. Accordingly, an ABPP workflow was established and in a second step applied to perform a hydrolase screening. The focus was put on

esterases and glycosidases which were identified by ABPP and also partly characterized. In addition, a full secretome analysis of *P. chrysosporium* after growth in different medium conditions was performed.

The full secretome analysis revealed more than 380 proteins in the secretome of *P. chrysosporium* (cf. section 4.2.3). Of note, 318 of these proteins were significantly regulated depending on the carbon substrate supplemented into the growth medium. Among them, 179 were annotated to be extracellular localized. This analysis so far displays the most comprehensive secretome analysis of *P. chrysosporium* as Wymelenberg *et al.* reported only about 140 proteins until now.[73] This analysis therefore may serve as a source for the detailed investigation of the secretome dynamics resulting from different nutrient environments. For example, the most regulated protein 138266 displays a BNR/Asp-box repeat which was shown to appear in different glycoside hydrolases.[109] Sequence alignment by BLASTp revealed homology (66% identity) to a GH74 protein of *Phanerochaete carnosa.* In the CAZy database, GH74 glycosidases are annotated as xyloglucanases. Indeed, this protein is most strongly downregulated in secretomes derived from MYP medium which makes sense as this medium lacks xylose and other hemicellulose sugars. In contrast, growth media containing polysaccharide substrates, like oak wood chips, display a high content of this protein.[73,110]

In the next experiments, a workflow for a gel-based ABPP analysis was established and subsequently used for profiling fungal hydrolases (cf. section 4.2.1). Wright and Overkleeft reported the use of ABPP to identify lignocellulolytic enzymes in fungal secretomes.[111-113] However, in these studies, *Trichoderma reseii* or *Aspergillus niger* were screened. Both of these fungal model organisms secrete a huge arsenal of cellulolytic enzymes, but they lack the ability to biosynthesize ligninases and therefore cannot completely degrade dead plant biomass.[68,69] Thus, *P. chrysosporium* as a ligninase biosynthesizer displays a more relevant candidate fungus for identifying enzymes for degrading dead plant biomass.

For the ABPP approach in *P. chrysosporium* secretomes, two established ABPs were used. To identify esterases, FP-based probes were employed while two glycosidase probes (JJB111 or JJB70) were used for profiling glycosidases. Overall, three esterases were successfully identified in the secretomes of *P. chrysosporium* grown in presence of wood medium, i.e. oak wood chips (cf. section 4.2.4). One protein (protein 126075) was further characterized and displayed a moderate heat stability (cf. section

4.2.7). This protein was annotated as a member of the CE1 family, a class of enzymes with acetyl xylan esterase activity. Such esterases are pivotal enzymes for the first steps in wood degradation.[29,30,114] Hemicellulose, which is the second most abundant natural polymer, contains acetyl side chains on several of its glucose monomer units. Acidification of the monomers protects the hemicellulose polymer from degradation by specific glycosidases. About 50% of the xylan polymers are acidified.[29,114] So far, only one acetyl xylan esterase was reported in the secretomes of *P. chrysosporium* (Uniprot ID: H2ESB9, JGI ID: 129015).[83] This protein was also identified by our approach, confirming the power of the established method. Additionally, two glucoronyl esterases were reported in 2009.[115] To conclude, the approach enabled to identify two unknown esterases with validated esterase activity in the secretome of *P. chrysosporium*.

Analogously to esterase profiling, also glycosidases were identified. Apparently, these glycosidases are overtaking the next steps in wood degradation via cleavage of cellulose polymers into smaller units. Three proteins were confirmed as specific targets of the glycosidase probe JJB111(cf. section 4.2.5). The subsequent protein annotation revealed that they were either GH3 or GH5 family members. However, one identified protein was annotated as an Armadillo/beta-catenin-like repeat domain-containing protein. Further studies are required to better understand if this protein harbours a so far unidentified glycosidase activity or is an off-target. The identification of glycosidases of the GH3 and GH5 family matches with the target selectivity of the used probe which was designed to target exo-glycosidases, particularly exo-β-glucosidases. Both the GH3 and GH5 families contain many exo-β-glucosidases. In order to confirm these GH3 and GH5 glycosidases as targets of the glycosidase probe, the glycosidase activity of *P. chrysosporium* in the presence of the probe (Fig. 40) was tested by a DNSA assay. Indeed, the glycosidase probe inhibited glucosidase activity in wood secretomes, confirming that this probe targets active glycosidases.

Moreover, glycosidases were also identified in secretomes of *P. chrysosporium* grown in MYP medium (cf. section 4.2.5). These were even more than in secretomes grown on wood chips. Four of the identified proteins were members of specific GH families, i.e. GH30 and GH6. Many GH30 glycosidases display a xylanase activity, while GH6 are frequently general endoglucanases. The identified glycosidases from the secretomes from growth on MYP or oak wood chips medium were thereby highly different as only one protein was found in both samples. This finding supports the notion that *P. chrysosporium* secretes specific proteins depending on the accessible

carbon source. ABPP of glycosidases was also performed in a temperature-dependent manner which revealed a high heat stability of the identified glycosidases (cf. section 4.2.7). The glycosidases were still labelled at similar levels even after a pre-incubation at 70 °C. In contrast, the esterases were only moderately heat stable, loosing activity at temperatures > 40 °C which fits with the optimum growth temperature of *P. chrysosporium*.

Recently, Overkleeft and coworkers introduced ABPP of xylan-degrading enzymes in the secretomes of fungi.[113] In this study, xylosidase ABPs were used to target enzymes form *Aspergillus* secretomes. This work delivered similar results regarding the identification of glycosidases with pronounced heat stability, even though *Aspergillus* is not a thermophilic fungus.[69] These results indicate that the observed heat stability is not directly dependent from the life form of the producing fungus but seems to be a more generic feature of fungal glycosidases. Moreover, although *Aspergillus* is a model organism for secretome analysis of fungi, it lacks the ability to completely degrade wood as it cannot metabolize lignin. Therefore, *P. chrysosporium* is a more relevant organism for identifying enzymes relevant for the degradation of dead plant material. Indeed, this study identified esterases that mediate the breakdown of acetylations on hemicellulose and cellulose, respectively. Overall, this thesis and the works of the Overkleeft group showed that ABPP can be used to identify enzymes from the secretomes of fungi. The generality of the established workflow is further proven by a transfer to another fungi species (*Rasamsonia emersonii*, Fig. 44).

Despite the advances that ABPP obviously has for characterizing and identifying enzymes from fungal secretomes, there are still some pitfalls. For example, as secreted proteins of fungi are highly glycosylated, these proteins are hard to identify by MS as standard analysis workflows will not identify glycosylated peptides leading to lower identification rates. Indeed, the labelling experiments in this thesis demonstrated that also proteins of *P. chrysosporium* are highly glycosylated (cf. section 4.2.6). As the activity of secreted proteins however often depend on glycosylation,[94,116] a deglycosylation reaction prior to ABPP analysis is not a viable option. Alternative MS workflows to better identify such proteins are thus still required.

Finally, first steps to establish an ABPP directly on substrates were undertaken (cf. section 4.2.9). It was shown that proteins bound to the wood substrate can also be labelled. With this method in hand, an alternative ABPP approach may be further developed that may help to identify enzymes that are not soluble in the medium but

strongly attached to the substrates. However, also here, further technical advances are however still required.

The presented workflow seems to be suitable for screening hydrolases also in other fungal secretomes which will enable alternative approaches to elucidate new enzymes of biotechnological relevance. An interesting application is thereby a growth time-dependent search, as protein secretion is highly dynamic and dependent on extracellular factors (cf. section 4.2.8). Therefore, an easy technology to analyze the enzyme repertoire at different physiological conditions is required and is given by the present ABPP approach. The ABPP approach can thereby be performed with or without gel-based analysis.

To summarize, an ABPP profiling approach was successfully established in *P. chrysosporium*. This approach also enabled a rapid characterization of the identified proteins, e.g. their heat stability. As *P. chrysosporium* is an organism capable to secrete the complete repertoire of lignocellulolytic enzymes, this approach may yield new biotechnologically useful enzymes for biomass degradation. In addition, the first identification of esterases which are pivotal for initiation of hemicellulose degradation, by ABPP was achieved. A broader application of this approach in other organisms and with other biotechnological aims is therefore warranted for the future. The established workflows seem to be compatible with many different future applications.

6 Outlook

This thesis shows that Zelkovamycin directly inhibits OXPHOS, most probably via complex II. Complex-specific OXPHOS inhibitors are known chemical tools for biological research. This study thus represents a promising starting point for further studies, e.g. the improvement of Zelkovamycin's bioactivity by chemical derivatization and a further characterization of its biological properties. For example, further studies to validate that Zelkovamycin indeed targets complex II are required. Complex II enrolls a bidirectional activity, on the one hand it functions as an electron carrier in the ETC and on the other hand it is part of the citrate cycle with its SDH subunit.[117] Moreover, only a few inhibitors for complex II are known. These inhibitors have to be used in micromolar or higher concentrations, for example TTFA, 3-nitropropionic acid or Triclosan.[118,119] Zelkovamycin thus may represent a better inhibitor for this difficult to target complex, warranting further studies. Additionally, an alternative interesting line of research could be to better characterize the molecular consequences resulting from the Zelkovamycin-induced metabolic switch. To this end, a thorough metabolomics analysis of Zelkovamycin-treated cells could give interesting insights. Accordingly, Zelkovamycin remains an interesting natural product for further chemical biology investigations.

The established ABPP-based hydrolase profiling in the thermophilic fungus *P. chrysosporium* identified a set of esterases and glycosidases. An ABBP-driven characterization of these hydrolases revealed – at least partly – favorable properties like heat stability, which makes them interesting for probable biotechnological approaches, like e.g. in the paper industries. To this end, these hydrolases however have to be studied in more detail. In addition, this work shows that ABPP is a suitable tool to identify hydrolases in thermophilic fungi. The established workflow has already been tested in another thermophilic fungus (*R. emersonii*), in which esterases were successfully enriched and labelled by FP, confirming the general applicability of the presented workflow (data in preparation). In addition, ABPP on-substrate labelling was demonstrated. However, these approaches need further optimizations and applications on other fungi or substrates to fully define their overall scope. Therefore, this thesis only represents the starting point for broader ABPP studies for identifying enzymes from fungal secretomes.

7 References

1 Darwin, C. *On the origin of species, 1859*. (Routledge, 2004).

2 Colegate, S. M. & Molyneux, R. J. *Bioactive natural products: detection, isolation, and structural determination*. (CRC press, 2007).

3 Tabata, N., Tomoda, H., Zhang, H., Uchida, R. & Ōmura, S. Zelkovamycin, a new cyclic peptide antibiotic from Streptomyces sp. K96-0670. *The Journal of antibiotics* **52**, 34-39 (1999).

4 Atsumi, S. *et al.* Production, isolation and structure determination of a novel β-glucosidase inhibitor, cyclophellitol, from Phellinus sp. *The Journal of antibiotics* **43**, 49-53 (1990).

5 Withers, S. & Umezawa, K. Cyclophellitol: a naturally occurring mechanism-based inactivator of beta-glucosidases. *Biochemical and biophysical research communications* **177**, 532-537 (1991).

6 Overkleeft, H. S. & Florea, B. I. *Activity-based proteomics : methods and protocols*. (Humana Press, 2017).

7 Liu, Y., Patricelli, M. P. & Cravatt, B. F. Activity-based protein profiling: the serine hydrolases. *Proceedings of the National Academy of Sciences* **96**, 14694-14699 (1999).

8 Mander, L. & Liu, H.-W. *Comprehensive natural products II: Chemistry and Biology*. Vol. 1 (Elsevier, 2010).

9 Fleming, A. Penicillin. *British medical journal* **2**, 386 (1941).

10 Bentley, R. The development of penicillin: genesis of a famous antibiotic. *Perspectives in biology and medicine* **48**, 444-452 (2005).

11 Zhang, H. *et al.* Zelkovamycin, a New Cyclic Peptide Antibiotic from Streptomyces sp. K96-0670. *The Journal of antibiotics* **52**, 29-33 (1999).

12 Krahn, D. *Total synthesis and biological evaluation of Zelkovamycin*, University of Duisburg-Essen, (2016).

13 Sasse, F. *et al.* Argyrins, immunosuppressive cyclic peptides from myxobacteria. I. Production, isolation, physico-chemical and biological properties. *J Antibiot (Tokyo)* **55**, 543-551 (2002).

14 Nickeleit, I. *et al.* Argyrin a reveals a critical role for the tumor suppressor protein p27(kip1) in mediating antitumor activities in response to proteasome inhibition. *Cancer Cell* **14**, 23-35 (2008).

15 Nyfeler, B. *et al.* Identification of elongation factor G as the conserved cellular target of argyrin B. *PLoS One* **7**, e42657 (2012).

16 Bülow, L. *et al.* Synthesis and Biological Characterization of Argyrin F. *ChemMedChem* **5**, 832-836 (2010).

17 Chen, X. *et al.* Therapeutic effects of Argyrin F in pancreatic adenocarcinoma. *Cancer letters* **399**, 20-28 (2017).

18 Tanaka, K. & Matsuda, N. Proteostasis and neurodegeneration: the roles of proteasomal degradation and autophagy. *Biochimica et Biophysica Acta (BBA)-Molecular Cell Research* **1843**, 197-204 (2014).

19 Bogyo, M. & Wang, E. in *The Proteasome—Ubiquitin Protein Degradation Pathway* 185-208 (Springer, 2002).

20 Bachovchin, D. A. & Cravatt, B. F. The pharmacological landscape and therapeutic potential of serine hydrolases. *Nature reviews Drug discovery* **11**, 52 (2012).

21 Rauwerdink, A. & Kazlauskas, R. J. How the same core catalytic machinery catalyzes 17 different reactions: the serine-histidine-aspartate catalytic triad of α/β-hydrolase fold enzymes. *ACS Catalysis* **5**, 6153-6176 (2015).

22 Simon, G. M. & Cravatt, B. F. Activity-based proteomics of enzyme superfamilies: serine hydrolases as a case study. *J Biol Chem* **285**, 11051-11055 (2010).

23 Van Esbroeck, A. C. *et al.* Activity-based protein profiling reveals off-target proteins of the FAAH inhibitor BIA 10-2474. *Science* **356**, 1084-1087 (2017).

24 Zweerink, S. *et al.* Activity-based protein profiling as a robust method for enzyme identification and screening in extremophilic Archaea. *Nature communications* **8**, 15352 (2017).

25 Kaschani, F. *et al.* Diversity of serine hydrolase activities of unchallenged and botrytis-infected Arabidopsis thaliana. *Molecular & Cellular Proteomics* **8**, 1082-1093 (2009).

26 Henrissat, B. & Davies, G. Structural and sequence-based classification of glycoside hydrolases. *Current opinion in structural biology* **7**, 637-644 (1997).

27 Cantarel, B. L. *et al.* The Carbohydrate-Active EnZymes database (CAZy): an expert resource for glycogenomics. *Nucleic acids research* **37**, D233-D238 (2009).

28 Lombard, V., Golaconda Ramulu, H., Drula, E., Coutinho, P. M. & Henrissat, B. The carbohydrate-active enzymes database (CAZy) in 2013. *Nucleic acids research* **42**, D490-D495 (2014).

29 Koutaniemi, S. *et al.* Distinct roles of carbohydrate esterase family CE16 acetyl esterases and polymer-acting acetyl xylan esterases in xylan deacetylation. *Journal of biotechnology* **168**, 684-692 (2013).

30 Koseki, T., Miwa, Y., Akao, T., Akita, O. & Hashizume, K. An Aspergillus oryzae acetyl xylan esterase: molecular cloning and characteristics of recombinant enzyme expressed in Pichia pastoris. *Journal of biotechnology* **121**, 381-389 (2006).

31 Chandrasekar, B. *et al.* Broad-range glycosidase activity profiling. *Molecular & Cellular Proteomics* **13**, 2787-2800 (2014).

32 Li, K.-Y. *et al.* Exploring functional cyclophellitol analogues as human retaining beta-glucosidase inhibitors. *Organic & biomolecular chemistry* **12**, 7786-7791 (2014).

33 Witte, M. D. *et al.* Activity-Based Profiling of Retaining β-Glucosidases: A Comparative Study. *ChemBioChem* **12**, 1263-1269 (2011).

34 Speers, A. E., Adam, G. C. & Cravatt, B. F. Activity-based protein profiling in vivo using a copper (I)-catalyzed azide-alkyne [3+2] cycloaddition. *Journal of the American Chemical Society* **125**, 4686-4687 (2003).

35 Speers, A. E. & Cravatt, B. F. Activity-Based Protein Profiling (ABPP) and Click Chemistry (CC)–ABPP by MudPIT Mass Spectrometry. *Current protocols in chemical biology* **1**, 29-41 (2009).

36 Speers, A. E. & Cravatt, B. F. Profiling enzyme activities *in vivo* using click chemistry methods. *Chemistry & biology* **11**, 535-546 (2004).

37 Bachovchin, D. A. *et al.* Superfamily-wide portrait of serine hydrolase inhibition achieved by library-versus-library screening. *Proceedings of the National Academy of Sciences* **107**, 20941-20946 (2010).

38 Serwa, R. & Tate, E. W. Activity-based profiling for drug discovery. *Chemistry & biology* **18**, 407-409 (2011).

39 Simon, G. M., Niphakis, M. J. & Cravatt, B. F. Determining target engagement in living systems. *Nature chemical biology* **9**, 200 (2013).

40 Cravatt, B. F., Simon, G. M. & Yates, J. R., 3rd. The biological impact of mass-spectrometry-based proteomics. *Nature* **450**, 991-1000 (2007).

41 Jessani, N., Liu, Y., Humphrey, M. & Cravatt, B. F. Enzyme activity profiles of the secreted and membrane proteome that depict cancer cell invasiveness. *Proceedings of the National Academy of Sciences* **99**, 10335-10340 (2002).

42 Kelleher, N. L Top-Down Proteomics. *Analytical chemistry* **76**, 197-203 (2004).

43 Aebersold, R. & Mann, M. Mass spectrometry-based proteomics. *Nature* **422**, 198 (2003).

44 Aebersold, R. & Mann, M. Mass-spectrometric exploration of proteome structure and function. *Nature* **537**, 347-355 (2016).

45 Fenn, J. B., Mann, M., Meng, C. K., Wong, S. F. & Whitehouse, C. M. Electrospray ionization for mass spectrometry of large biomolecules. *Science* **246**, 64-71 (1989).

46 Whitehouse, C. M., Dreyer, R. N., Yamashita, M. & Fenn, J. B. Electrospray interface for liquid chromatographs and mass spectrometers. *Analytical chemistry* **57**, 675-679 (1985).

47 Yamashita, M. & Fenn, J. B. Electrospray ion source. Another variation on the free-jet theme. *The Journal of Physical Chemistry* **88**, 4451-4459 (1984).

48 Tanaka, K. *et al.* Protein and polymer analyses up to m/z 100,000 by laser ionization time-of-flight mass spectrometry. *Rapid communications in mass spectrometry* **2**, 151-153 (1988).

49 Makarov, A. & Scigelova, M. Coupling liquid chromatography to Orbitrap mass spectrometry. *Journal of Chromatography A* **1217**, 3938-3945 (2010).

50 Zubarev, R. A. & Makarov, A. Orbitrap Mass Spectrometry, *Analytical chemistry* **85**, 5288-5296 (2013)

51 Hu, Q. *et al.* The Orbitrap: a new mass spectrometer. *Journal of mass spectrometry* **40**, 430-443 (2005).

52 Cox, J. *et al.* Accurate proteome-wide label-free quantification by delayed normalization and maximal peptide ratio extraction, termed MaxLFQ. *Mol Cell Proteomics* **13**, 2513-2526 (2014).

53 Cox, J. & Mann, M. MaxQuant enables high peptide identification rates, individualized ppb-range mass accuracies and proteome-wide protein quantification. *Nature biotechnology* **26**, 1367 (2008).

54 Cox, J. *et al.* A practical guide to the MaxQuant computational platform for SILAC-based quantitative proteomics. *Nature protocols* **4**, 698 (2009).

55 Rappsilber, J., Mann, M. & Ishihama, Y. Protocol for micro-purification, enrichment, pre-fractionation and storage of peptides for proteomics using StageTips. *Nature protocols* **2**, 1896 (2007).

56 Picotti, P., Bodenmiller, B., Mueller, L. N., Domon, B. & Aebersold, R. Full dynamic range proteome analysis of S. cerevisiae by targeted proteomics. *Cell* **138**, 795-806 (2009).

57 Cox, J. & Mann, M. Is proteomics the new genomics? *Cell* **130**, 395-398 (2007).

58 Gholami, A. M. *et al.* Global proteome analysis of the NCI-60 cell line panel. *Cell reports* **4**, 609-620 (2013).

59 De Godoy, L. M. *et al.* Comprehensive mass-spectrometry-based proteome quantification of haploid versus diploid yeast. *Nature* **455**, 1251 (2008).

60 Legrain, P. *et al.* The human proteome project: current state and future direction. *Molecular & cellular proteomics* **10**, M111. 009993 (2011).

61 Humphrey, S. J., Azimifar, S. B. & Mann, M. High-throughput phosphoproteomics reveals *in vivo* insulin signaling dynamics. *Nat Biotechnol* **33**, 990-995 (2015).

62 Humphrey, S. J., Karayel, O., James, D. E. & Mann, M. High-throughput and high-sensitivity phosphoproteomics with the EasyPhos platform. *Nat Protoc* **13**, 1897-1916 (2018).

63 Nickel, S., Kaschani, F., Colby, T., van der Hoorn, R. A. & Kaiser, M. A para-nitrophenol phosphonate probe labels distinct serine hydrolases of Arabidopsis. *Bioorganic & medicinal chemistry* **20**, 601-606 (2012).

64 Shevchenko, A., Tomas, H., Havli, J., Olsen, J. V. & Mann, M. In-gel digestion for mass spectrometric characterization of proteins and proteomes. *Nature protocols* **1**, 2856 (2006).

65 Weerapana, E., Speers, A. E. & Cravatt, B. F. Tandem orthogonal proteolysis-activity-based protein profiling (TOP-ABPP)—a general method for mapping sites of probe modification in proteomes. *Nature protocols* **2**, 1414 (2007).

66 Lamar, R. T., Larsen, M. J., Kirk, T. K. & Glaser, J. A. Growth of the white-rot fungus Phanerochaete chrysosporium in soil. *Land disposal, remedial action, incineration and treatment of hazardous waste: Proceedings of the 13th annual research symposium*, 419-424 (1987).

67 Tien, M. & Kirk, T. K. *Methods in enzymology* Vol. 161, 238-249 (Elsevier, 1988).

68 Kirk, T. K. Degradation and conversion of lignocelluloses. *The filamentous fungi* **4**, 266-295 (1983).

69 Hamed, S. A. M. *In-vitro* studies on wood degradation in soil by soft-rot fungi: *Aspergillus niger* and *Penicillium chrysogenum*. *International Biodeterioration & Biodegradation* **78**, 98-102 (2013).

70 Agger, J. W. *et al.* Discovery of LPMO activity on hemicelluloses shows the importance of oxidative processes in plant cell wall degradation. *Proceedings of the National Academy of Sciences* **111**, 6287-6292 (2014).

71 Vaaje-Kolstad, G., Forsberg, Z., Loose, J. S., Bissaro, B. & Eijsink, V. G. Structural diversity of lytic polysaccharide monooxygenases. *Current opinion in structural biology* **44**, 67-76 (2017).

72 Bao, W. & Renganathan, V. Cellobiose oxidase of *Phanerochaete chrysosporium* enhances crystalline cellulose degradation by cellulases. *FEBS letters* **302**, 77-80 (1992).

73 Wymelenberg, A. V. *et al.* The *Phanerochaete chrysosporium* secretome: database predictions and initial mass spectrometry peptide identifications in cellulose-grown medium. *Journal of biotechnology* **118**, 17-34 (2005).

74 Kazmi, M. Z. H., Karmakar, A., Michaelis, V. K. & Williams, F. J. Separation of cellulose/hemicellulose from lignin in white pine sawdust using boron trihalide reagents. *Tetrahedron* **75**, 1465-1470 (2019).

75 Lin, L., Yan, R., Liu, Y. & Jiang, W. In-depth investigation of enzymatic hydrolysis of biomass wastes based on three major components: cellulose, hemicellulose and lignin. *Bioresource Technology* **101**, 8217-8223 (2010).

76 Ramsden, M. & Blake, F. A kinetic study of the acetylation of cellulose, hemicellulose and lignin components in wood. *Wood science and technology* **31**, 45-50 (1997).

77 Martinez, D. *et al.* Genome sequence of the lignocellulose degrading fungus *Phanerochaete chrysosporium* strain RP78. *Nat Biotechnol* **22**, 695-700 (2004).

78 Ohm, R. A. *et al.* Genomics of wood-degrading fungi. *Fungal Genet Biol* **72**, 82-90 (2014).

79 Blanchette, R. A., Burnes, T. A., Leatham, G. F. & Effland, M. J. Selection of white-rot fungi for biopulping. *Biomass* **15**, 93-101 (1988).

80 Bumpus, J. A. Biodegradation of polycyclic hydrocarbons by *Phanerochaete chrysosporium*. *Appl. Environ. Microbiol.* **55**, 154-158 (1989).

81 Thakkar, A., Dhamankar, V. & Kapadnis, B. Biocatalytic decolourisation of molasses by *Phanerochaete chrysosporium*. *Bioresource technology* **97**, 1377-1381 (2006).

82 Wariishi, H., Valli, K. & Gold, M. H. *In vitro* depolymerization of lignin by manganese peroxidase of *Phanerochaete chrysosporium*. *Biochemical and biophysical research communications* **176**, 269-275 (1991).

83 Huy, N. D., Thiyagarajan, S., Kim, D.-H. & Park, S.-M. Cloning and characterization of a novel bifunctional acetyl xylan esterase with carbohydrate binding module from *Phanerochaete chrysosporium*. *Journal of bioscience and bioengineering* **115**, 507-513 (2013).

84 Grosse-Holz, F. *et al.* The transcriptome, extracellular proteome and active secretome of agroinfiltrated Nicotiana benthamiana uncover a large, diverse protease repertoire. *Plant biotechnology journal* **16**, 1068-1084 (2018).

85 Neilson, A., Teich, J., Wu, M. & Ferrick, D. Analysis of metabolic activity in cells using extracellular flux rate measurements. U.S. Patent Application Nr. 11/545,714, 2007

86 Adeva-Andany, M. *et al.* Comprehensive review on lactate metabolism in human health. *Mitochondrion* **17**, 76-100 (2014).

87 Chen, Y. J. *et al.* Lactate metabolism is associated with mammalian mitochondria. *Nat Chem Biol* **12**, 937-943 (2016).

88 Storch, A., Kaftan, A., Burkhardt, K. & Schwarz, J. 6-Hydroxydopamine toxicity towards human SH-SY5Y dopaminergic neuroblastoma cells: independent of mitochondrial energy metabolism. *Journal of neural transmission* **107**, 281-293 (2000).

89 Scatena, R., Bottoni, P., Pontoglio, A., Mastrototaro, L. & Giardina, B. Glycolytic enzyme inhibitors in cancer treatment. *Expert Opin Investig Drugs* **17**, 1533-1545 (2008).

90 Webb, B. A. *et al.* Structures of human phosphofructokinase-1 and atomic basis of cancer-associated mutations. *Nature* **523**, 111-114 (2015).

91 Roesch, A. *et al.* A temporarily distinct subpopulation of slow-cycling melanoma cells is required for continuous tumor growth. *Cell* **141**, 583-594 (2010).

92 Roesch, A. *et al.* Overcoming intrinsic multidrug resistance in melanoma by blocking the mitochondrial respiratory chain of slow-cycling JARID1B(high) cells. *Cancer Cell* **23**, 811-825 (2013).

93 Copley, R. R., Russell, R. B. & Ponting, C. P. Sialidase-like Asp-boxes: sequence-similar structures within different protein folds. *Protein Science* **10**, 285-292 (2001).

94 Deshpande, N., Wilkins, M. R., Packer, N. & Nevalainen, H. Protein glycosylation pathways in filamentous fungi. *Glycobiology* **18**, 626-637 (2008).

95 Su, Y.-Y. & Cai, L. Rasamsonia composticola, a new thermophilic species isolated from compost in Yunnan, China. *Mycological progress* **12**, 213-221 (2013).

96 Perez-Escuredo, J. *et al.* Lactate promotes glutamine uptake and metabolism in oxidative cancer cells. *Cell Cycle* **15**, 72-83 (2016).

97 Amoroso, F., Falzoni, S., Adinolfi, E., Ferrari, D. & Di Virgilio, F. The P2X7 receptor is a key modulator of aerobic glycolysis. *Cell Death Dis* **3**, e370 (2012).

98 Arrell, D. K. *et al.* Proteomic analysis of pharmacological preconditioning: novel protein targets converge to mitochondrial metabolism pathways. *Circulation research* **99**, 706-714 (2006).

99 Hinerfeld, D. *et al.* Endogenous mitochondrial oxidative stress: neurodegeneration, proteomic analysis, specific respiratory chain defects, and efficacious antioxidant therapy in superoxide dismutase 2 null mice. *Journal of neurochemistry* **88**, 657-667 (2004).

100 Pfleger, J., He, M. & Abdellatif, M. Mitochondrial complex II is a source of the reserve respiratory capacity that is regulated by metabolic sensors and promotes cell survival. *Cell Death & Disease* **6**, e1835-e1835 (2015).

101 Boekema, E. J. & Braun, H.-P. Supramolecular structure of the mitochondrial oxidative phosphorylation system. *Journal of Biological Chemistry* **282**, 1-4 (2007).

102 Chaban, Y., Boekema, E. J. & Dudkina, N. V. Structures of mitochondrial oxidative phosphorylation supercomplexes and mechanisms for their stabilisation. *Biochimica et Biophysica Acta (BBA)-Bioenergetics* **1837**, 418-426 (2014).

103 Vander Heiden, M. G., Cantley, L. C. & Thompson, C. B. Understanding the Warburg effect: the metabolic requirements of cell proliferation. *Science* **324**, 1029-1033 (2009).

104 Warburg, O. H. *Ueber den stoffwechsel der tumoren*. (Springer, 1926).

105 Ashton, T. M., McKenna, W. G., Kunz-Schughart, L. A. & Higgins, G. S. Oxidative phosphorylation as an emerging target in cancer therapy. *Clinical Cancer Research* **24**, 2482-2490 (2018).

106 Vogel, F. C. *et al.* Targeting the H3K4 demethylase KDM5B reprograms the metabolome and phenotype of melanoma cells. *Journal of Investigative Dermatology* (2019).

107 Bélanger, M., Allaman, I. & Magistretti, P. J. Brain energy metabolism: focus on astrocyte-neuron metabolic cooperation. *Cell metabolism* **14**, 724-738 (2011).

108 Wallace, D. C. Mitochondria and cancer. *Nature Reviews Cancer* **12**, 685 (2012).

109 Gaskell, A., Crennell, S. & Taylor, G. The three domains of a bacterial sialidase: a β-propeller, an immunoglobulin module and a galactose-binding jelly-roll. *Structure* **3**, 1197-1205 (1995).

110 Manavalan, A., Adav, S. S. & Sze, S. K. iTRAQ-based quantitative secretome analysis of *Phanerochaete chrysosporium*. *Journal of proteomics* **75**, 642-654 (2011).

111 Anderson, L. N. *et al.* Activity-based protein profiling of secreted cellulolytic enzyme activity dynamics in Trichoderma reesei QM6a, NG14, and RUT-C30. *Molecular BioSystems* **9**, 2992-3000 (2013).

112 Liu, Y. *et al.* Advancing understanding of microbial bioenergy conversion processes by activity-based protein profiling. *Biotechnology for biofuels* **8**, 156 (2015).

113 Schröder, S. P. *et al.* Dynamic and functional profiling of xylan-degrading enzymes in *Aspergillus* Secretomes using activity-based probes. *ACS central science* **5**, 1067-1078 (2019).

114 Zhang, J., Siika-aho, M., Tenkanen, M. & Viikari, L. The role of acetyl xylan esterase in the solubilization of xylan and enzymatic hydrolysis of wheat straw and giant reed. *Biotechnology for Biofuels* **4**, 60 (2011).

115 Ďuranová, M., Špániková, S., Wösten, H. A., Biely, P. & De Vries, R. P. Two glucuronoyl esterases of Phanerochaete chrysosporium. *Archives of microbiology* **191**, 133 (2009).

116 Payne, C. M. *et al.* Hallmarks of processivity in glycoside hydrolases from crystallographic and computational studies of the *Serratia marcescens* chitinases. *Journal of Biological Chemistry* **287**, 36322-36330 (2012).

117 Bezawork-Geleta, A., Rohlena, J., Dong, L., Pacak, K. & Neuzil, J. Mitochondrial Complex II: At the Crossroads. *Trends Biochem Sci* **42**, 312-325 (2017).

118 Mandavilli, B. S., Boldogh, I. & Van Houten, B. 3-nitropropionic acid-induced hydrogen peroxide, mitochondrial DNA damage, and cell death are attenuated by Bcl-2 overexpression in PC12 cells. *Molecular brain research* **133**, 215-223 (2005).

119 Ajao, C. *et al.* Mitochondrial toxicity of triclosan on mammalian cells. *Toxicology reports* **2**, 624-637 (2015).

8 Appendix

8.1 Supporting MS data

Additional MS data are part of the digital appendix of this work.

8.2 Zelkovamycin affects OXPHOS complexes

8.2.1 Zelkovamycin interferes with the Ubiquinone/Ubiquinol redox system

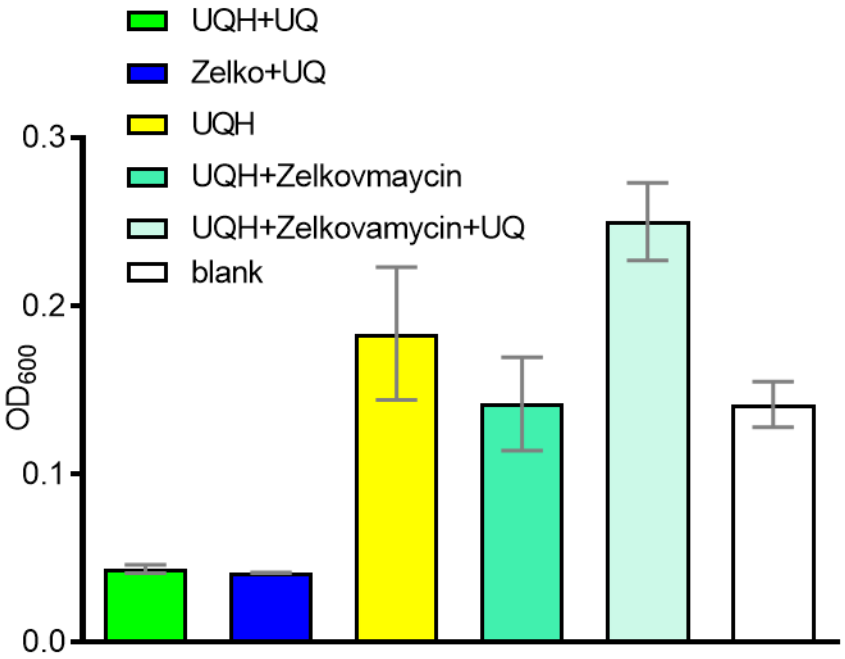

Figure 46: Zelkovamycin interferes with the reduction of DCPIP by Ubiquinone/Ubiquinol. Ubiquinone (UQ), Ubiquinol (UQH) and Zelkovamycin were incubated for 10 min at a 1:1:1 ratio (50 µM). The reaction was started by adding 50 µM DCPIP and the resulting OD_{600} was determined. Error bars indicate standard deviation from three replicates.

The production of ubiquinol can be monitored by the addition of DCPIP (2,6-dichlorophenolindophenol), which upon ubiquinol reduction recycles the substrate ubiquinone, resulting in a loss of its blue color. This can be measured by a UV absorption measurement at 600 nm. (ab109904 MitoTox Complex II OXPHOS Activity Assay protocol, 2017 Abcam).

Monitored reactions:

Complex I: NADH + H^+ + Ubiquinone → NAD^+ + Ubiquinol

Complex II: Succinate + Ubiquinone → Fumarate + Ubiquinol

8.2.2 Western Blot analysis of OXPHOS complexes

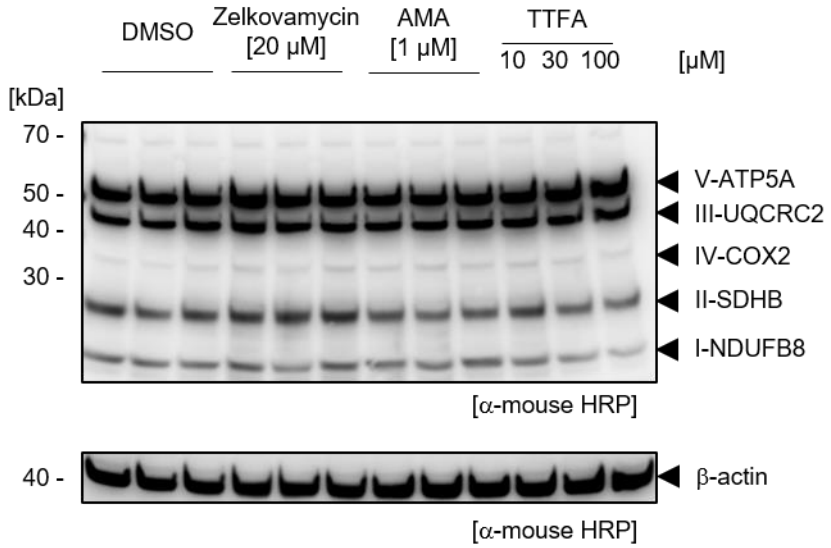

Figure 47: Zelkovamycin does not change the abundance of OXPHOS complex subunits. In order to elucidate the molecular target of Zelkovamycin, HeLa cells were treated with Zelkovamycin for 24 h. Lysates were separated by gel electrophoresis. Subsequently, proteins were analyzed by a Western blot using an OXPHOS antibody-cocktail (1:1000, Abcam ab110411) that stains subunits of all OXPHOS complexes. As a secondary antibody, IgG HRP (1:10000, GE NA931) was used. AMA and TFFA served as positive controls. For control of protein loading, actin was stained with mouse anti-actin (1:500 MP #691001) and visualized by anti-mouse IgG HRP (1:10000, GE NA931). Digitalization and Western blotting were performed as described in section 3.6.3.

8.3 Activity-based probes, competitors and inhibitors

8.3.1 Serine hydrolases

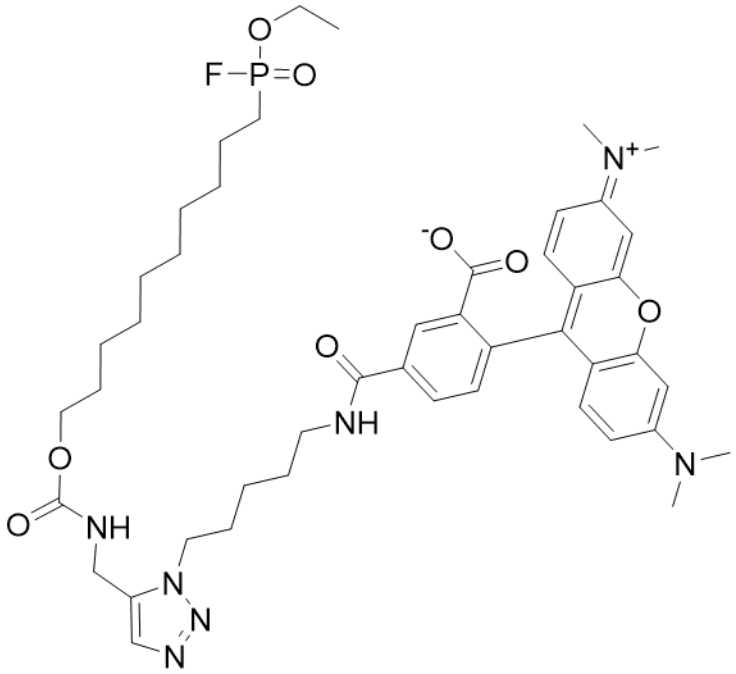

Figure 48: Chemical structure of FP-Rh.

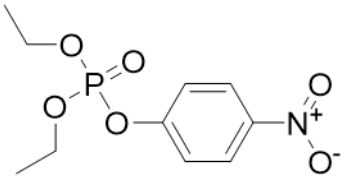

Figure 49: Chemical structure of Paraoxon, a competitor of FP labelling.

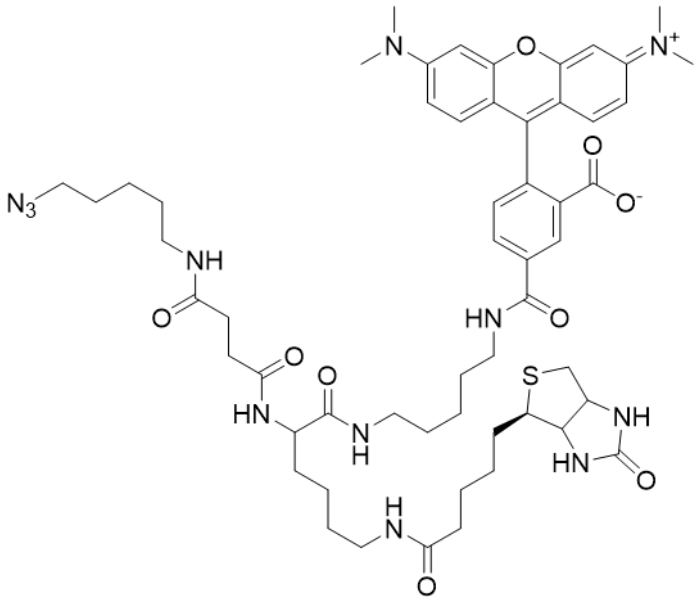

Figure 50: Tri-azide tag

8.3.2 Glycosidases

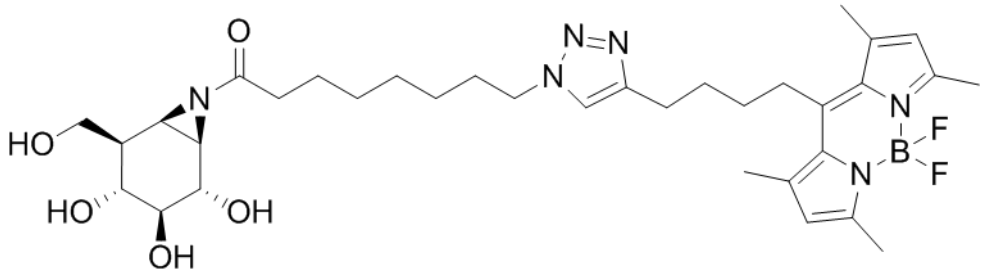

Figure 51: Chemical structure of JJB70, a β-glucosidase probe with a fluorophore-tag.

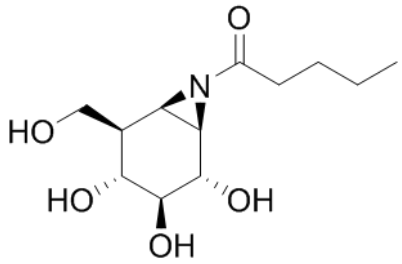

Figure 52: Chemical structure of KY358-acyl, a competitor of JJB70 labelling.

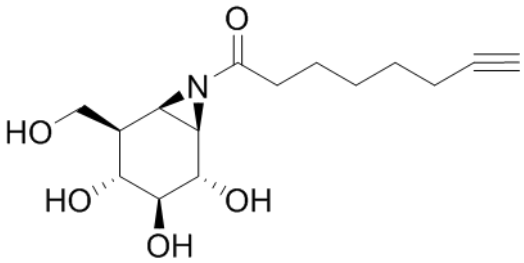

Figure 53: Chemical structure of KY371, a β-glucosidase click-probe and competitor.

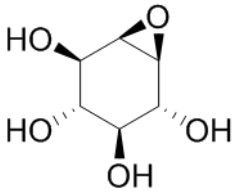

Figure 54: Chemical structure of Conditurol epoxide B, a broad-range glycosidase inhibitor

8 Appendix

Table 11: Overview of probes, competitors and inhibitors used in this thesis. Probes, competitors and inhibitors are reported in conjunction with their molecular weight and function in the ABPP workflow.

Name	Molecular weight (Da)	Function
FP-alkyne	234.25	Click-probe
Tri-azide	1079.33	Click-tag
FP-Rh	890.01	Fluorescent probe for SH labelling
FP-tri	1448.66	Fluorescent and enrichment probe for SH labelling
Paraoxon	275.20	SH competitor
Cyclophellitol	176.17	Glycosidase competitor
Cyclophellitol-aziridine	175.18	Glycosidase competitor
JJB70	670.61	Fluorescent probe for GH labelling
JJB111	736.93	Enrichment probe for GH labelling
KY358-acyl	259.30	Glycosidase competitor
KY371	297.35	Click-probe for GH labelling and Glycosidase competitor

8.4 Supplementary material and methods

8.4.1 Natural products and probes

Zelkovamycin was purchased from Abcam (ab144389). Zelkovamycin derivatives were synthesized in-house by Daniel Krahn. FP-probes were either synthesized in-house or by the van der Stelt laboratory (Leiden, Netherlands). Tri-N3-tag (MK109) was synthesized in-house. Cylclophellitol-based glycosidase probes and competitors were synthesized by the Overkleeft laboratory (Leiden, Netherlands). Further probes and competitors were purchased and are listed in chemicals section 8.4.2.

8.4.2 Chemicals

Chemicals are listed in alphabetical order together with the manufacturer and the article or catalog number. Purchased quantities varied.

3-(*N*-morpholino)propane sulfonic acid	Sigma-Aldrich®, #M1254-250G
Acetic acid (glacial)	Fisher Chemical, A/0400/PB17
Acetone	Sigma-Aldrich®, Chormasolv #270725
Acrylamide/Bisacrylamide	Serva, #10688.01
Ammonium bicarbonate	Sigma-Aldrich®, #11213
Ammonium persulfate	Sigma -Aldrich®, #A7460
Ammonium sulfate	Sigma -Aldrich®, #A5132
anti-mouse IgG HRP	GE lifesciences, #NA931
Antimycin A	Sigma-Aldrich®, #A8674
Avidin-beads	Pierce™, #20219
BSA (Protein standard)	Sigma-Aldrich®, #P5619
BSA (Western blot)	VWR, #4223519
C18 column beads	Reprosil-Pur Basic C18, 1.9 µm, #r119.b9.
Carbonylcyanid chlorphenylhydrazone	Sigma-Aldrich®, #C2759
Chloroform	Sigma-Aldrich®, #C2432
Coomasie G-250	Alfa Aesar, #43318
Copper sulfate	Sigma -Aldrich®, #C1297

Dimethylformamide	Fisher Chemical, #D/3841/17
Disodium hydrogenphosphate	VWR – Prolabo, #28.029.292
DMSO	Sigma-Aldrich®, #D8418
DTT	Sigma-Aldrich®, #D9779
Ethanol p.a.	Fisher Chemical, #E/0650DF/17
Fetal bovine serum	Gibco®, #16140-071
Hydrochloric acid	Sigma Aldrich®, #H9892
Iodo acetamide	Acros Organics, #122270050
Lithium dodecyl sulfate	AppliChem, #A1385,0100
Lys-C	Wako Chemicals, #125-05061
Mouse anti-actin	MP Biomedicals, #691001
MS-grade acetonitrile	Honeywell, Chormasolv LCMS-Ultra, #14261
MS-grade formic acid	Fisher Chemical, #A117-50
MS-grade methanol	Honeywell, Chormasolv LCMS-Ultra, #14262
MS-grade water	Honeywell, Chormasolv LCMS-Ultra, #14263
N,*N*,*N*′,*N*′-Tetramethylethylendiamine	Sigma Aldrich®, #T9281
Sodium acetate	VWR – Prolabo, #27.652.298
Sodium chloride	VWR – Prolabo, #27.810.364
Ortho-phosphoric acid	Merck, #1.005.631.000
OXPHOS antibody cocktail	Abcam, #ab110411
Paraoxon	Fluka Analytical, #36186
Pen/Strep	Gibco®, #15140-122
Potassium dihydrogenphosphate	AppliChem, #A3620,1000
Protease and Phosphatase Inhibitor	Sigma-Aldrich®, MSSAFE-1VL
Protein ladder	Thermo Fisher, #26623

Rotenone	Abcam, #ab143145
Roti®-Nanonquant	Roth, #K880.1
Sodium dodecyl sulfate	Roth, #2326.2
Streptavidin-HRP	Sigma-Aldrich®, #S2438
Thenoyltrifluoroacetone	Cayman Chemical, #15517
Thiazolyl Blue Tetrazolium Bromide	Sigma-Aldrich®, #M2128
Trifunctional tag	MK109, synthesized in-house
Tris[(1-benzyl-1H-1,2,3-triazol-4-yl)methyl]amine)	Sigma-Aldrich®, #678937
Tris-base	VWR – Prolabo, #28808.294
Trochloric acid	Sigma-Aldrich®, #T0699
Trypan blue	Invitrogen, #T10282
Trypsin (MS-grade)	Pierce™, #90057
Tween-20	AppliChem, #A1389,0500
Ubiquinol	United States Pharmacopeia, #1705334
Ubiquinone	Coenzyme Q10, Sigma-Aldrich®, #C9538
Urea	GE Healthcare, #17-1319-01

8.4.3 Buffers and Media

DMEM	Gibco®, #31966-047
DMEM low glucose	Gibco®, #31885-023
DMEM/F12	Gibco®, #31330-038
Phosphate-buffered saline (cell culture)	Gibco®, #14190-094
Trypsin (cell culture)	Gibco®, #25300-062

8.4.4 Consumables

C18 membrane	Supelco Analytical, #6688-3U
Cell culture dishes:	

10 cm Ø	Sarstedt, #83.3902
6-well	Sarstedt, #83.3920
12-well	Sarstedt, #83.3921
96-well	Sarstedt #83.3924
Cell Scraper	Sarstedt, #83.1830.
Dispenser tips	
0.1 mL	#702402
0.5 mL	#702370
1 mL	#702406
5 mL	#705710
12.5 mL	#702378
25 mL	#702380
Glass fiber membrane	GE Healthcare, #1822-204
Low-bind tubes and tips:	
1.5 mL tubes	Eppendorf, #022431081
2 mL tubes	Eppendorf, #022431102
15 mL tubes	Eppendorf, #0030122.151
50 mL tubes	Eppendorf, #0030122.178
10 µL tips	Eppendorf, #022493018
200 µL tips	Eppendorf, #022493022
1000 µL tips	Eppendorf, #022493024
96-well plate	Eppendorf, #0030601.300
Sealing mat	Eppendorf, #0030127.978
MS autosampler plates	Thermo Scientific, #AB-800-L
MWCO cut-off filter	Amicon Ultra-0.5 Centrifugal Filter Unit,

	Merck, #UFC501096
Needles	Sterican®, Braun, #4665791
Nitrocellulose membrane	Immobilon-P, Millipore, #T831.1
Pestles	VWR, #47747.358
Plates for spectroscopy applications:	
colorless	Sarstedt, #821581
black	Greiner bio-one, #655096
Sealing mats MS autosampler	Axygen, #AM-96-PCR-RD
Serological pipettes:	
5 mL	Sarstedt, # 86.1253.001
10 mL	Sarstedt, #86.1254.001
25 mL	Sarstedt, #86.1685.001
Sterile filters	Filtropur S 0.2, Sarstedt, #831826.001
Syringes	Braun, #4606205V
Tubes:	
1.5 mL	Roth, #XC63.1
2 mL	Sarstedt, #72.691
15 mL	Sarstedt, #62.554.502
50 mL	Sarstedt, #62.547.254
Tips:	
10 µL	Starlab, #S1111-3700
200 µL	Starlab, #S1111-1706
1000 µL	Starlab, #S1112-1720
Wipes	Kimtech, #05511

8.4.5 Devices and Software

8.4.5.1 Devices for biological works

Bioruptor	Diagenode, UCD-200TM-EX
Blotting Chamber	Biorad, Mini-PROTEAN® Tetra-system
Cell counter	Labor Optik, Neubauer, #631-0926
Centrifuges:	
Small tube centrifuge	Eppendorf, 5430 R
Big tube centrifuge	Eppendorf, 5810 R
Dispenser	Brand, HandyStep®
Fluorescence scanner	Typhoon FLA 9000 (+Software)
Gel electrophoresis:	
Comb (10 pockets)	C.B.S. Scientific, #MVC-1010
Comb (14 pocekts)	C.B.S. Scientific, #MVC-1014
Glass plates	C.B.S. Scientific, #MGP-100R
Gel scanner	Intas, 140S
Incubator	New Brunswick, Galaxy 170R
Lyophilizer	Christ, Alpha 2-4 LD plus
Microscope	Olympus, CK2
Pipettes	Eppendorf, Research plus
Power supply	VWR, 300V
Scale	Mettler Toledo, XS105 Dual range
Shaker	Eppendorf, Thermomixer C
Table top centrifuge	Sprout, #6.254604
Vortexer	VWR, VV3

8.4.5.2 Software for biological works

Adobe Illustrator C24	v. 14.0.0

Adobe Photoshop C24 Extendend	v. 11.0
GraphPad Prism	v. 5.04
ImageJ	v. 1.51n
Microsoft office 2016	Microsoft
Sparkcontrol Dashboard	v. 2.2.0
Typhoon FLA 9000 control	v. 1.2

8.4.5.3 Mass Spectrometry devices

8-channel pipettes	Eppendorf, Research plus
Centrifuges:	
Small tube centrifuge	Eppendorf, 5430 R
Big tube centrifuge	Eppendorf, 5810 R
Vacuum concentrator	Eppendorf, Concentrator plus
Column oven	Sonation
EASY-nLC™1000	Thermo Fisher
EASY-nLC™1200	Thermo Fisher
Electric dispenser	Eppendorf, Xplorer
Nanospray flex ion source	ES071 and ES072
Orbitrap Elite™	Thermo Fisher
Orbitrap Fusion™ Lumos™ Tribrid™	Thermo Fisher
Pipettes	Gilson, Pipetman
Siliica capillary	PicoFrit emitter, New Objective

8.4.5.4 Mass Spectrometry labor software

Freestyle	Thermo Fisher, v. 1.6
MaxQuant	v. 1.5.3.30 and v. 1.6.7
Perseus	v. 1.6.2.1 and v. 1.6.2.3
XCalibur	Thermo Fisher v. 3.063 and v. 4.3.73.11

Tune	Thermo Fisher, v. 2.7.0 and v. 3.3.2782.28
Column oven control	Sonation CO Control, v. 3.4
Proteome databases:	
Homo sapiens	Uniprot
Phanerochaete chrysosporium	v. 2.2 Joint Genome Institute

Danksagung

Diese Arbeit entstand im Rahmen meiner Zeit als Doktorand in der Arbeitsgruppe Kaiser (Chemische Biologie, Zentrum für medizinische Biotechnologie, Universität Duisburg-Essen). Ich bedanke mich bei Herrn Prof. Dr. Kaiser und seinen Mitarbeitern für die stets konstruktive und kollegiale Zusammenarbeit. Ferner danke ich allen Kooperationspartnern für ihre wichtigen Beiträge zu dieser Arbeit.

Die Arbeitsgruppe belegt, dass wissenschaftliche Exzellenz und Spaß bei der Arbeit nicht in Widerspruch miteinander stehen. Die letzten vier Jahre werden mir aufgrund unzähliger positiver Ereignisse immer in Erinnerung bleiben. Es war ein Privileg, mit euch zusammen zu arbeiten.

Ich widme diese Arbeit meinen Eltern, für ihre andauernde Unterstützung während meines Studiums. Ohne euren Rückhalt hätte ich es niemals bis zu diesem Punkt geschafft – danke! Zudem möchte ich meiner Freundin und meinen Freunden danken, dass ihr meine Freizeit immerzu positiv gestaltet habt und mir bis heute meine unzähligen Fehler und Macken verzeiht. Hervorzuheben bleibt die Bedeutung der Familien Rossié, Grefkes und Hoffmanns, welche mich schon lange auf meinem Weg begleiten und fortwährend unterstützt haben.

Curriculum vitae

Curriculum vitae